Very preterm birth and fetal growth restriction in adolescence - Cardiovascular and renal aspects

Liefke, Jonas

2022

Document Version:
Publisher's PDF, also known as Version of record

Link to publication

Citation for published version (APA):
Liefke, J. (2022). *Very preterm birth and fetal growth restriction in adolescence - Cardiovascular and renal aspects*. [Doctoral Thesis (compilation), Department of Clinical Sciences, Lund]. Lund University, Faculty of Medicine.

Total number of authors:
1

Very preterm birth and fetal growth restriction in adolescence

Cardiovascular and renal aspects

JONAS LIEFKE
DEPARTMENT OF CLINICAL PHYSIOLOGY | FACULTY OF MEDICINE | LUND UNIVERSITY

Very preterm birth and fetal growth restriction in adolescence

Very preterm birth and fetal growth restriction in adolescence

Cardiovascular and renal aspects

Jonas Liefke, M.D.

LUND
UNIVERSITY

DOCTORAL DISSERTATION

Doctoral dissertation for the degree of Doctor of Philosophy (Ph.D.) at the Faculty of Medicine at Lund University to be publicly defended on the 7th of December 2022 at 13.00 in Lecture Hall 1 at Skåne University Hospital, Lund, Sweden.

Thesis advisors: Associate Professor Erik Hedström, M.D., Associate Professor Katarina Steding-Ehrenborg, and Professor David Ley, M.D.

Faculty opponent: Professor Jan Engvall, M.D.

Organization LUND UNIVERSITY Skåne University Hospital, Clinical Sciences, Department of Clinical Physiology Entrégatan 7 SE—22242 Lund Sweden	**Document name** DOCTORAL DISSERTATION **Date of issue**
Author(s) Jonas Liefke	Sponsoring organization

Title and subtitle
Very preterm birth and fetal growth restriction in adolescence – Cardiovascular and renal aspects

Abstract
This thesis applied magnetic resonance imaging (MRI) to investigate to what extent very preterm birth due to early onset fetal growth restriction (FGR) impacts the cardiovascular system and kidneys in adolescence. The thesis further investigated whether FGR exacerbates the organ-specific effects of very preterm birth.

Study I validated a widely available non-contrast enhanced MRI method for quantification of renal cortical and medullary parenchymal volumes and showed that kidney volumes can be quantified with high accuracy and precision.

Study II validated an MRI method for pulse wave velocity (PWV) acquisition in neonates and adolescents and showed how the acquired PWV was influenced by commonly used MRI methods. The study proposed the use of 3D angiography images and the time-to-foot method for accurate and precise PWV acquisition.

Study III implemented the proposed PWV method from Study II and 24-hour ambulatory blood pressure measurements and showed that very preterm birth due to early onset FGR was associated with higher, yet normal, blood pressure in adolescent boys while very preterm birth was associated with higher arterial stiffness in girls.

Study IV showed that very preterm birth was associated with smaller ventricular volumes without alterations in left or right longitudinal and radial pumping. Early onset FGR did not exacerbate the effects of very preterm birth.

Study V implemented the newly validated non-contrast enhanced MRI method from Study I together with biomarkers of kidney function. Very preterm birth due to FGR was associated with smaller total kidney and medullary kidney volumes, but not with markers of kidney dysfunction or renin-angiontensin-aldosterone system activation in adolescence.

This thesis concludes that adolescents born very preterm with and without preceding fetal growth restriction show alterations in cardiovascular and renal morphology. Changes were more pronounced in girls. Cardiovascular and kidney function were however normal, possibly indicating a decreased long-term effect of very preterm birth and fetal growth restriction on these organ systems compared to earlier studies, where clear signs of increased risk were observed already in childhood and adolescence. As indicated by increases in blood pressure, male sex and fetal growth restriction might increase cardiovascular risk in those born preterm. Morphological changes in the heart and in the kidneys may still precede functional decline in this population, and the alterations observed could potentially be used as prognostic markers in the future.

Key words
Very preterm birth, Fetal growth restriction, magnetic resonance imaging, Cardiovascular function, Kidney function, Kidney volumes, Pulse wave velocity, Arterial stifness, Atrioventricular plane displacement

Classification system and/or index terms (if any)

Supplementary bibliographical information	**Language** English
ISSN and key title ISSN: 1652-8220 Lund University, Faculty of Medicine Doctoral Dissertation Series 2022:159	**ISBN** 978-91-8021-321-9

Recipient's notes	**Number of pages** 136	Price
	Security classification	

Signature Date 2022-10-31

Very preterm birth and fetal growth restriction in adolescence

Cardiovascular and renal aspects

Jonas Liefke, M.D.

LUND
UNIVERSITY

Faculty Opponent

Professor Jan Engvall
Linköping University
Linköping, Sweden

Evaluation Committee

Assoc Prof. Elisabeth Olhager
Lund University
Lund, Sweden

Assoc Prof. Kristofer Hedman
Linköping University
Linköping, Sweden

Assoc Prof. Lina Bergman
Göteborg University
Göteborg, Sweden

Cover: “Cardiovascular aspects of a Ph.D. student”. A coronal view of Jonas Liefke. Artwork was created with “Fotor” Chengdu Everimaging Science & Technology Co., Ltd. (https://www.fotor.com/)

Faculty of Medicine Department of Clinical Physiology
ISSN 1652-8220
ISBN 978-91-8021-321-9

Lund University, Faculty of Medicine Doctoral Dissertation Series 2022:159
Printed in Sweden by Media-Tryck, Lund University, Lund 2022

GOOD

Jocko Willink

Table of Contents

List of publications

This thesis is based on the following publications and manuscripts:

I. **Non-contrast-enhanced magnetic resonance imaging can be used to assess renal cortical and medullary volumes-A validation study.**
J Liefke, K Steding-Ehrenborg, D Asgeirsson, D Nordlund, S Kopic, E Morsing, E Hedström. *Acta Radiol Open. 2022;11(1):20584601211072281.*

II. **Pulse wave velocity measurements by magnetic resonance imaging in neonates and adolescents: Methodological aspects and their clinical implications.**
S Lundström, **J Liefke**, E Heiberg, E Hedström. *Pediatr Cardiol. 2022. 10.1007/s00246-022-02894-0.*

III. **Higher blood pressure in adolescent boys after very preterm birth and fetal growth restriction.**
J Liefke, K Steding-Ehrenborg, P Sjöberg, D Ryd, E Morsing, H Arheden, D Ley, Erik Hedström. *Accepted Pediatric Research 2022-10-14.*

IV. **Smaller ventricles but preserved cardiac pumping in adolescents born very preterm.**
J Liefke, K Steding-Ehrenborg, E Morsing, D Ley, H Arheden, E Hedström. *Manuscript.*

V. **Fetal growth restriction followed by very preterm birth is associated with smaller kidneys but preserved kidney function in adolescence.**
J Liefke, C Heijl, K Steding-Ehrenborg, E Morsing, H Arheden, D Ley, E Hedström. *Accepted Pediatric Nephrology 2022-10-06.*

Abbreviations

ABPM Ambulatory blood pressure measurements

AVPD Atrioventricular plane displacement

CKD Chronic kidney disease

CVD Cardiovascular disease

EF Ejection fraction

FGR Fetal growth restriction

IUGR Intrauterine growth restriction

LV Left ventricle

LVM Left ventricular mass

MRI Magnetic resonance imaging

PWV Pulse wave velocity

RV Right ventricle

SGA Small for gestational age

THV Total heart volume

Acknowledgements

This thesis would not have been what it is today without the strong foundation of which I have had the great fortune to not only stand, but also to build upon. There are many things and many people to be grateful for. Thank you everyone in the Cardiac MR group, all past and present members, for forming me to the person and researcher I am today. Thank you everyone at the Department of Clinical Physiology and Nuclear Medicine for great collaboration and discussions regarding work, life, and career. You all inspire me to improve.

I would also like to direct special gratitude to the following:

To my supervisors.

My main supervisor **Erik Hedström** for challenging me, from the first to the last step, and for making me not just a better researcher but also a better human. This has not been easy, which was your purpose. Thank you.

My co-supervisor **Katarina Steding-Ehrenborg** for seeing potential in me from the start and for guiding me through this work, both professionally and personally. Looking forward to years of class parenting.

My co-supervisor **David Ley** and **Eva Morsing** for including me and letting me take part in your important work. It has been a pleasure and a joy working with you both. I hope that this work will help future generations of infants admitted to the neonatal intensive care unit.

To my colleagues

Håkan Arheden, for all wisdom, your directness, and your honesty in all situations. For training me in how to lead.

Jonathan Berg for all discussions and for becoming a close friend to the family also outside of work. **Daniel Ryd**, for great collaboration and important discussions, but especially for all the fun. **Petter Frieberg** for being helpful and kind, you are a true inspiration. **Per Arvidsson** for being a lifelong friend and an inspiration in both work and in life. **Felicia Seeman**, for being awesome, in science as well as in life. **David Nordlund**, you are a true inspiration. **Tom Gyllenhammar**, for all the guidance throughout the years. **Anders Nelsson** for all guidance and clinical work

together, looking forward to years together as class parents. **Anthony Lindholm**, for a great time together doing research.

Fredrik Hedeer, Barbro Kjellström, Johannes Töger, Sebastian Bidhult, Robert Jablonowski, Mikael Kanski, Martin Johansson, Mariam Al-Mashat, Shahnaz Akil, Björn Östenson, Jonathan Edlund, Anna Székely, Marjolein Piek, Julius Åkesson, Elsa Bergström, Karin Pola, Tania Lala, Kristian Dimovski and Theodor Lav for all discussions. It has been great working with you all.

A special thanks to **Ashwin Venkateshvaran, Marjolein Piek, Petter Frieberg, David Nordlund, Barbro Kjellström, Martin Johansson, Anders Nelsson, Mikael Kanski and Jonathan Berg** for helping me improve the thesis.

Henrik Engblom, Ellen Ostenfeld, Einar Heiberg, Anthony Alethras, and **Marcus Carlsson**, for forming the group as we know it and for teaching me new things every single day.

Jane Tufvesson, for always being helpful. **Karin Larsson** and **Kerstin Brauer**, for solving everything.

Margareta Gebka and the research nurses at the NICU. It has been a privilege working with you all.

All research **techs**, helping with this project over the years.

To my friends and family

Joel Cehlin for challenging me when needed and supporting me when needed more. **Johan Joelsson**, my oldest friend, for always being there.

Mom and dad, **Lena Klasson** and **Torgny Karlsson** for all your love and guidance throughout the years and the continuous support in all possible ways. Thank you also for teaching me to work hard, never quit and to dig in.

Evelin, Adrian and Estelle, for making me dig deeper, work harder and for making me want to be a better human. This is for you. I'll hope that you someday will read this and be inspired to do great things.

Madeleine Liefke, for everything. For being my best friend and the best wife and mom that anyone could ever ask for.

Lund, 31 October 2022

Populärvetenskaplig sammanfattning

Med förbättrad förlossningsvård ökar chanserna för foster i riskgraviditeter att överleva. Vissa tillstånd, så som för tidig födsel och tillväxthämning i livmodern, utgör en ökad risk för fosterdöd och sjukdom i spädbarnsåldern. Tillväxthämning i livmodern är ett allvarligt tillstånd där fostret riskerar att avlida om man inte tidigarelägger förlossningen till mycket tidigt i graviditeten, detta trots att alla organsystem då inte är fullt utvecklade. Det finns ett starkt samband mellan för tidig födsel och tillväxthämning i livmodern med ökad risk för hjärtkärlsjukdomar och njursjukdom senare i livet. Det är dock inte helt kartlagt varför detta sker eller vilka organ som främst är drivande i den ökade risken. Det är inte heller känt hur tillväxthämning påverkar långtidseffekterna av att födas för tidigt.

Denna avhandling undersöker ungdomar som på grund av hotande syrebrist och otillräcklig blodcirkulation efter tidigt isättande tillväxthämning i livmodern förlöstes före graviditetsvecka 30. Ungdomarna föddes vid Skånes universitetssjukhus i Lund 1998–2004 och jämförs i denna avhandling med två grupper födda med normal födelsevikt, en grupp som också föddes i liknande graviditetsvecka och en som föddes med normal vikt efter en normal graviditetslängd.

Magnetkamera (MR) användes för att studera hjärtats, kärlens och njurarnas struktur och funktion. Deltagarna fick även utföra 24-timmars blodtrycksundersökning och lämna blod och urin för undersökning av markörer som kan visa på ökad risk för nuvarande eller framtida sjukdom.

Avhandlingen inkluderar fem delarbeten. Två av dessa är arbeten testar och validerar nya metoder för att studera njurarnas struktur respektive pulsvågshastighet, ett mått på kärlstyvhet, i stora kroppspulsådern. Dessa metoder används i avhandlingens senare delarbeten.

Det övergripande syftet med denna avhandling var att ta reda på i vilken utsträckning mycket för tidig födsel och tillväxthämning i livmodern påverkar hjärta, kärl och njurar i ungdomsåren. Syftet var också att ta reda på om effekterna av mycket för tidig födsel på de olika organen förstärks av tillväxthämning i livmodern. De ingående studierna omfattar i korthet följande:

Delarbete I. Njurarnas olika delar mättes med hjälp av en fritt tillgänglig och MR-metod varefter de uppmätta volymerna jämfördes med de faktiska volymerna. MR-metoden stämde väl överens med de faktiska volymerna och metoden visade på hög tillförlitlighet vid upprepade mätningar och mellan olika individer.

Delarbete II. Pulsvågshastigheten i stora kroppspulsådern mättes med olika MR metoder i nyfödda samt i ungdomar. Arbetet visade att olika vanligt använda metoder för att mäta denna hastighet ger olika resultat och därmed inte säkert kan jämföras. Den mest tillförlitliga metoden i delarbetet gavs som förslag att användas i framtida studier.

Delarbete III. Blodtrycksvariation över dygnet och pulsvågshastigheten och styvheten i stora kroppspulsådern i de tre grupperna undersöktes och metoden från Studie II implementerades. Studien visade att blodtrycket hos pojkar var högre efter mycket för tidig födsel jämfört med att vara född i normal tid. Studien visade även att tillväxthämning i livmodern förstärker denna skillnad. Studien antydde även att pulsvågshastigheten var högre hos flickor födda mycket för tidigt jämfört med att vara född i normal tid.

Delarbete IV. Magnetkamera användes för att undersöka hjärtats struktur och funktion. Studien visade på skillnader i hjärtvolymer men också att hjärtats funktion under tonåren inte var påverkad av mycket för tidig födsel, oavsett föregående tillväxthämning i livmodern. Skillnaden i hjärtats volymer var mest uttalad hos flickor.

Delarbete V. Njurens olika volymer mättes med metoden som validerades i delarbete I. Studien visade att mycket för tidig födsel på grund av tillväxthämning i livmodern var associerad till mindre njurvolymer. En skillnad som var mest markant hos flickor. Detta utan att njurfunktionen var påverkad.

Sammanfattningsvis har denna avhandling tagit ett helhetsgrepp kring de organsystem som visats påverkas av mycket för tidig födsel och tillväxthämning i livmodern. Helt nya validerade metoder har använts tillsammans med tidigare väl kända metoder för att bedöma hjärta, aorta och njurar. Sammantaget indikerar avhandlingen minskade långtidseffekter och lägre grad av kardiovaskulär påverkan och njurpåverkan av mycket för tidig födsel, med eller utan tillväxthämning.

Popular summary in English

Improved obstetric and neonatal care have increased the number of fetuses in high-risk pregnancies that can be identified, surveilled, and who eventually survive. Early onset fetal growth restriction is a clinical syndrome in which the fetus risks intrauterine death due to dysfunctional fetal placental circulation. At Skåne University Hospital in Lund, Sweden, it has been the clinical practice to actively deliver fetuses, due to early onset fetal growth restriction, even in very early gestation, when organ maturation has not yet been completed. The long-term effects of this management are not known. There is, however, a strong association between both preterm birth and fetal growth restriction with an increased risk of cardiovascular disease (CVD) and kidney disease later in life. Whether the heart, the vasculature or the kidneys drives this increased risk is not known. It is further not known whether early onset fetal growth restriction adds to the effects of very preterm birth.

This thesis included a cohort of adolescents born very preterm due to early onset fetal growth restriction at Skåne University Hospital between the years 1998-2004. Two sex-matched control groups with appropriate birth weight were included, one in similar gestational and one born at term after a healthy pregnancy.

To diagnose and quantify organ specific alterations, magnetic resonance imaging (MRI) was used. This method is the reference method for quantification of cardiovascular structure and function and is central in assessing kidney structure. 24-hour ambulatory blood pressure measurements were performed and biochemical markers in blood and urine for the assessment of cardiovascular risk, kidney function and inflammatory activity were sampled.

This thesis includes five studies. Two are validation studies in which methods for the quantification of kidney volumes and pulse wave velocity in the aorta, a measure of arteria stiffness, respectively, are developed and assessed. These methods are then applied to assess differences between groups in the primary cohort.

The overall aim of this thesis was to investigate to what extent very preterm birth due to fetal growth restriction effects the heart, the vasculature, and the kidneys in adolescence. The aim was also to investigate whether the organ specific alterations induced by very preterm birth was exacerbated by fetal growth restriction.

Study I. Validated renal cortical and medullary volume assessment with a readily available non-contrast-enhanced MRI method. For comparison, renal cortical and medullary volumes were quantified with Archimedes' principle, after dissection of

extracted kidneys. The MRI method agreed with ex-vivo measurements and the intra-and interobserver variability was low.

Study II. Validated a method for pulse wave velocity acquisition with MRI in neonates and in adolescents. A computer phantom was created to determine the temporal resolution needed for reliable quantification of pulse wave velocity in the respective cohort, with the actual physical parameters as input. The study showed what method for pulse wave velocity that should be used and determine the temporal resolution needed for reliable assessment of pulse eave velocity in the respective group.

Study III. Investigated blood pressure variability and aortic stiffness in the three groups, born very preterm with and without preceding fetal growth restriction and born at term. 24-hour ambulatory blood pressure measurements and the validated method for pulse wave velocity measurements were used. The study showed that blood pressure is higher in boys born very preterm and that fetal growth restriction exacerbates this increase. The study further showed, in contrast to earlier studies of adolescents born very preterm with and without fetal growth restriction, that arterial stiffness was similar between groups.

Study IV. Cardiac structure and function were assessed with common clinical and new MRI methods. The study showed that very preterm birth was associated with smaller cardiac volumes but also that cardiac function was unaffected after very preterm birth and fetal growth restriction in adolescence.

Study V. Cortical and medullary kidney volume were assessed with the validated method from *Study I*. The study showed that very preterm birth due to fetal growth restriction was associated with smaller kidney volumes. This volume change was mostly driven by smaller medullary volumes. Kidney function was not affected.

In summary, this thesis has taken a comprehensive approach to assess the effects of very preterm birth and fetal growth restriction on the cardiovascular system and the kidneys in adolescence. Potential prognostic biomarkers of future cardiovascular and renal disease have been assessed using new validated MRI methods together with standard clinical methods. Overall, this thesis indicates lessened long-term effects and degree of cardiovascular impact of very preterm birth with and without preceding fetal growth restriction.

Part I

Research context

1 Introduction

Word wide, the incidence of preterm birth is approximately 10 percent and preterm birth is the leading cause of death in children under 5 years of age, with worsening outcomes related to degree of prematurity (1,2). Fetuses presenting with early onset fetal growth restriction (FGR) due to pathological fetal-placental blood flow, are at particular risk for adverse perinatal outcomes (3). Preterm birth and low birth weight has further been associated with increased risk of future disease burden, including cardiovascular and renal disease, showing an inverse relationship between gestational age and birth weight to cardiovascular morbidity (4–7). Low birth weight and birth weight deviation have been used as a proxy for FGR in studies on both perinatal and long-term outcomes, resulting in inclusion of heterogeneous groups, since not all small fetuses are subject to restricted intrauterine growth.

Several landmark improvements in obstetric and neonatal management, such as antenatal corticosteroid and postnatal surfactant administration, both implemented just prior to the birth of the current study population, have decreased perinatal morbidity and mortality (8–10). The short-term outcome of both preterm birth and low birth weight has improved substantially over the last decades (11,12), and the limit of viability has been pushed further and further back in gestation (13–15). Since the second half of the 1990's, the clinical management of fetuses with early onset FGR, verified with pathological fetal-placental Doppler velocimetry, presenting at Skåne University Hospital, Lund, Sweden, has been to deliver the compromised fetus with emergency or elective cesarean section early in gestation (16).

The long-term cardiovascular outcomes after very preterm birth due to early onset fetal growth restriction in adolescents born with access to modern neonatal intensive care has not yet been studied.

The overall aim of this thesis was therefore to investigate whether very preterm birth with or without preceding early onset fetal growth restriction is associated with cardiovascular and renal dysfunction in adolescence. This thesis also sought to investigate whether fetal growth restriction exacerbated the effects of very preterm birth.

1.1 Fetal origin of adult disease

In 1990 David Barker and colleagues proposed the "fetal origin of adult disease" (or "Barker hypothesis") hypothesis, postulating that the fetal environment and maternal and early infant health impacts the incidence of metabolic and cardiovascular disease later in life (17).

Epidemiological data to support this hypothesis had been gathering from across the world and studies in Finland, Norway and England all showed similar findings (6,18–24). The incidence of cardiovascular disease was greater in areas with poor socioeconomic living conditions and in areas with increased childhood and maternal morbidity (18,19,22,23). Studies included populations born in the late 1800s up to the end of the second world war.

Other epidemiological data to support the hypothesis were observations that adult height was inversely related to cardiovascular mortality (24) and that low birth weight in infancy increased the risk of ischemic heart disease later in life (6). In these historical cohorts, an increased incidence in maternal and infant death as well as drastic alterations in height and weight, may be seen as a direct proxy for poor socioeconomic living conditions with lack of food and basic healthcare as underlying factors to changes in anthropological metrics. The conclusion that poor nutrition in early life increases susceptibility to the effects of future nutrition rich diet was drawn early (19,24) and has since been observed in recent studies showing an increased risk of cardiometabolic and cardiovascular disease after being born with low birth weight (25) and after childhood malnutrition (26). An intensive compensatory nutritional strategy and subsequent catch-up growth in infancy (27) and in childhood (28) has further been shown to increase the risk of cardiometabolic and cardiovascular disease after low birth weight.

One of the most known study cohorts are those surviving and living through the "Dutch famine" between the years 1944-1945 when Nazi Germany occupied the western parts of the Netherlands and imposed an embargo on all transport and food. The famine raged from October in 1944 to May 1945, after which the German forces surrendered to the Allies (29,30). Follow-up studies on these cohorts have confirmed previous findings in line with the work by Barker et al, that factors in fetal life and infancy affects long-term morbidity and mortality (29,31).

These historical populations, surviving and living through the Depression and the great wars, have given us valuable insights into future consequences of early programming, otherwise only available through animal experiments. However, considering the continuous development of obstetric and neonatal care, these populations might not be representative of today's cohorts of fetuses born preterm with low birth weight and fetal growth restriction.

1.2 Pregnancy

The human pregnancy lasts for approximately 40 weeks, or 280 days. The first day of the last menstruation counts as day one and the following days and weeks are counted as "gestational week + days".

The developmental stages in pregnancy are categorized and subdivided in three trimesters. The 1st trimester 0 to 13+6 days, the 2nd trimester 14+0 to 27+6 days and the 3rd trimester ≥ 28+0 days (32).

Time of birth is further categorized based on gestational weeks

- Extremely preterm < 28+0
- Very preterm 28+0 to 31+6
- Preterm birth 32+0 to 36+6
- Term 37+0 – 41+6

1.2.1 Maternal and fetal surveillance during pregnancy

The maternal surveillance program in Sweden was implemented in the first part of the 20th century and has since evolved to a week-per-week program for risk stratification and management of the pregnant woman and the developing fetus. In Skåne, Sweden, the program is called "Basprogram för graviditet och eftervård i Region Skåne" and is subsidized and offered to all.

The routine program for a healthy woman includes serial visits to the midwife for assessment of weight, height, blood pressure, proteinuria, symphysis-fundus measurements, and later in pregnancy also examination of fetal movement, fetal palpation, and fetal sound. Blood is initially sampled for more thorough testing, including blood grouping, testing for sexually transmittable diseases, and anemia. An oral glucose tolerance test is performed in the beginning of the third trimester.

An early ultrasound is usually performed in the first trimester for dating of the pregnancy and for fetal diagnostics. A combination of ultrasound and blood sampling (KUB) is offered for fetal diagnostics. Pregnancy associated plasma protein-a (PAPP-A) and human chorionic gonadotropin (β-hCG) are sampled from maternal blood and the result is used together with variables from the fetal ultrasound and maternal parameters to calculate the risk for trisomy 21, 18 and 13. Noninvasive prenatal testing (NIPT) with maternal sampling of cell-free DNA (cfDNA) might also be offered in similar gestation and offers further certainty into potential chromosomal abnormalities.

The second ultrasound is performed in the second trimester. Fetal growth and size assessment, and further anatomical examination of the fetus and the placenta are performed.

For high-risk pregnancies, an individual plan for increased surveillance will be put in place together with the obstetrician and the midwife. A deviant symphysis-

fundus measure, non-normal findings on ultrasound, or other clinical signs of maternal or fetal stress, will cause referral to the responsible obstetrician.

1.2.2 Dating of pregnancy

The expected date of birth and thus gestational age can be calculated using Naegele's rule: adding 9 months and seven days to first day of the last menstruation (33). However, the preferred and most accurate method for dating the pregnancy is ultrasound at 8-14 weeks of gestation by measuring crown -rump length (CRL). The precision at this gestational age is ±7days (2SD), meaning that 95% of all fetuses will be born within two weeks from he calculated date. The risk of overestimating the gestational age, and thus underestimating fetal weight and growth is lessened with early ultrasound as compared to using Naegele's rule. An accurate estimation of gestational age is needed to assess whether the estimated fetal weight is appropriate for gestational age (AGA).

1.2.3 Fetal biometry

In addition to the planned ultrasound measurements, fetal growth is assessed by the midwife throughout the second half of the pregnancy using the symphysis- fundus measurement. In Sweden, a measure of more than two standard deviations below reference standard is used as cut off for referral to obstetric ultrasound while the 10th percentile is often used internationally. Also, a growth curve that deviates from its original shape might also cause a referral for more accurate diagnostics. These deviations are however seldom noticed before 30 gestational weeks and might thus rather be a sign of late onset FGR rather than early onset FGR, especially if no signs of growth restriction were observed during the second ultrasound. Using the internationally used reference cutoff, the 10th percentile, sensitivity is about 50% while the specificity is about 80% for finding SGA fetuses and both increase with increased gestational age (34,35). Using two standard deviations (as opposed to the 10th percentile) would thus improve specificity at the expense of sensitivity.

Fetal size and subsequently growth is determined by serial measurements of head circumference (HC) biparietal diameter (BPD), abdominal circumference or diameter (AC/AD) and femur diaphysis length (FL). Several formulae have been presented. In an international multicenter study, the INTERGROWTH-21st project sought to establish internationally valid estimations of fetal weight (36), however the estimations provided may be less accurate than the commonly used Hadlock formula (37), at least in early gestation (38). In Sweden, the Person and Weldner formula is used for estimation of fetal weight (39). A Swedish population with growth curves based on serial intrauterine measures of healthy fetuses who continued to grow until full term is used for reference (40). Internationally, a fetus with an estimated fetal weight between the 10th and 90th percentiles is termed AGA

while a fetus with an estimated fetal weight below the 10th percentile below the reference standard is termed small for gestational age (SGA). In Sweden, a cutoff of more than two standard deviations, or more than 22% below, the reference for gestational age is used to define SGA.

Birth weight is further categorized as:

- Extremely low birth weight (ELBW) < 1000g
- Very low birth weight (VLBW) weighing less than 1500g
- Low birth weight (LBW) weighing less than 2500g
- Macrosomia weighing > 4500g

1.2.4 Fetal growth restriction

1.2.4.1 Definitions

In this thesis, adolescents with early onset fetal growth restriction (FGR) are included. Definitions are in accordance with the Delphi Criteria, also adopted by The International Society of Ultrasound in Obstetrics and Gynecology (ISUOG) guidelines (Table 1.1) (3,41). However, as stated above, in Lund, Sweden, the cut off in birth weight deviation used for determining SGA is 2SD. The previously used terms "symmetric" and "asymmetric" FGR, indicating early and late onset FGR (42) should not be used, as the classification does not add information regarding neither etiology nor prognosis (43).

Fetal growth restriction, or 'intrauterine growth restriction (IUGR)', indicates that the fetus has not reached its genetic growth potential. These fetuses are not only smaller, as the constitutionally small SGA fetuses, they are small because of poor placental function, impairing fetal blood flow and thus nutrient and oxygen delivery (41). Risk stratification and correct definitions and diagnosis is important as the FGR fetus is at higher risk for adverse perinatal outcomes compared to the SGA fetus (41,44,45). Historically, and in many recent studies, birth weight deviation per se is used to define FGR. This will, however, overestimate the number of FGR fetuses and may also expose the mother and fetus in unnecessary surveillance and potentially harmful procedures.

Table 1.1 Definitions for early-and late-onset fetal growth restriction, based on Deplhi consensus criteria's.

Early fetal growth restriction	Late fetal growth restriction
Gestational age < 32w, in absence of congenital anomalities	Gestational age > 32w, in absence of congenital anomalities
AC/EFW < 3rd centile or umbilical artery absent end diastolic flow	AC/EFW < 3rd centile
Or	*Or 2/3 of the following*
1. AC/EFW < 10th centile *combined with*	1. AC/EFW < 10th centile
2. UtA-PI > 95th centile *and/or*	2. AC/EFW crossing centiles >2 quartiles on growth centiles
3. UA-PI >95th centile	3. CPR <5th centile or UA-PI >95th centile

AC=fetal abdominal circumeference, EFW=estimated fetal weight, UA=umbilical artery, UtA=Uterine artery, PI=pulsatile index, CPR=cerebrplacental ratio. Reproduced and adapted from Gordijn et al. (41).

1.2.4.2 Epidemiology and incidence

Between 115.000 and 120.000 children are born in Sweden each year. Of these, five to six percent are born preterm, while approximately one percent are born very preterm. Approximately four to five percent of babies are born with low birth weight (<2500g) (46). Both preterm birth and FGR are important causes of low birth weight, and both constitutes clinical problems, especially in combination. Early onset FGR constitutes 20-30 percent of all FGR cases. In low- and middle-income countries almost one in five is born SGA and approximately one in ten is born preterm, significantly contributing to infant mortality. Although infant mortality is high in these populations, the majority of these infants survive, increasing the global prevalence of individuals born preterm with birth weight deviation (1,47).

1.2.4.3 Etiology and risk factors for fetal growth restriction

The etiology of FGR is often not known but common risk factors for early onset FGR include preeclampsia or other maternal hypertensive disorders, multiple pregnancy, primipara, chronic diseases of the mother, malnutrition and socioeconomic factors and substance abuse, such as smoking (48,49). Risk factors for preterm birth includes multiple pregnancy, bacterial vaginosis, systemic diseases such as thyroid disease or diabetes and local or systemic inflammation. Other factors, such as stress, smoking and substance abuse and socioeconomic characteristics and race are also important risk factors (42).

Fetuses with genetic abnormalities were excluded in the current thesis but constitute a portion of fetuses presenting with early onset FGR. Further, prenatal infections, especially TORCH infections, is an important cause to early onset FGR, at least word wide. As all pregnant women in Sweden are screened for these diseases, the incidence of early onset FGR due to these infections is most probably low.

1.2.4.4 Pathophysiology of fetal growth restriction

Factors influencing uteroplacental blood flow also impact fetal circulation and can thus lead to fetal hypoxia and subsequent asphyxia. Increased resistance in the

maternal vasculature and in the fetoplacental circulation are common pathways towards early-onset FGR (50). Causes include poor placental implantation and a faulty trophoblast invasion, spiral artery abnormalities and maternal vasculopathy (51–54). Abnormal Doppler velocity measurements in the umbilical and uterine arteries are indicative of increased placental fetoplacental resistance and are prognostic of both preeclampsia and FGR, especially in high risk pregnancies (55). The uteroplacental vasculature is not subject to autonomic regulation and thus lacks innervation, making it susceptible to changes in systemic vascular pressure. The increased resistance in the uteroplacental vasculature, as observed with doppler ultrasound, is an effect of endothelial activation and vasoconstriction and impaired angiogenesis, where blood vessels within the terminal villi are abnormal and dysfunctional, increasing fetoplacental vascular resistance and limiting adequate oxygen and nutritional exchange across the villi (56). Trophoblast invasion of myometrial spiral arteries, as needed for low resistance uteroplacental blood flow, has been shown to be faulty in up to 75% of preeclamptic pregnancies, also showing high correlation to pathological doppler findings in the uterine artery (53). Further, in pregnancies with FGR fetuses, the placenta has been shown to be smaller, the villi having thicker walls and smaller lumens, indicative of a poor gaseous exchange and high vascular resistance, changes also correlating to pathological umbilical artery blood flow (52).

1.2.4.5 Diagnosis and management

Early onset FGR might not be detectable using symphysis fundus measurements. Instead, other factors, such as high blood pressure, proteinuria and maternal symptoms cause referral for an obstetric ultrasound. Figure 1.1 shows a flow chart for surveillance and clinical management of fetuses identified as being SGA and Table 1.1 shows the diagnostic criteria for early onset FGR. Diagnosis and management are based on biophysical examination, i.e., expected fetal weight ≥ 2SD (-22%) below the reference for gestational age, and doppler velocimetry in the umbilical artery, the uterine artery, ductus venosus and in the middle cerebral artery.

Fetoplacental Doppler velocimetry is central for the identification of uteroplacental insufficiency associated with FGR, allowing for differentiation of constitutionally small fetuses (SGA) from FGR (3). The blood flow patterns in the feto- placental circulation show characteristic changes with severity of FGR and has been shown to be predicative of future fetal demise. These measures are therefore used for grading of the severity and to decide when to induce labor (3,57).

In addition to doppler ultrasound, analysis of fetal heart rate, usually by cardiotocography (CTG), is used for identifying fetal distress and may, if pathological support the decision to induce labor (3). However, alterations in blood flow patterns might precede pathological CTG patterns and thus support active management in the absence of abnormal CTG findings.

Reduced and abnormal uterine artery blood flow has been observed in preeclampsia and in pregnancies with FGR fetuses (58–60) and the bilateral

notching (end-diastolic velocity increase) and increased pulsatility index (PI) (61) indicates up to a 50% reduction in uterine blood flow to the fetus (50,62). Pulsatility index is measured in the umbilical artery and is defined as peak velocity in systole minus the velocity in end-diastole divided by the average velocity. Uterine artery score further classifies the PI and the blood flow in the uterine artery. Ranging from 0-4, worsening uterine artery score is predictive of adverse perinatal outcomes such as 5 minute Apgar score <7, preterm delivery, NICU admission and birth weight deviation (63).

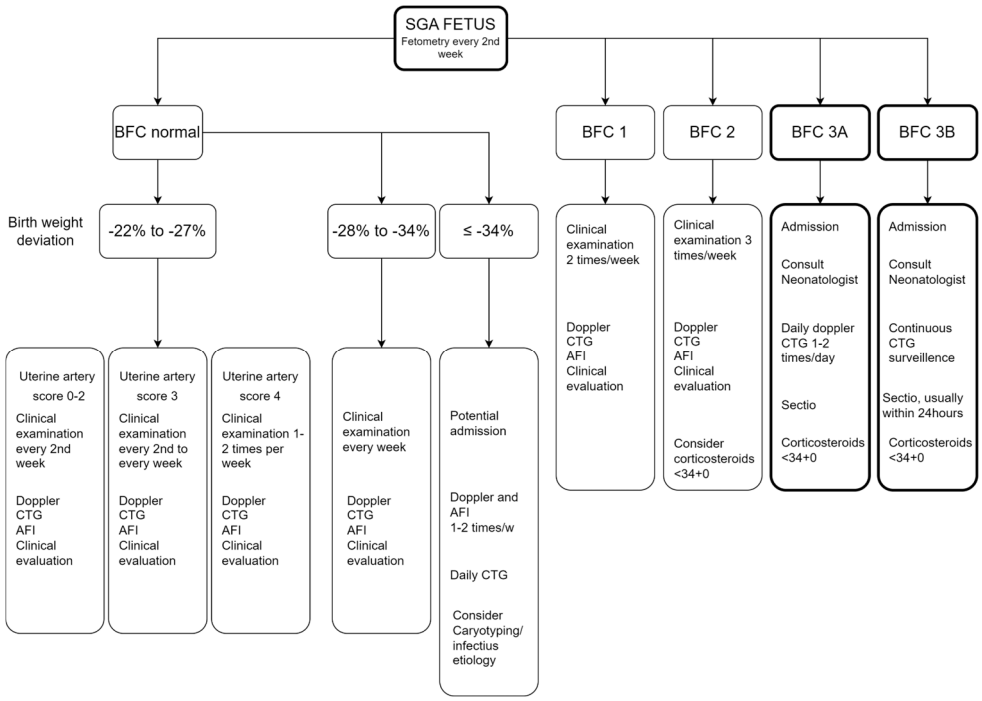

Figure 1.1 Flow chart for surveillence and clinical management of SGA fetuses.
The SGA fetus will undergo fetometry every other week. Management will differ depending weight deviation and blood flow findings. Sections with bold linings indicate the scheme for surveillence and clinical management of the current FGR study population. SGA=small for gestational age, BFC= blood flow class, CTG=cardiotocographi, AFI=amniotic fluid index.

Similarly, on the fetal side, umbilical arterial blood flow, assessed with doppler ultrasound, is lower and shows abnormal blood flow patterns in pregnancies with preeclampsia and/or FGR, changes that are prognostic of perinatal death (64–67). Pulsatility index decreases continuously in a healthy pregnancy but increases in a sequential and typical manner in fetuses with early onset FGR. The continuous measure pulsatility index (PI) is subdivided and categorized in to blood flow classes, from 1 to 3A and 3B, where 3A corresponds to arrested end-diastolic blood flow and 3B to reversed end-diastolic blood flow in the umbilical artery (Figure 1.2) (68).

Increasing PI and changes in the blood flow pattern show a progressive correlation to an increasing resistance and a functional loss of blood flow between the fetus and the placenta, resulting in an up to 70% loss of placental blood flow in the FGR fetus with reversed end diastolic blood flow in the umbilical artery (69,70).

The blood flow pattern in the middle cerebral artery (MCA) in FGR fetus displays an increased end-diastolic blood flow, indicative of a "brain-sparing effect" and has been shown to be of prognostic value in these fetuses (71). The cerebral-placental ratio indicates a redistribution of blood flow to the brain and is calculated as the middle cerebral artery PI divided by the umbilical artery PI. An abnormal cerebral-placental ratio is strongly associated with adverse perinatal outcome and improves risk prediction as compared to using umbilical artery assessment alone (72,73).

Further, abnormal blood flow in the ductus venosus is highly predicative of infant mortality and severe morbidity in FGR fetuses (74,75). In Lund, Sweden, ductus venosus blood flow assessment is, together with CTG and the above blood flow measurements, used to aid decision making for the induction of labor of the FGR fetus.

1.2.4.6 Perinatal mortality and morbidity

Survival has improved for infants born early in gestation (13,14) and intensive surveillance of SGA fetuses and active management of fetuses with early onset FGR limits and prevents fetal demise. Today, mortality after early onset FGR with active management is comparable to that of fetuses born AGA at similar gestational ages (76,77). Studies evaluating neonatal morbidity and mortality in SGA and FGR fetuses, show that gestational age seems to be the most important risk factor for adverse outcome (45). The susceptibility for adverse outcomes and neonatal morbidity will thus depend on gestational week at birth as well as the degree of placental insufficiency and subsequent growth restriction. Although mortality rates after both very and extremely preterm birth and FGR have decreased, adverse perinatal and neonatal outcomes remain as important challenges (13,76–78). The incidence of neonatal morbidity has not seen similar trends in reductions as that of infant mortality, and for some conditions, such as bronchopulmonary dysplasia (BPD) and respiratory distress syndrome (RDS) the incidence has rather increased (13,76).

The FGR infant has an increased risk for postnatal hypoglycemia. The increased risk is mainly due to depleted glycogen stores but may also be due to hypoxia leading to acidosis, and the metabolism shifting to a non-oxygen dependent and ineffective pathway for glucose utilization. Transient hypoglycemia is often present also in the term infant, although subclinical. The term infant utilizes energy substrates such as fatty acids and ketone bodies from fat storage in order to compensate for transient hypoglycemia, a process which is limited in the FGR infant.

Antenatal corticosteroid administration increases maturation of several organs, and lowers mortality and morbidity in the very preterm infant (8,9). The effect of

antenatal corticosteroid administration is especially effective in reducing the risk for RDS by increasing synthesis and release of surfactant (32). Respiratory distress syndrome is a major cause of morbidity and mortality in the very preterm infant, affecting up to ~90% of those born very preterm FGR (76). The cause of RDS is a lack of surfactant and subsequent high surface tension at the air-liquid interface within the alveoli, causing the lungs to collapse during respiration. RDS often presents immediately post-partum, and the incidence and severity are inversely related to gestational age. Surfactant is produced by Type II alveolar cells which are not fully differentiated and functional until 34 gestational weeks (79). To decrease the risk of relying on invasive mechanical ventilation, surfactant is usually administered via the INSURE method (intubation-surfactant-extubation) whereafter the infant, if possible, is ventilated via continuous positive airway pressure (CPAP), nasal intermittent positive pressure ventilation (NIPPV) or high flow nasal cannula (HFNC). If necessary, the infant will be intubated and ventilated using conventional mechanical ventilation or high frequency oscillatory ventilation (HFOV) (32).

Bronchopulmonary dysplasia is also a common lung disease in the preterm infant, indicated by the need for supplemental oxygen at an age corresponding to 36 gestational weeks. Risk factors are prolonged ventilatory support, RDS and early gestation. Immature lungs, pulmonary injury and a faulty healing process characterize the disease. The incidence of BPD is about 75% in infants born very preterm with FGR as compared to ~50% for very preterm AGA infants born at similar gestation (76). Postnatal corticosteroid administration is the major treatment strategy for BPD (80), used to reduce oxygen requirement and to facilitate extubation.

Intraventricular hemorrhage (IVH) and periventricular leukomalacia (PVL) are two complications of preterm birth. Blood vessels in the germinal matrix are delicate and sensitive to changes in blood pressure and blood flow, making them prone for rupture. Severe IVH affects 10-15 percent of the extremely preterm population. Intraventricular hemorrhage is sensitively detected as all infants below 30 gestational weeks undergo frequent ultrasound examinations of the brain to screen for IVH. Hypoxia and general inflammation contribute to injury to the white matter close to the ventricular system in the brain causing periventricular leukomalacia (PVL) with motor dysfunction, such as spastic diplegia and cognitive delay as sequele. The risk for both of these serious complications of the immature brain is reduced by antenatal corticosteroid administration (8,32).

Both septicemia and necrotizing enterocolitis (NEC) are common in the very preterm FGR infant. Septicemia may be due to maternal fetal spread or nosocomial infection and affects up to 45% of FGR infants born <30weeks of gestation as compared to ~35% in term AGA infants born at similar gestation (76). The cause of NEC is not fully understood but it is thought that an abnormal perfusion of the colon is a contributing factor. Inflammation of the wall of the colon with subsequent necrosis and perforation may be observed.

1.2.4.7 Active clinical care at the limit of viability

The first national consensus guideline on perinatal management at extremely early gestational age was issued in 2016 by the Swedish society of perinatal medicine and provided specific recommendations on centralization of care, antenatal corticosteroid treatment, mode of delivery and a neonatologist attending at the birth. These guidelines formulated that antenatal steroid treatment and active resuscitation of the newborn infant should be considered from 22+0 GW and are recommended from 23+0 GW. Existing national guidelines do not specify gestational-age related recommendations for the extremely preterm FGR fetus. The current guidelines from the American College of Obstetricians and Gynecologists and the Society for Maternal-Fetal Medicine (15), was updated in 2021 and corresponding recommendations state that antenatal steroid treatment and active resuscitation of the newborn infant should be considered from 22+0 GW and are recommended from 24+0 GW, also with no specific statement regarding FGR. In current clinical practice globally, delivery on fetal indication due to early onset FGR is very rarely considered before 24+0 GW.

1.2.4.8 Long term consequences of preterm birth and fetal growth restriction

Preterm birth and low birth weight are associated with long term adverse outcomes such as hypertension (5,81), ischemic heart disease and heart failure (82,83) and chronic kidney disease (4,84). These quite recent studies support the validity of the Barker hypothesis (17), indicating that both preterm birth in itself and the intrauterine environment affects future cardiovascular and renal disease (85). However, studies with the objective of relating FGR to health outcomes have used birthweight as a proxy for FGR (6,86,87), potentially mixing the constitutionally small infants with truly growth-restricted infants. Also, using the 10^{th} percentile (in comparison to the >2SD) as cutoff for significant birth weight deviation and for FGR diagnosis greatly increase the number of fetuses included.

For comparison between studies, gestational age, birth weight deviation and presence of FGR verified with doppler ultrasound, and year of birth (and thus clinical management) must be accounted for. The full impact of FGR on future morbidity after preterm birth is therefore difficult to assess. It is further not known which organ system driving the increased cardiovascular and renal risk in these populations. Biomarkers indicative of future cardiovascular and kidney disease have been observed from infancy to adulthood after preterm birth and FGR.

Cardiac changes after preterm birth and birth weight deviation have been observed from childhood to adulthood and preterm birth has even been proposed as its own cardiomyopathy (88). Increased blood pressure and increased arterial stiffness and RAAS activation are commonly observed after preterm birth (81,89–91). It might thus be hypothesized that long term cardiac structural changes after preterm birth, such as increased left ventricular mass (92,93), are mainly a result of increased afterload. However, studies also suggest impaired cardiac function in utero (94,95) and in infancy (96–98), indicative of hemodynamic and potentially

also structural changes in the preterm heart. These changes also seem to persist from infancy to pre adolescence (99).

Fetal growth restriction may further impair vascular growth (100) and several studies have shown that both preterm birth and low birth weight are associated with increased arterial stiffness (87,91,101). Arterial stiffness is a surrogate marker for the atherosclerotic process and is an independent risk factor for CVD and all-cause mortality in differing populations (102–104) including patients with known renal disease (105).

In line with the Barker hypothesis (17), Brenner et al. (106,107), suggested the "Hyperfiltration theory"; that a low nephron count at birth, as observed after preterm birth and FGR (108–110), increases the risk for future hypertension and progressive decline in renal function. Hyperfiltration of the remaining glomeruli as a response to increased hydrostatic pressures at the glomerular level is suggested to result in accelerated renal dysfunction (106,107). Increased birth weight correlate to increased number of glomeruli but shows an inverse relationship to glomerular size (110). Preterm birth and FGR independently impede renal development resulting in a low nephron count at birth (108,109,111,112). As both prematurity and low birth weight are associated with smaller kidney volumes (113–117), kidney volume quantification has been used as a proxy for nephron count in these populations. Both preterm birth (4,5,118) and a low nephron count (107,119,120) increases the risk for future renal functional decline and development of chronic kidney disease (CKD) (4,5,118) and several studies have shown associations between preterm birth and low birth weight with reduced kidney function (4,118,121). Biochemical markers of RAAS activation have been shown to be elevated in populations born preterm, with increases observed after preeclamptic pregnancies and after prenatal corticosteroid administration (89,122). Angiotensin II derived vasoconstriction and aldosterone derived plasma volume expansion due to increased absorption and decreased excretion of sodium and water will increase both preload and afterload and could thus be a contributing factor to the increased risk for CVD and CKD in the preterm population.

1.2.5 Preeclampsia

Gestational hypertension affects up to 10% of all pregnancies. About 3-7% of these will also develop preeclampsia (123,124), approximating 5000 women per year in Sweden. Gestational hypertension increases the risk of both preterm birth and FGR, with preeclampsia being the major contributor, causing ~15% of all preterm births and up to ~40% of all FGR cases (76). Both states increases perinatal maternal and fetal morbidity and mortality (125,126) as well as long term morbidity of both the offspring and the mother (123,127–129). Risk factors for preeclampsia includes chronic hypertension and kidney disease, blood clotting disorders, diabetes and obesity. Previous preeclampsia and a family history of preeclampsia are both strong risk factors (42).

Preeclampsia is defined as blood pressure ≥140/90 mmHg commencing after 20 gestational weeks with simultaneous proteinuria (>0.3g/24 hours or an albumin-creatinine ratio (ACR) > 30mg/mmol). Blood pressure should be verified on two separate occasions, at least 4-6 hours apart. Serial blood pressure measurements and urine analysis for proteinuria during pregnancy are thus an important screening tool for ensuing preeclampsia (130). In addition, uterine artery PI >90th percentile detects ~50% of women who will develop early preeclampsia and could also be used for screening (131). Preeclampsia is associated with endothelial activation and general inflammation affecting not only the uteroplacental circulation. A general vasoconstriction in the pregnant woman increases the peripheral resistance lowering glomerular filtration and also increases preload and afterload, inducing left ventricular hypertrophy and in some cases even heart failure (132). In severe cases of preeclampsia, liver function gets severely affected, with ensuing hemolysis, elevated liver enzymes and low platelets, collectively called the HELLP syndrome (133). Eclampsia describes the most sever complication, affecting central nervous system with general seizure and tonic-clonic seizures (134).

1.2.6 Human embryology

1.2.6.1 The placenta

During the first 36 hours after fertilization the egg undergoes multiple cleavage stages and at the 16-cell stage it becomes a mass of cells called morula, which shortly after gets fluid filled to form the blastocyst. By day 6-7 the blastocyst, now containing an inner cell layer of cytotrophoblasts and an outer layer of syncytiotrophoblats, attach to and penetrate the endometrium as a result of invasion and phagocytosis of endometrial stromal cells. A subset of trophoblasts, the extra villous trophoblasts, penetrates deeper into the endometrial stroma and invade the spiral arteries, creating lacunae, filled with maternal blood. These will eventually join to form the intervillous space, making up the area where the fetal and maternal blood exchanges nutrients and waste products.

By the 13th day after conception, cords of cytotrophoblasts called “Langhan’s cells” protrudes in the area of the intervillous space and forms the primary villi, eventually branching into secondary, and then subclasses of vascularized tertiary villi, in different developmental stages. These vessels will form the end-capillaries of the fetal circulation, i.e., from the umbilical arteries, towards the placenta. About 10-16 generations of branching of the villi occurs before complete maturation of the placenta. Gas exchange is taking place between the distal terminal villi and the intervillous space (50,135).

As the trophoblasts invade the endometrium a portion of the smooth muscle walls of the maternal spiral arterioles are destroyed making the vessels flaccid and dilated. During maternal systole this facilitates high flow at low pressures in the intervillous space. Blood flow in uterine artery at term is ~500-750 ml/min. The oxygen

saturation of maternal blood reaching the intervillous space is 90-100% and as fetal hemoglobin is at higher concentrations and has a higher affinity for oxygen than maternal blood, delivery of oxygen from the mother to the fetus will be favored. The umbilical cord contains two arteries who carries deoxygenated blood from the fetus to the placenta and one vein carrying oxygenated blood from the placenta to the fetus. The vessels grow in a spiral shape inside a polysaccharide structure called "Wharton's jelly". At term, the blood flow is approximately 350ml/min and the umbilical arterial blood pressure is about 70/60mmHg while the venous pressure is ~25mmHg (136).

1.2.6.2 Fetal circulation

The fetal circulation differs quite extensively from the adult circulation. Three shunts make up the main differences between the pre- and post-natal circulation. More than half of the venous return passes from the right to the left atrium through the *foramen ovale.* The rest enters the right chamber where it is pumped through the pulmonary artery. Most of this blood is redirected to the aorta through the *ductus arteriosus* and only a small portion, 8-10%, passes through the pulmonary vasculature. The two umbilical arteries branch from the internal iliac arteries and carry deoxygenated blood from the fetus via the umbilical cord to the placenta, finally branching out as capillaries in tertiary villi. The oxygenated blood from the placenta returns to the fetus via the umbilical vein which branches to the liver, and the portal vein, and about 50-60% reaches the inferior vena cava directly though the *ductus venosus*, and thus bypasses the liver, before returning back to the heart (32,137).

1.2.6.3 Cardiac development

The first heartbeat is initiated at gestational day 22 but the heart first becomes functional by the 4th gestational week. The heart goes through several developmental stages finally becoming the 4-chamber heart during the 7th week of gestation (137). Cardiomyocyte proliferation is active throughout fetal life but significantly tapers by the end of the third trimester, although with some proliferative function persisting also in infancy (138). Animal studies show cardiac myocyte hypertrophy and increased deposits in collagen and abnormal changes in cardiomyocyte nuclear numbers after preterm birth (139) and that the switch from intrauterine to extrauterine life induces cell cycle arrest, indicating arrested cardiomyocyte proliferation (140). Human studies of infants born preterm show an abruptly arrested cardiomyocyte proliferation and the initiation of a hypertrophic growth pattern of the myocytes (141). These findings together indicates that the premature change from intrauterine to infant life induces permanent changes in the myocardium, possibly relating to the increased CVD risk observed in those born preterm.

1.2.6.4 Vascular development

During early embryonic life groups of mesodermal cells differentiate to angioblasts, endothelial precursor cells, and joins to form rudimentary blood vessels. Vasculogenesis refers to the de novo synthetization of blood vessels from endothelial precursors whereas angiogenesis refers to the process of generating new vessels from existing ones. Following the initial vasculogenesis, capillaries will begin to form mostly though angiogenesis, which entails proteolysis of the surrounding extracellular matrix and the following proliferation, migration, and lumen formation of endothelial cells. Several signaling molecules are crucial for normal vascularization, and one of these factors, the vascular endothelial growth factor (VEGF) and its pathways have been shown to be essential for both vasculogenesis and angiogenesis (142). Vessels will remodel and/or regress according to the environment and the stress and need of blood flow in the area. The circulatory system remains plastic throughout life with examples in wound healing, the formation of collaterals and increased capillarization as an adaptation to exercise.

Studies suggest that preterm birth interrupts the normal elastin composition of the aorta, lessening the elastin component at birth (143). Elastin is the major component of the large elastic arteries, such as thoracic and abdominal aorta, and during normal aging, the elastin/collagen ratio decreases (144). An altered elastin composition in the vessel walls after preterm birth and impaired growth is suggested to increase arterial stiffness, blood pressure and cardiovascular disease (145).

1.2.6.5 Renal development

The urogenital system develops from the intermediate mesoderm forming the urogenital ridge on both sides of the aorta at the caudal parts of the embryo. The urogenital ridge develops into the pronephros, the mesonephros and the metanephros. The most cranial region, the pronephros, induces nearby intermediate mesoderm to form the mesonephric tubules which filtrates blood until the 8th week. The pronephros itself will regress in the 4th gestational week. The metanephros, will form the functional kidneys and appears in the 5th week of gestation becoming functional by the 12th week.

Functional glomeruli are first observed in the juxtaglomerular zone at 22 weeks of gestation. Glomerular filtration increases as the number of glomeruli and blood pressure increases. In the fetus, only about 2% of cardiac output is directed through the kidneys, to be compared with approximately 20% of the adult cardiac output. Although the placenta is responsible for excretion of waste products the larger portion of the amniotic fluid is produced from fetal excretion via the kidneys. The majority of nephrons are formed in the second half of the pregnancy with the completion of nephrogenesis by ~36 gestational weeks (108). The number of nephrons at birth are however highly individual, ranging from 200.000 to 2.000.000. Both preterm birth and fetal growth restriction hinders nephrogenesis and renal development and thus lowers nephron count at birth (108,109,119).

The preterm infant has fewer and less mature nephrons, lower mean arterial blood pressure and comparably higher renal vascular resistance, all factors contributing to lower glomerular filtration rate (GFR). Glomerular filtration rate is lower in the preterm infant compared to a term infant at similar gestation.

As the tubular function and the ability to concentrate urine are impaired there is an increased risk for hyponatremia and metabolic acidosis. Neonatal acute kidney injury is common (146) and both maternal and neonatal medication may impact neonatal and future renal function (147,148). Antenatal corticosteroid administration has been shown to accelerate renal maturation, increasing kidney function by increasing the number of developed glomeruli (149), potentially lessening the negative impact of preterm birth. In the case of fetuses with early onset FGR, where the mother often is inpatient and continuously surveilled with fetal Doppler velocimetry, most if not all mothers will receive prenatal corticosteroids before induction of delivery. Growth of the embryo causes the kidneys to ascend from the pelvis to the lumbar region. As they ascend, new vessels, renal arteries, are formed while the pelvic branches regress.

1.3 Cardiovascular anatomy and function

1.3.1 Cardiac anatomy

Figure 1.2 shows cardiac anatomy. The heart is situated in the pericardial cavity within the inferior mediastinum, a central compartment of the thoracic cavity. The pericardial sac encapsulates and protects the heart and restricts the outward movement of the myocardium during cardiac pumping. The heart consists of 4 chambers, the left and right atria, separated by the interatrial septum, and the left and the right ventricles, separated by the muscular interventricular septum. The fibrous atrioventricular plane separates the atria from the ventricles and contains the mitral valve enabling blood flow between the left atria to the left ventricle and the tricuspid valve enabling blood flow between the right atria to the right ventricle. The left ventricle connects to the systemic circulation via the aortic valve and the ascending aorta whereas the right ventricle connects to the pulmonary artery via the pulmonary valve. The left atria receive oxygenated blood from the pulmonary arteries and the right atria receives deoxygenated blood from the superior and inferior vena cava. The heart provides blood flow to two interconnected systems: the low resistance pulmonary circulation and the high resistance systemic circulation.

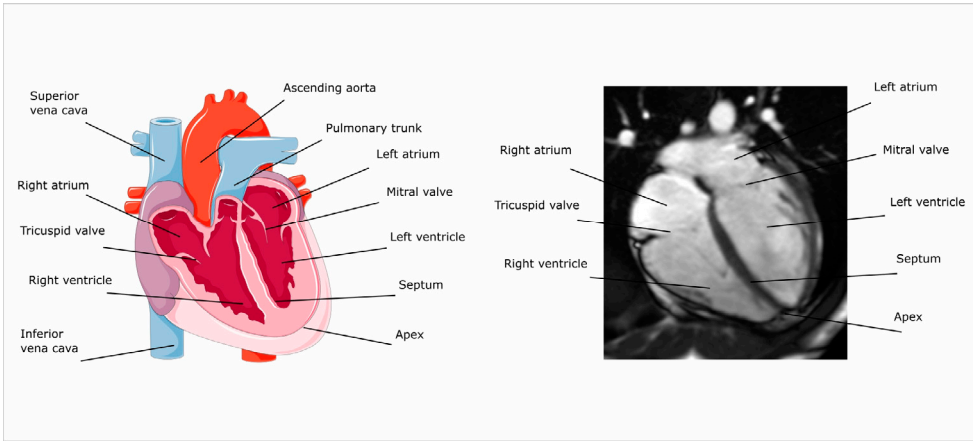

Figure 1.2 Cardiac anatomy.
A schematic image of the heart (**left**) and an MRI image (**right**) showing the " 4-chamber view " of the heart with the corresponding anatomical landmarks labled (if visible) as appropriate. *Labelling were added in the left figure from Servier Medical Art. Servier Medical Art by Servier is licensed under a Creative Commons Attribution 3.0 Unported License (https://creativecommons.org/licenses/by/3.0/).*

1.3.2 Cardiac pumping

The right atrium receives deoxygenated blood from the body via the inferior and superior vena cava and serves as a reservoir of blood for the right ventricle. During diastole i.e., ventricular filling, the right ventricular myocardium relaxes, lowering intraventricular pressure so that the tricuspid valve opens and blood flows from the atria to the ventricle, ending with a "atrial kick" where the atria contracts and forces blood to the ventricle. At the start of systole, the ventricles will contract, increasing intraventricular pressures and closing the tricuspid and mitral valves. When the intraventricular pressure surpasses the pulmonary and the systemic pressure, respectively, the pulmonary and aortic valves will open, and blood will be ejected.

It was long believed, and is, in many places, still taught, that the heart pumps blood in a squeezing pattern with the epicardial borders and the whole myocardium "contracting" inwards squeezing and pushing the blood upward to the aorta and pulmonary artery, respectively. Using MRI, Carlsson et al. (150–152), in a series of papers showed that ~60% of left ventricular stroke volume is generated by longitudinal motion, i.e., atrioventricular plane displacement (longitudinal contribution to stroke volume) and that approximately 40% is generated by an inward-squeezing motion by radial contraction (radial contribution to stroke volume). Notably, the other border of the heart only changes 5-8% throughout the cardiac cycle and the apex is almost fixed in place (152). The radial contribution to stroke volume is mainly due to the inward contraction and bulging of the myocardium, not an outer volume change of the entire heart as previously believed. For the right ventricle, the longitudinal contribution to stroke

volume is even higher, contributing to 80%, with 20% of the stroke volume generated by radial contraction (150).

1.3.3 Arterial structure and function

The arterial tree can be divided into elastic arteries such as the aorta and carotids, muscular arteries such as coronary arteries and renal arteries, and arterioles. The arterioles make up the last part of the arterial three and resides within tissues and organs before finally branching to capillaries through which diffusion of oxygen and carbon dioxide takes place. Arterial wall thickness decreases as vessels become smaller but the ratio of wall thickness to the lumen of the vessel increase, enabling the muscular arteries and arterioles to control blood flow and blood pressure. Three concentric layers makes up all arteries (Figure 1.3).

The inner cell layer of all blood vessels, the endothelium, consists of a single layer squamous epithelial cells attached to a basal membrane. This layer is referred to as the *tunica intima.* Initially believed to be only a physical barrier between the blood and the outer parts of the blood vessel, the endothelium has been shown to be central to vascular function but also to the atherosclerotic process.

The middle layer, *tunica media,* is separated to the intima by the internal elastic lamina and consists of smooth muscle cells in well-organized concentric layers. The thickness, the collagen, and elastin content of the *tunica media* differs across the arterial tree. The elastic arteries, e.g., the aorta, has a high degree of elastin fibers, enabling the vessel to distend during systole and to recoil in diastole, whereas muscular arteries and arterioles are less distensible and have a higher proportion of media-to-lumen ratio than the elastic arteries. Arterioles are the major contributors to changes in blood pressure and has via a larger intima media the ability to change vessel diameter, in turn altering blood flow and peripheral resistance.

The outermost layer, the *tunica adventitia*, is separated from media by the external elastic lamina and consists of connective tissue, mostly collagen, and the vasa vasorum, blood vessels supplying the blood vessel and nerve fibers (153).

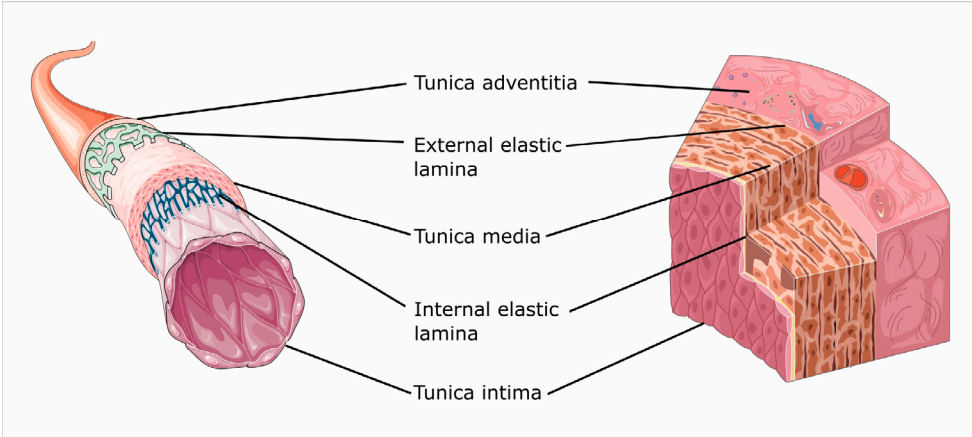

Figure 1.3 Arterial morphology.
Overview of the histology of the arterial wall. The innermost layer *tunica intima* consisting of endothelial cells, the *tunica media*, containing smooth muscle cells, elastin and collagen, and the *tunica adventitia,* containing the supportive vessels and nerves to supply the artery. *The figure was modified and put in a collage by using pictures from Servier Medical Art. Servier Medical Art by Servier is licensed under a Creative Commons Attribution 3.0 Unported License (https://creativecommons.org/licenses/by/3.0/).*

1.3.3.1 Arterial stiffness

Arterial stiffness increases with age and may be attributed to two separate processes in the arteries. The atherosclerotic process affecting mostly the tunica intima and a change in the elastic properties of the arteries, mainly affecting the tunica media.

The atherosclerotic process, although starting in childhood and adolescence (154,155), is strongly associated with high cholesterol, dyslipidemia, diabetes, smoking and hypertension. The process affects elastic and muscular arteries and starts off with endothelial dysfunction and a following cascade of endothelial activation, cell migration, proliferation and thickening of the intimal wall (153). Atherosclerotic disease may in turn lead to myocardial infarction, stroke and peripheral vascular disease and is the leading cause of death and disease world-wide and is and is thus an important target for disease prevention (156).

Elastin and collagen make up the elastic properties and strength the aorta. Changes in the relation between these connective fibers within the vessel walls, i.e., a lower elastin to collagen ratio, leads to lower compliance and increased arterial stiffness and increased afterload (157). The amount of both collagen and elastin increases with age but the ratio of elastin to collagen decrease, indicating stiffer blood vessels with age, a relationship that seems to be augmented in older patients with hypertension (158).

1.4 The kidney

1.4.1 Renal anatomy and physiology

Figure 1.4 shows an illustration of the kidneys with gross anatomy and histology visualized. The kidneys are situated retroperitoneally in the abdominal cavity, right next to the lumbar spine along the TH12- L3 vertebrae. The left kidney is usually more cranially located than the right. The renal fascia encapsulates the kidneys, with pararenal fat on the outer side and perirenal fat towards the fibrous renal capsule that protects the kidneys and surrounds the renal parenchymal tissue. The renal parenchymal tissue is in turn divided into renal cortex and medulla. The renal medulla is subdivided into medullary pyramids where the apex of the pyramid, the papilla, connects with the minor calyx, in turn forming the major calyx and the renal pelvis.

The renal arteries, on the left and right side, respectively, branch directly from the abdominal aorta. The renal artery first branches into segmental arteries, then into interlobular arteries which pass through the renal capsule and extend into the renal columns and eventually branch out into the afferent arterioles, leading blood towards the glomeruli.

The functional unit of the kidney is the nephron (Figure 1.4). The nephron is in turn comprised of the renal corpuscle, dispersed throughout the renal cortex, and the renal tubule and collecting duct, which passes through both cortex and medulla. The renal corpuscle encompasses the afferent arteriole and its tuft of glomerular capillaries responsible for filtering blood into the tubular system. Blood that circulates through the glomeruli without being filtered leaves the corpuscle in the efferent arteriole which travels along the tubular system and form peritubular capillaries and the vasa recta. Both are important for reabsorption and excretion along the tubular system. These blood vessels will thereafter form efferent venules and eventually renal veins, which connects to the inferior vena cava. The nephron is where filtration, reabsorption and potential excretion of solutes takes place. The kidneys play an integral role in homeostasis and the regulation of blood pressure, electrolyte balance, pH and is responsible for most of the excretion of waste products produced during metabolism. The amount of filtration is mainly governed by changes in blood pressure, both through direct sympathetic innervation and hormonal influence and also through local feedback systems within the kidney i.e., tubuloglomerular feedback. All of these systems affect the hydrostatic pressure within the glomeruli to manipulate the nephron to filtrate or to retain water.

1.4.2 Blood pressure regulation

The heart acts as a pump to create a pressure gradient to enable blood flow from the heart to the tissues. Besides tissue specific intrinsic feedback systems impacting blood flow, such as tissue autoregulation in muscles and the "Frank Starling mechanism" and the "Bainbridge effect" in the heart, blood pressure is mainly regulated by two systems, the sympathetic nervous system and the renin-angiotensin-aldosterone system (RAAS). These systems are highly interconnected, and both rely mostly on signals from baroreceptors, situated mainly in the carotid sinuses and the aortic arch. These receptors get activated depending on stretch of the arterial wall, i.e., high blood flow, high stretch and vice versa. The hormonal system responsible for long-term blood pressure regulation is the RAAS system and is regulated by the kidneys.

As part of keeping homeostasis, when blood pressure decreases, cells in the juxtaglomerular apparatus (Figure 1.4) cleaves circulating prorenin to renin, which in turn activates angiotensinogen, synthesized in the liver, to angiotensin I. Angiotensin I gets cleaved to angiotensin II by angiotensin-converting enzyme (ACE), a main drug target in cardiovascular disease, which are mostly expressed in endothelial cells in the lungs. Angiotensin II and its derivates stimulate the adrenal glands to produce and release aldosterone, which in turn increases sodium retention from the tubular system and from the intestines, and excretion of potassium, both resulting in increased extracellular volume. Angiotensin II is a strong vasoconstrictor, causing redistribution of blood flow and increased peripheral resistance. Plasma concentration of antidiuretic hormone is increased, causing increased thirst and retention of water by the increasing the numbers of aquaporins in the distal and cortical collecting tubules (153).

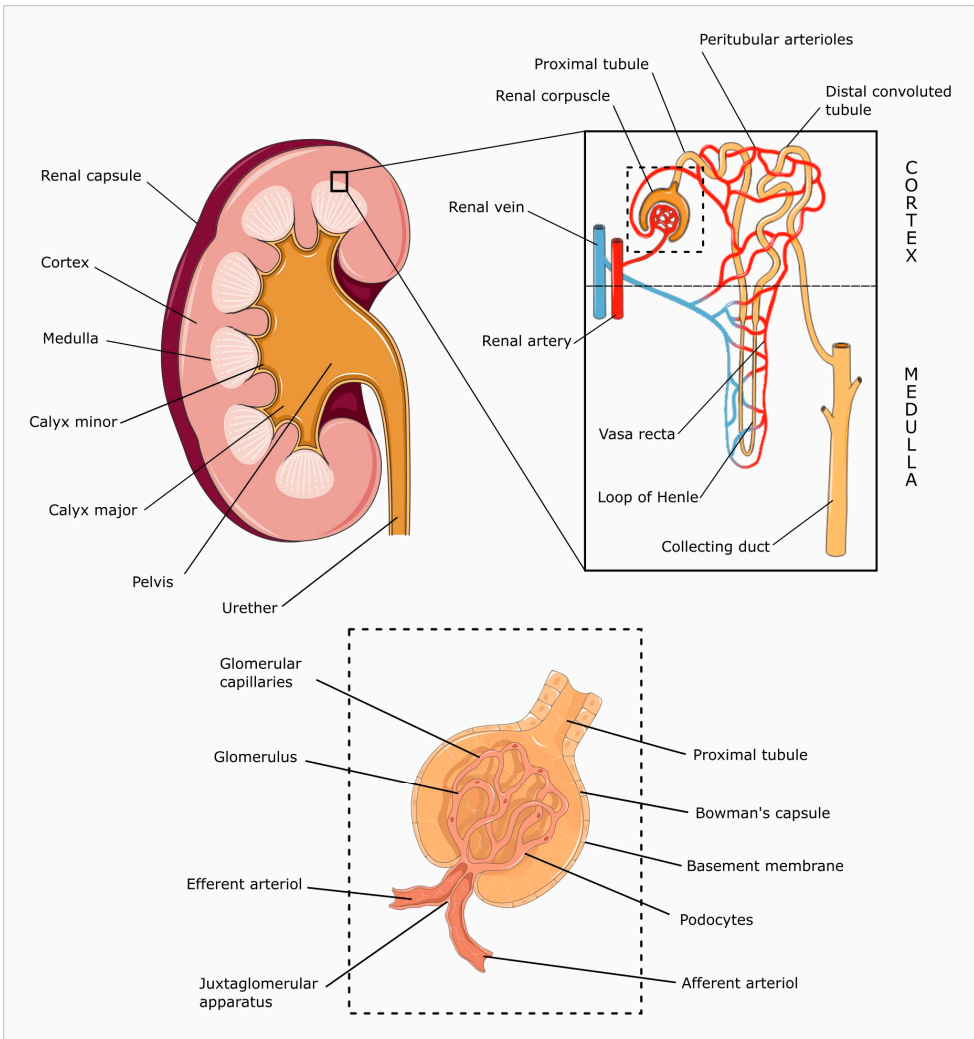

Figure 1.4 Renal anatomy and histology.
A schematic view of the right kidney (**upper left**) with gross anatomy outlined, a juxtaglomerular nephron (**upper right**) with blood supply and collecting duct outlined and the renal corpuscle (**lower image**) with histological landmarks outlined. *Figure modified and text added from Servier Medical Art by Servier, licensed under a Creative Commons Attribution 3.0 Unported License" (https://creativecommons.org/licenses/by/3.0/).*

1.4.3 Renal function

1.4.3.1 Measures of renal function

Renal function is measured though estimations of glomerular filtration rate (eGFR) based on plasma concentration of cystatin C and creatinine. Plasma concentration of these waste products of metabolism increases a result of a decrease in filtration

capacity and thus reflect kidney function. In this thesis the Caucasian, Asian, Pediatric and Adult (CAPA) equation based on Cystatin C was used for the assessment of $eGFR_{Cystatin\ C}$ (159) while the updated Schwartz method (160) was used for calculating $eGFR_{Creatinine}$. Clinically, at Skåne University Hospital, Lund, Sweden, only the CAPA method is used in children and adolescents (<18 years old). A wide range of glomerular filtration rates have been investigated using both creatinine and cystatin C, and especially the Cystatin C based method shows low bias versus reference standard iohexol plasma clearance (159,161).

1.4.3.2 Chronic kidney disease (CKD)

According to the KDIGO (Kidney Disease Improving Global Outcome) guidelines the definition for CKD diagnosis is "abnormalities of kidney structure or function persistent >3 months, with implications for health". Imaging thus has a place already in the diagnostic stage. The staging and prognosis of CKD is based on both eGFR (G1-5) and degree of albuminuria (A1-3) (162,163).

The global prevalence of chronic kidney disease (CKD) is between 11-13% and as hypertension and diabetes are the main drivers of the disease (164) the prevalence are set to increase (165,166). The cardiorenal syndrome describes the interplay between kidney function and cardiac function, where dysfunction of one organ negatively impacts the other (167,168). A decrease in kidney function and an increase in albumin creatinine ratio (ACR) is prognostic for heart failure and all-cause mortality and the combination of ACR with eGFR improves risk stratification, also in individuals without CKD (169–172).

The number of nephrons in the general population ranges from 200,000 to 2,000,000 per kidney (119,120,173). The average loss of nephrons due to aging in healthy population is ~6500 per year, potentially corresponding to half the nephrons lost from young adulthood to old age (70-75 years). This gradual loss of nephrons is proportional to the decline in GFR accompanied with aging (174) and it is believed that a low nephron count increases susceptibility for future renal insults and also increase the risk for hypertension and chronic kidney disease.

1.4.4 Hypertension

The prevalence of hypertension is high and increasing (165), affecting ~25% of men and women worldwide (175). Increased blood pressure is strongly associated with cardiovascular and renal morbidity and all-cause mortality and is one of the main targets for cardiovascular disease prevention (156,175). Office blood pressure measurements are often used for screening but ambulatory blood pressure measurements are reference standard and more sensitive to predict adverse outcomes (175–177). The definition and diagnosis of hypertension differs between children and adolescents as compared to adults, where cutoff values for the former group is based on percentiles of sex, height and age while the cutoff for the latter is

defined as ≥140/90 mmHg. In the most recent guidelines for children and adolescents, hypertension is defined as systolic and/or diastolic blood pressures ≥95th percentile for those under the age of 15, while ≥140/90 mmHg is used as a cutoff for boys and girls 16 years old and older (178). Sixteen year old's thus follows the same guidance as adults (175).

1.5 Imaging modalities

In this thesis, non-contrast-enhanced magnetic resonance imaging (MRI) is used for the assessment of cardiovascular and renal morphology and function. Magnetic resonance imaging and other modalities which could be used for non-invasive imaging of these organ systems are briefly discussed below.

1.5.1 Magnetic resonance imaging

Magnetic resonance imaging is the reference method for non-invasive quantification of blood flow and cardiovascular morphology and function (179). It is possible to acquire detailed images of any organ, creating a complete 3D image independent of orientation in space. There is thus no limit in either x, y, or z direction. Body habitus has practically no impact on field of view or image quality. The MRI technique is free of ionizing radiation and instead uses hydrogen atoms in the human body to generate images. These factors make MRI particularly suitable for imaging during pregnancy, in pediatric cohorts, in cohorts with planned successive imaging, such as patients with polycystic kidney disease, and for imaging in patients with renal failure who might get worsening renal function if contrast a is given.

1.5.1.1 MRI scanner

An MRI scanner consists of a strong superconducting magnet, three gradient coils, shim coils and radiofrequency (RF) coils. Magnetic resonance imaging uses radiofrequency waves to generate an image of the patient. The MRI scanner is enclosed in a copper-lined examination room, a "Faraday cage" with the purpose of keeping interfering radio signals outside. The main magnet generates a constant magnetic field called B_0 along the z axis. The strength of the magnetic field is measured in units of tesla (T) and is for cardiovascular imaging usually 1.5 or 3.0 T. For perspective, one tesla is equivalent to approximately 20.000 times the earth's magnetic field. The three gradient coils, in the x, y, and z directions, respectively, generate a superimposed magnetic field to that of B_0. The shim coil is used to homogenize the magnetic field in the specific area of interest, e.g., over the thorax for cardiac imaging or over the abdomen for renal imaging. The RF coils are used to add energy to the tissue by applying a radiofrequency field (B_1) while another RF coil is on the receiving end and collects the signal back from the tissue.

1.5.1.2 The MR signal

The source of the MRI signal used to generate images is the hydrogen nucleus, containing a single proton with a positive charge. The proton is spinning around its own axis creating a small magnetic field with a north and a south pole, practically creating a tiny bar magnet. These magnets are referred to as "spins". These spins are, without a strong magnetic field present, randomly oriented in space. When an external magnetic field, B_0, is applied, the spins will start to align and precess around the axis of B_0. Precessing protons can be seen as small vectors which cancel each other out in all directions except the z-axis, along B_0. The sum of these vectors, the net magnetization vector (M_0), is parallel to the magnetic field and is referred to as longitudinal magnetization. The precession frequency, or the Larmor frequency, ω_0, is defined by the Larmor equation:

$$\omega_0 = \gamma \cdot B_0$$

Where γ, the gyromagnetic ratio is a constant for the specific nuclear species e.g., 42.58 MHz/T for hydrogen. Hydrogen thus precesses at ~64MHz at 1.5T. The Larmor equation states that the precession frequency is proportional to the strength of the external magnetic field.

For the patient lying supine in the MRI scanner in the z direction, the net magnetization will be in the direction of the external magnetic field, B_0, and thus not measurable. By applying an external radiofrequency (RF) pulse along B_0, in the same frequency (on resonance) as the precessing protons, these protons can be manipulated to align to the new magnetic component, the B_1 field. As the protons align in the B1 direction they will now begin to precess around the z-axis in phase. The RF pulse thus excites the protons, causing flipping of the longitudinal magnetization to the x-y plane. The flip angle is dependent on the strength and duration of the RF pulse. As the RF pulse is terminated, the spins will return to their low-energy state, along B_0. The return of the longitudinal magnetization, from the x-y plane to the z-axis makes up the basis for the MRI contrast and signal. Two independent processes can describe the tissue specific relaxation towards the low energy state

T1, or longitudinal relaxation, is referred to as the spin-lattice relaxation and is due to transfer of energy from the spinning protons to the surrounding tissue. Simply put, T1 is a time constant for the recovery of the longitudinal magnetization along the z axis. T1 is defined as when the z magnetization has recovered 0.63 times its original value and is tissue specific. Difference in T1 relaxation time makes up the contrast between the tissues being imaged. By acquiring multiple images at different time-points after a single RF pulse, the tissue specific T1 curve can be reconstructed and the tissue specific T1 value be calculated.

T2, or transverse relaxion, refers to the spin-spin interactions between the spinning protons making them dephase and lose coherent transverse magnetization in the x-y plane. The rate of dephasing and decay of transverse magnetization is

governed by T2. When time equals T2 the transverse magnetization will have decayed to 0.37 of its original value. The T2 value is tissue specific, where tissues with high amounts of water have a long T2. The combination of spin-spin interactions (T2) and dephasing as a result of field inhomogeneities is defined as T2*. It is possible to acquire serial images at different times after an RF pulse to reconstruct and calculate the T2 or T2*(180).

1.5.1.3 The MR image

To acquire an image needed for visualization of the organ of choice, the coordinates in the x, y and z directions need to be defined. Gradient coils are used to encode spatial information. The signals detected by the scanner are gathered in what's called k-space. k-space can be viewed as a coordinate system holding spatial information about the imaged tissue. Each coordinate in k-space contains information about all the pixels in the image. In order to get an MR image, the radiofrequency signal from the chosen tissue, now stored in k-space must be transformed using the mathematical Fourier transform.

1.5.1.4 Limitations and potential drawbacks

Motion during image acquisition will distort the image, giving motion artefacts, possibly lessening diagnostic quality. Motion artefacts due to breathing can be avoided by using breath-hold sequences, with repeated image acquisition at a similar breathing depth. A similar technique is used during gated image acquisition, where imaging is coupled to diaphragmatic movement. Artefacts due to cardiac motion can be avoided by ECG-gating where imaging is synchronized to the patients ECG. Images acquired with ECG gating can be sorted and compiled as a "movie" of one heartbeat, called "cine" imaging.

Potential limitations with the MRI method are mostly due to patient specifics. Some objects constitute an absolute contraindication for scanning while other, non-magnetic objects, constitute a partial contraindication, potentially distorting the image. Atrial fibrillation makes it difficult to properly synchronize and then sort the images and is another limitation. Claustrophobia is a potential patient specific factor usually overcome by administering sedatives and could be completely overcome by putting the patient under general anesthesia.

Other "limitations" often discussed when comparing MRI to echocardiography are the lack of availability, both of MRI scanners and staff, the cost and the time allotted for the examination. One could however argue that these examples are rather a resource problem and not limitations in the method per se.

1.5.2 Computed Tomography

Computed tomography (CT) uses rapidly rotating X-ray tubes to image and visualize the tissues as a highly detailed 3D image. The penetration of the X-rays in

the tissue, or attenuation, is proportional to the density of the tissue. The radio density of the tissues is measured in Hounsfield units (HU). To calculate the attenuation coefficient for each tissue within the sample, air (~-1000 HU) and distilled water at standard temperature and pressure (0 HU) are used for standardization. The attenuation for the tissue within the image is depicted in greyscale. Tissues with high density has positive values and appear white while tissues with low densities have negative values and appears dark. The range of HU between tissues are ~-1000 HU (air) to ~+2000 HU for dense bone (181).

1.5.3 Ultrasound

Ultrasound represents the region of the sound spectrum with frequencies >20kHz. Medical ultrasound employs frequencies between 1 and 20 megahertz to create sonographic images of anatomical structures. Ultrasound transducers, also referred to as probes, are compiled of piezoelectrical crystals in which electrical energy, by inducing vibrations in the crystals, is transformed to ultrasound and vice versa. The transducer thus acts as both a sender and receiver of signals.

The acoustic impedance is a physical property of the tissue and describes the interaction of ultrasound with tissue. The acoustic impendence depends on tissue density and the velocity of the sound wave. As the sound wave propagates through tissues with different densities, some of the energy will be reflected. The higher the acoustic impedance between different tissues, the stronger the reflected wave. The amplitude of the sinusoidal sound wave is a measure of the strength of the sound and is measured in decibel. When reflective ultrasonic waves reach the transducer, electrical impulses in proportion to the amplitude of the ultrasonic wave are created. As ultrasonic waves propagate with near constant speed of around 1500 m/s in tissue, the depth of where the reflections originated can be calculated. The reduction in amplitude and intensity of the ultrasonic wave as it propagates through tissues (attenuation) is mainly due to refraction, reflection and absorption. By decreasing the frequency, signal penetration can be increased, however at the expense of spatial resolution, in ultrasound divided into axial and lateral resolution (182).

1.5.3.1 Doppler ultrasound

When ultrasound reflects against moving objects the frequency will change in proportion to the velocity of the moving object. If the object, e.g., erythrocytes, moves towards the transducer, the reflected frequency will be higher than the transmitted frequency and vice versa. When the angle between the transducer and the measured moving object increases, the frequency and the speed of the moving object will be underestimated. When employing Doppler, it is thus important to quantify velocities placing a sample volume parallel to blood flow, with as small a deviation with respect to the blood vessel as possible.

There are two types of Doppler techniques at use, continuous wave (CW) Doppler and pulsed wave (PW) Doppler. Continuous wave Doppler continuously transmit and receive ultrasound signals, and plots this as a velocity waveform on the screen. Velocity of blood flow towards the transducer is displayed above the baseline while flow from the transducer is displayed below the baseline. This technique is especially good for assessing high blood flow velocities and for detecting the highest velocity within the field of view. An example of when to use CW Doppler is to estimate blood flow velocities across stenotic valves, or in the setting of regurgitation. As no pulses are emitted, it is not possible to assess velocity at a specific depth using CW Doppler. This is however possible using PW Doppler in which short bursts of ultrasound are transmitted and received before the following bursts are sent out. The method enables quantification of velocities within a specific area, at a specific depth called "sample volume". If the velocity measured exceeds the maximum pulse interval, the phase shift measured will be made on wrong assumptions, creating aliasing artefacts, limiting the use of this technique at high flow velocities.

Color Doppler uses a pulsed wave technique where several pulses of ultrasound continuously are transmitted to the tissue. This enables the calculation and color coding of the direction and velocity of flow in the respective sample volume. The area of interest is divided into a multitude of sample volumes, which together creates a "map" of differing velocities and blood flow directions within the field. These are visualized as a color map overlaying the anatomical 2D image of the area at hand. Blood flow away from the transducer is depicted as cold colors and blood flow towards the transducer is often depicted as warm colors (182).

1.5.4 Cardiovascular imaging

Magnetic resonance imaging, Computed Tomography (CT) and Echocardiography are the main modalities of choice for assessment of cardiac morphology and function. Table 1.2 shows a simplified comparison of the pros and cons between these cardiac imaging modalities in relation to relevant measures included in the current thesis.

Table 1.2. Comparison of cardiac imaging techniques

	Magnetic resonance imaging	Computed tomography	Echocardiography
Cardiac morphology	+++	+++	++
Cardiac function	+++	++	++
Blood flow	+++	-	+++
Aortic morphology	+++	+++	+
Spatial resolution	++	+++	+
Accuracy/precision	+++	+++	++
Typical temporal resolution	++	+(+)	+++
Ionizing radiation	No	Yes	No
Contrast agents	Yes/No	Yes/No	Yes/No
Major limitations	Incompatible devices, costs and availability.	Ionizing radiation, availability	Operator dependence, acoustic window

Grading +++= excellent, ++=good, +=ok, - = non existing.

1.5.4.1 Cardiovascular magnetic resonance imaging

Magnetic resonance imaging is the gold standard for the assessment of cardiac volumes and, cardiac function and blood flow (179,183). The method enables imaging of the entire heart including accurate measurements of atrial and ventricular volumes as well as total heart volume. In this thesis, cardiac volumes, and measures of cardiac pumping as well as blood flow in the thoracic and abdominal aorta were assessed using non-contrast enhanced MRI.

Stroke volume can either be calculated using anatomical images and comparing the end-diastolic and end-systolic volumes or by using phase contrast imaging of the ascending aorta. The ejected stroke volume is a direct result of both longitudinal and radial pumping which both can be assessed using MRI. Longitudinal function can be measured as atrioventricular plane displacement (AVPD) whereas longitudinal contribution to stroke volume is calculated as the portion of the ejected stroke blood volume that is derived from the AVPD. By calculating the inward movement of the myocardial borders during the cardiac cycle the radial function and radial contribution to stroke volume can be calculated (150,152,184). The AVPD corresponds to, but is not equal, to the echocardiographic measures mitral annular plane systolic excursion (MAPSE) for the left ventricle and tricuspid annular plane systolic excursion (TAPSE) for the right ventricle and show low variability between the measurements (185).

Pulse wave velocity and distensibility of the thoracic aorta are both used as proxies for arterial stiffness and can be assessed using MRI, showing high agreement with invasive measurements (186).

Further, MRI decreases the number of subjects needed to detect clinically relevant changes in left ventricular volumes (~10ml), left ventricular mass (~10g) and ejection fraction (~3%), up to 95% (50–95%) as compared to 2D echocardiography (187,188). Reproducibility of RV volume and function show similar reproducibility as left ventricular quantification (189).

1.5.4.2 Cardiac computed tomography (CT)

The clinical question at hand dictates the choice of modality, cardiac CT versus cardiac MRI, but as both modalities have wide and overlapping capabilities (179,190), the choice also depends on availability and clinical praxis. Cardiac CT can be used for a wide range of clinical indications (191,192). Two big draw backs in comparison with MRI is the inability to measure blood flow and the ionizing radiation.

Because of the high spatial resolution, cardiac CT is the preferred choice for the assessment of vessel morphology and coronary artery disease (190). Cardiac CT can also provide "Coronary calcium score" which is one of the strongest predictors of cardiovascular risk, also in a asymptomatic population (193). Further, CT angiography (CTA) is gold standard for non-invasive assessment and visualization of the presence of atherosclerotic plaques in the coronary arteries. Visualization of coronary arteries can be performed using MRI but is not clinical standard and the sensitivity for plaque identification is lower than for CTA (194).

1.5.4.3 Echocardiography

Ultrasound cardiography, or Echocardiography, is today most often the first line of cardiac imaging for diagnosis and management of patients with suspected or manifest heart disease.

The first known experiment utilizing ultrasonic waves was conducted in the 1880s (195), but it wasn't until 1954 the first paper on cardiac applications was published (196). In the paper, Swedish cardiologist Inge Edler and physicist Carl Helmuth Hertz were able to visualize the cardiac wall motion in situ, using what's now known as "motion mode" or "M-mode". M-mode is still widely utilized given its high temporal resolution (~1000 frames per second) which permits accurate visualization of fast-moving structures such as heart valves or the vessel wall. In comparison, the temporal resolution of a 2D echocardiographic image is around 50 frames per second, and standard MRI is around 30 frames per second (197). AVPD for the right ventricle free wall can be measured by tracking the annular motion of the tricuspid valve during systole or TAPSE and for the left ventricle using the mitral annular motion or MAPSE.

The standard echocardiographic examination uses transthoracic imaging (TTE) but probes for transesophageal (TEE), intravascular and intracardiac images are also available.

The method is widely available, low-cost and very versatile, with the possibility to image virtually any structure and blood flow within the field of view. Echocardiography, however, is an operator dependent diagnostic evaluation that is limited by narrow acoustic windows, high interobserver variability, and suboptimal image resolution in patients with obesity or lung disease. Air in the lungs distorts the sound waves limiting the quality of the images and as the ultrasonic waves are directly reflected against the costae, the intercostal spaces for cardiac imaging. When the ultrasonic wave reaches a structure of high density, such as bone or a

calcification, all energy is reflected, creating a shadow behind the structure. It is thus not possible to completely visualize the right ventricle and atria.

1.5.5 Renal imaging

Several conditions affecting renal function, either acutely or chronically, will eventually show also as alterations in renal macrostructure. Clinically, imaging of the kidneys is performed using computed tomography (CT) or ultrasound. Computed tomography is accurate in measuring renal parenchymal volumes (198–200), but uses radiation and might not be generally available. The risk/ benefit of serial assessment or imaging in pediatric populations using imaging with radiation should be carefully considered.

Ultrasound is on the other hand widely available and is thus a low-cost non-invasive imaging alternative with no radiation or potential harm to the patient. However, the acoustic window and field of view is limited, especially in adults and in overweight patients. As the entirety of the kidneys cannot be visualized using ultrasound, several proxies for renal morphology and volymes have been used. Examples include renal width at different locations, length and cortical or pyramidal thickness (201–203). Repeated measurements of renal length with ultrasound in children up to adolescent age show intra- and interobserver variability comparable with the expected annual increase in renal length (202). This indicates that serial measurements of renal length should not be performed within at least 12 months in these cohorts, and these data were from experienced observers. Repeatability and observer variability are thus an issue with ultrasound (204,205). Renal volumes are usually calculated by measuring the three axes of the kidney assuming an ellipsoid shape. The ellipsoid method (renal volume = length x width x thickness x $\pi/6$) is the most commonly used method for the assessment of kidney volumes (206). However, although commonly used, several studies have shown that this method underestimates total renal volume by an average of 24%, independent on whether measurements were done using ultrasound or MRI (204,206).

Renal volumes may instead be quantified using non- contrast enhanced MRI, showing low variability and low observer variability for total kidney and cortical volume (206–208). In addition to volume measurements, blood flow and tissue characteristics using T1 and T2* mapping can be performed in the same session, possibly adding prognostic information (209–211).

2 Aims

The overall aim of this thesis was to investigate to what extent very preterm birth due to early onset fetal growth restriction impact the heart, the vasculature, and the kidneys in adolescence. The thesis further sought to investigate whether fetal growth restriction exacerbates the organ-specific effects of very preterm birth.

The specific aims were

Study I
To validate a non-contrast enhanced MRI method for the quantification of renal cortical and medullary volumes.

Study II
To validate MRI methods for quantification of thoracic pulse wave velocity in neonates and in adolescents.

Study III
To investigate to what extent very preterm birth and early onset fetal growth restriction impact blood pressure and arterial stiffness in adolescence, and to investigate whether fetal growth restriction exacerbates the effect of very preterm birth on these parameters.

Study IV
To investigate to what extent very preterm birth and early onset fetal growth restriction impact cardiac volumes and function in adolescence, and to investigate whether fetal growth restriction exacerbates the effect of very preterm birth on these parameters.

Study V
To investigate to what extent very preterm birth and early onset fetal growth restriction impact kidney structure and function in adolescence, and to investigate whether fetal growth restriction exacerbates the effect of very preterm birth on these parameters.

3 Methods and material

3.1 Study population

3.1.1 Ethical permits

Studies were performed in accordance with the declaration of Helsinki (212) and all participants or their guardians when appropriate, provided written informed consent before participation.

3.1.1.1 Adolescents

The Regional Ethical Review board in Lund, Sweden, approved *Studies I–V* (DNR 2013/244) and (DNR 2014/431). The application is a follow-up to the original application titled "Uppföljningsundersökning av kärl-och nervutveckling samt glykosreglering hos barn och unga vuxna med tillväxthämning och hotande asfyxi under fosterperioden" (DNR 197/2006), with inclusion in childhood and retrospective analysis of perinatal outcome in the three groups.

One healthy adolescent volunteer was included in *Study II* for method development (DNR 2019-01966, original ethics application: 741/2004).

3.1.1.2 Neonates

Neonates who underwent CMR were included in *Study II* with ethical permits "2018/172" and "2009/616".

3.1.1.3 Animals

The experimental part of *Study I* was performed in agreement with the guide for the care and use of Laboratory Animals (213) and was approved by the Swedish Board of Agriculture and the Malmö/Lund Ethics Committee on Animal Testing; DNR M94-14 and 5.8.18-05681/2017, respectively.

3.1.2 Inclusion

3.1.2.1 Adolescents

Inclusion for this thesis was conducted at Skåne University Hospital, Lund, Sweden, between 2014-2019. The study population was born between 1998-2004 at Skåne university Hospital, Lund Sweden and were for this thesis prospectively included for follow-up in adolescence (Figure 3.1).

The index group consisted of fetuses with early onset fetal growth restriction, defined in line with current guidelines (3,41). Fetuses had a birth weight > 2 standard deviations below the Swedish reference standard (40), absent or reversed end-diastolic blood flow in the umbilical artery (blood flow class II-III) assessed with Doppler velocimetry, and were actively delivered on fetal indication before 30 gestational weeks. Forty-two live born fetuses with early onset fetal growth restriction (*preterm FGR*) were delivered and included in a retrospective 2 year outcome study (16). A control group consisting of all children born in the same period (1998-2004) of all live born infants (n =371) admitted to the neonatal intensive care unit in Lund during this time period was included. A subgroup (n =42) of this control group was matched to the index group for sex, gestational age at birth and year of birth (*preterm AGA*). The causes for premature birth in this group were ablatio placentae, preterm premature rupture of the membranes chorioamnionitis and being delivered as the healthy same sex twin to an individual in the preterm FGR group. Thirty-four individuals in the preterm FGR group were available for follow-up in childhood and were included together with the matched pair from the preterm AGA group. A third control group, born vaginally after a healthy pregnancy, with birth weight appropriate for gestational age, born at the same time-period were included (*term AGA*). Studies on 2-year morbidity and mortality outcomes and follow up studies in childhood including neurocognitive, pulmonary and cardiovascular outcome have previously been reported (16,214–216).

All participants (n = 102) that were studied in childhood were asked to participate in this follow-up study in adolescence.

3.1.2.2 Inclusion flow chart

Figure 3.1 shows a flow chart of the inclusion of adolescents included in *Studies I – V*. Of those infants presenting with fetal growth restriction at Skåne University Hospital, Lund, Sweden, during 1998-2004, four died in utero and a total of 42 live born fetuses were admitted to the NICU, of these, four died during the admission. Of all fetuses born <30 weeks of gestation during the same time-period 24 were stillborn and four died during delivery.

At prospective inclusion in childhood, four of the 38 children in the preterm FGR group choose not to participate, finalizing the number of children born preterm due to FGR available for follow up, to 34 individuals, with a total of 102 children in the three matched groups.

At prospective inclusion in adolescence, two individuals in the preterm FGR group and one in the preterm AGA group were unreachable. Eight individuals in the preterm FGR group, six in the preterm AGA group and five in the term AGA group choose not to participate. Although initially accepting to participate several participants chose to abort examinations and one individual in the preterm FGR group were 19 years old at the time of MRI examination.

3.1.2.3 Study overlap

Table 3.1 shows overlap in study participants between studies. *Study I* included study participants born term AGA (i.e., healthy controls). *Study II* included all participants who underwent MRI from the three groups. *Study III* included all participants who underwent either MRI or 24-hour ABPM. *Study IV-V* included all participants who underwent MRI examination, excluding the individual who were 19 years old at MRI examination.

Table 3.1. Overlap in study participants between studies included in the thesis.

	Study I	*Study II*	*Study III*	*Study IV*	*Study V*
Study I	-	24	24	24	24
Study II	24	-	71	70	70
Study III	24	71	-	70	70
Study IV	24	70	70	-	70
Study V	24	70	70	70	-

3.1.2.4 Neonates

Study II included 15 neonates (14 (6 – 45 days old) born at Skåne University Hospital, Lund, Sweden, between November 2018 and October 2020 with surgically corrected aortic coarctation but without associated major congenital heart disease. Neonates underwent CMR 5 days [IQR 4–8] after surgery.

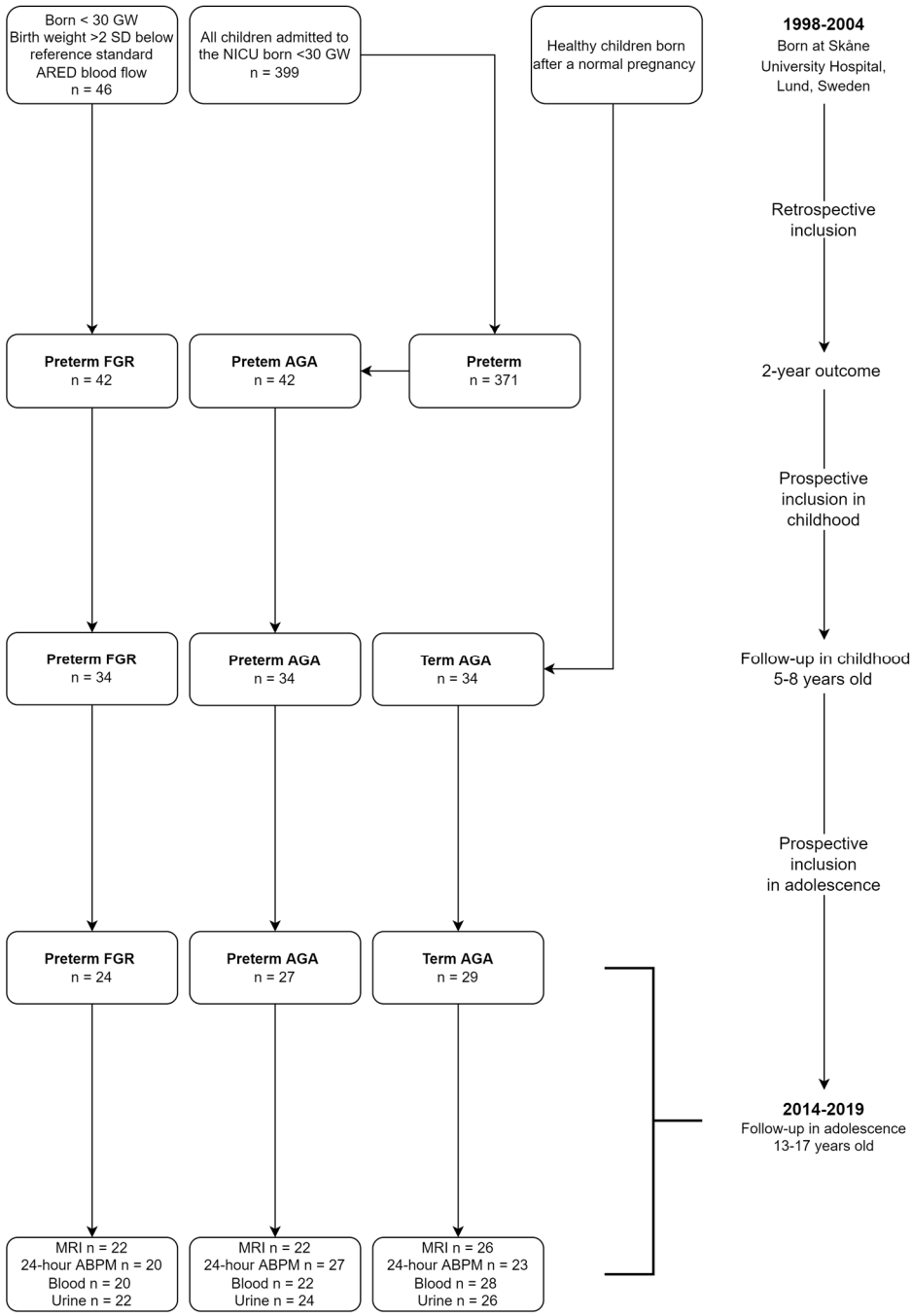

Figure 3.1 Inclusion flow chart.

GW=gestational weeks, SD=standard deviations, ARED=arrested or reversed blood flow in the umbilical artery, NICU=neonatal intensive care unit, FGR=fetal growth restriction, AGA=birth weight appropriate för gestational age, MRI=Magnetic Resonance Imaging, 24-hour ABPM=24-hour ambulatory blood pressure measurements.

3.1.2.5 Animals

Six pigs (weight 44 – 47kg) were included for validation of renal cortical and medullary volume quantification. Animals were premedicated with Ketamine 15 mg/kg (Ketaminol, Intervet, Danderyd, Sweden) and Midazolam 0.5 mg/kg intramuscularly (Dormicum, Roche AB, Stockholm, Sweden). Animals were held fasting overnight with free access to water. General anesthesia was induced with Propofol 20 mg/kg (Propofol Sandoz AS, Copenhagen, Denmark) and maintained using Isoflurane (Isoflurane, Baxter Medical AB, Kista, Sweden) using a disposable administration system (Anaconda, Sedana Medical AB, Uppsala, Sweden). Animals were intubated and mechanically ventilated using volume-controlled mode regulated towards a pCO2 of 5–6 kPa. A 5% glucose infusion, 0.9% NaCl infusion, norepinephrine, and fentanyl were administered as needed. Following MRI, still under general anesthesia, the animals were euthanized with a rapid infusion of potassium chloride, whereafter the renal vessels and ureter were clamped, and kidneys excised. Cortical and medullary tissue were dissected and quantified separately using the reference standard water displacement method (100 mL volumetric flask with 2 mL increments, tolerance ±2.0 mL at 20°C) according to Archimedes' principle.

3.2 Magnetic resonance imaging

3.2.1 MR image acquisition

Animals, neonates, and adolescents underwent non-contrast-enhanced MRI and were imaged in supine position. Neonates were positioned in a vacuum infant immobilizer. In all five studies, a 1.5T Philips Achieva, (Best, the Netherlands) or a 1.5T Magnetom Aera (Siemens Healthineers, Erlangen, Germany) with a 32-channel coil (Philips) or an 18-channel and spine coil combination (Siemens) was used. For neonates, a small flexible coil was chosen. For adolescents, cardiac and kidney images were acquired during the same session. Imaging of kidney volumes were not performed in neonates.

Neonates were imaged using "feed and sleep" (217) and more detailed information about the management of the neonates is described by Sjöberg et al. (218).

3.2.1.1 Kidney volumes

Fast low angle shot (FLASH) MR images were acquired as transaxial stacks during breath hold for humans and with free breathing for animals. Typical parameters were 1.3 x 1.3 x 6 mm, TR/TE = 152/5.57 ms, FA = 80°, bandwidth = 270 Hz/px, GRAPPA = 2 with 24 reference lines, water excitation and 50 mm saturation bands head/foot with gap 10 mm.

3.2.1.2 Renal T1 and T2 imaging*

Renal coronal T1 maps were based on a modified Look-Locker inversion recovery (MOLLI) sequence using a 5(3)3 scheme, with typical parameters: 1.4 x 1.4 x 8 mm, TR/TE = 281/1.12 ms, FA = 35°. Renal coronal T2* maps were based on a multi-echo gradient recalled echo sequence using 10 echoes with first echo 1.07 ms and step 1.36ms (i.e., range 3–13.3 ms). Typical parameters were 3.1 x 3.1 x 8 mm, TR = 200 ms, FA = 20°.

3.2.1.3 Flow measurements

For quantitative flow measurements, a 2D phase-contrast gradient recalled echo sequence with retrospective ECG gating were used. Typical image parameters for flow measurements in the renal arteries were TR/TE = 9.84/2.67 ms; flip angle = 20°; in-plane resolution 1.5 x 1.5 x 5 mm and VENC = 100 cm/s.

For adolescents, typical image parameters for the flow measurements in the ascending aorta and descending aorta at diaphragm level were TR/TE = 9.15/5.54 ms, FA = 15°, 1.2 x 1.2 x 6 mm (Philips); and TR/TE = 4.92/2.67 ms, FA = 20°, 1.5 x 1.5 x 5 mm (Siemens), VENC = 200 cm/s.

For neonates, typical image parameters for the quantitative flow phase-contrast sequence were TR/TE = 4.92/2.67 ms, FA = 20°, 1.5 x 1.5 x 5 mm (Siemens).

3.2.1.4 Pulse wave travelling distance

For the pulse wave travelling distance in adolescents, two separate sets of images were used: 1) “Coronal overview” coronal slices covering the entire thorax based on a bSSFP sequence with in plane resolution 1.66 mm and slice thickness 8 mm and slice gap 2.64 mm, and 2) “3D angiography“ with oblique sagittal slices covering the thoracic aorta based on a clinical routine T2-prepared bSSFP with isotropic resolution 0.88 mm (Philips) or 0.55 mm (Siemens). Respiratory gating using navigator echoes was used for the 3D angiography. The apex of the diaphragm, i.e., the liver-diaphragm border, was used as tracking point for the navigator. Only images acquired within a pre-specific acceptance window, based on a previously acquired scout, are saved; the rest are discarded.

In neonates a clinical routine 3D black-blood T1-weighed non-contrast-enhanced angiography sequence was used with isotropic resolution 1.04 mm (Siemens).

3.2.1.5 Cardiac volumes

Short axis cine images were acquired using a balanced steady state free precession (bSSFP) sequence with retrospective ECG gating. For short axis images, typical parameters were 30 reconstructed time frames per cardiac cycle, slice thickness 8 mm; slice gap = 0 mm; FA = 60°; TR/TE = 3.1/1.5 ms; in-plane resolution = 1.1 x 1.1 mm (Philips) or slice thickness = 6 mm; slice gap = 0 mm; FA = 51°; TR/TE = 73/1 ms; in-plane resolution = 0.8 × 0.8 mm (Siemens).

3.2.1.6 Atrioventricular plane displacement

Cine images were acquired in 2-, 3-, and 4-chamber long-axis views using a balanced steady state free precession (bSSFP) sequence with retrospective ECG gating. Typical image parameters were slice thickness = 8 mm; FA = 60°; TR/TE = 3.1/1.6 ms; in-plane resolution =1.1 x 1.1 mm (Philips) or slice thickness = 6 mm; FA = 51°; TR/TE = 73/1 ms; in-plane resolution = 0.8 x 0.8 mm (Siemens).

3.2.2 MR image analysis

MR images were analyzed using the image analysis software Segment (Medviso, Lund, Sweden) (219).

3.2.2.1 Kidney volumes

Figure 3.2 shows delineations of renal cortical and medullary volumes in pig and in human. The renal cortex and medulla were manually delineated on transversal images covering the entire kidneys. Cysts, renal pelvis, and other non-parenchymal tissue were excluded. Volumes were then calculated by adding the respective slice volumes. Total kidney volume was defined as the combination of cortical and medullary volumes, excluding renal pelvis, blood vessels and other non-parenchymal structures. The ratio between cortical and medullary volumes (corticomedullary ratio) was calculated as cortical volume divided by medullary volume. Kidney volumes were also normalized to BSA (220).

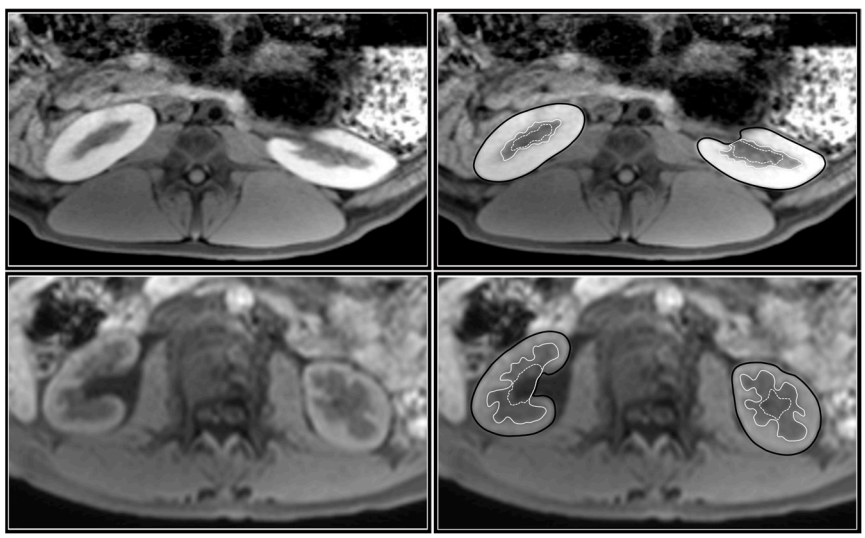

Figure 3.2 Renal MRI images in pig and human.
In-vivo renal MR images in pig (**top row**) and in human (**lower row**) without (**left column**) and with (**right column**) delineations of renal cortical and medullary borders. Cortical outer borders are depicted in solid black lines, medullary borders by solid white lines and non-parnehcymal tissue in dashed white lines. *Image adapted from Liefke et al. (221), Sage, through a CC BY 4.0 License (https://creativecommons.org/licenses/by/4.0/).*

3.2.2.2 Renal T1 and T2 mapping*

Figure 3.3 shows delineations for T1 and T2* maps. T1 maps were generated using motion-correction and a 3-parameter T1 fit with Look-Locker correction while T2* maps were generated using a 2-parameter mono-exponential fit (222). The region of interest (ROI) was drawn one pixel in from the outer contour of the respective parenchymal area and the renal column was not delineated all the way down to the renal pelvis. T1 values were acquired for renal cortex and medulla separately. Corticomedullary T1 differentiation, a marker of kidney dysfunction (223), was calculated as the ratio between cortical and medullary T1.

T2* values were acquired for the renal cortex and for the entire renal parenchyma combined (cortex and medulla). It was not possible to accurately distinguish between cortical and medullary parenchyma in all echo images that were used for creating T2* maps.

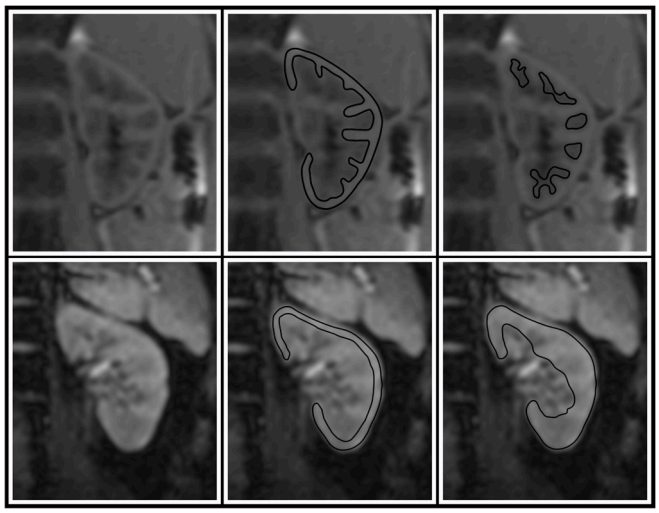

Figure 3.3 MR images with delineations for renal parenchymal T1 and T2* values.
Coronal images of the left kidney for T1 mapping measurements (**upper row**) and for T2* measurements (**lower row**). The kidney is shown without delineations (**left column**), with delineations of cortical parenchyma (**middle column**) and delineations of medullary parenchyma and total kidney parenchyma, respectively (**right column**). For both T1 and T2* values, delineations were placed to avoid partial volume effects. Both left and right kidneys were delineated. *Adapted from accepted manuscript, Pediatric Nephrology. The article will be published under a CC BY 4.0 license, http://creativecommons.org/licenses/by/4.0/.*

3.2.2.3 Flow measurements

Quantitative flow measurements were performed in the ascending aorta, the proximal descending aorta, the aorta at diaphragm level and in renal arteries. Delineations were performed in magnitude images throughout the cardiac cycle using an automated algorithm (224). Manual correction was used, and the phase-contrast images guided delineations when needed. Linear background phase correction was performed (225).

Glomerular filtration fraction, a measure of renal flow reserve (226), was calculated as eGFR divided by renal blood flow multiplied with 0.55 in boys and with 0.6 in girls to estimate the fraction of plasma in whole blood for the respective sex (227). The perfusion of the renal parenchyma was calculated as renal arterial blood flow divided by total kidney mass (density 1.05 g per 1 ml).

3.2.2.4 Pulse wave velocity

Figure 3.4 shows aortic PWV measurements in neonates and in adolescents for *Study II*.

Pulse wave velocity was calculated as the pulse wave travelling distance between flow planes, i.e., vessel length, (Δd), derived from 2D coronal overview images and the reference standard 3D angiography images (*Study II*). For neonates, only the 3D black-blood sequence was used to calculate vessel length (Δd) (*Study II*). Figure 3.5 shows the application in *Study III,* where only reference standard 3D angiography images were used. For both image types a manual frame-by-frame centerline vessel tracking method was used. Lengths reported are from the reference standard 3D angiography unless otherwise specified.

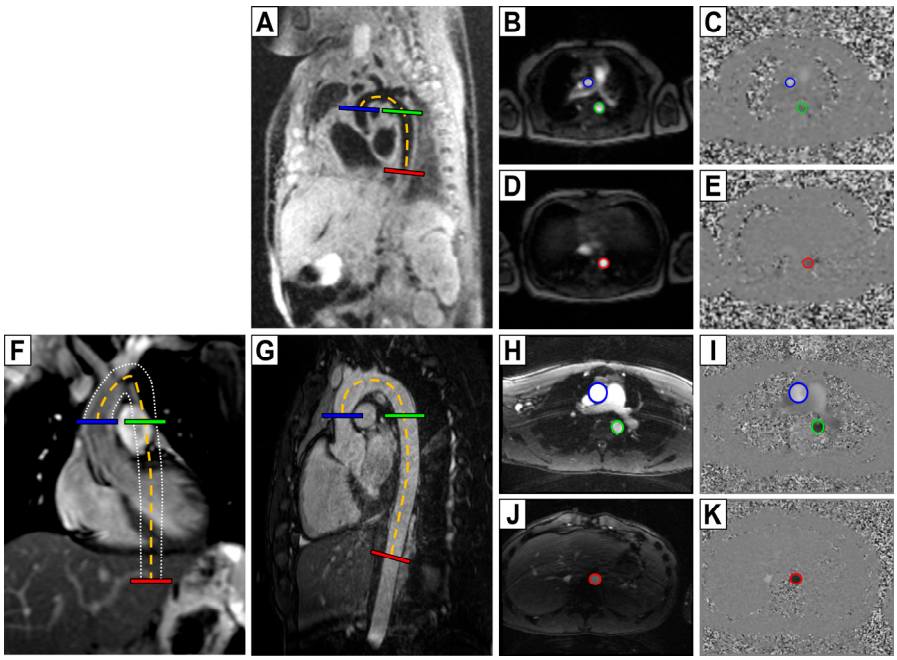

Figure 3.4 Image delineations for aortic length and flow mesaurements.
Neonatal black-blood (**A**) and adolescent white-blood (**G**) 3D angiography, and adolescent thoracic coronal overview image with white dotted lines outlining the aortic walls throughout the 2D image stack (**F**), all with length delineation (Δd) (dashed orange) and perpendicular flow imaging planes in the ascending aorta (**blue**), descending proximal aorta (green) and descending aorta at the level of the diaphragm (red). Magnitude and quantitative phase-contrast images at ascending and proximal descending aorta (**B–C, H–I)** and descending aorta at the level of the diaphragm (**D–E, J–K**), corresponding to the flow imaging planes localizations. Images from Lundström et al. (228), through a CC BY 4.0 license, SpringerNature. http://creativecommons.org/licenses/by/4.0/.

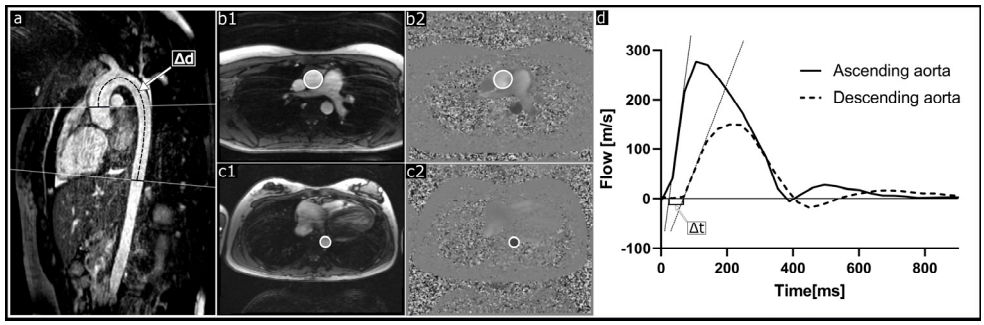

Figure 3.5 Application of pulse wave velocity measurements using the time to foot method.
Non-contrast-enhanced 3D angiography (**a**) of the thoracic aorta with flow measurement planes (solid lines) perpendicular to the ascending aorta and descending aorta at diaphragm level, and the aortic centerline distance (Δd; dashed line) between flow measurement planes. Delineations of the ascending aorta in a magnitude image (**b1**) and phase-contrast image (**b2**). Corresponding delineations of the descending aorta at diaphragm level (**c1** and **c2**). Flow curves for the ascending aorta (**d**) (solid line) and descending aorta (dashed line) were used to assess pulse wave velocity using the time-to-foot method. Pulse wave travelling time (Δt) was calculated as the time between upslope tangents intersecting the baseline. Pulse wave velocity was calculated by dividing the aortic centerline distance (Δd) with the time difference (Δt). *Manuscript accepted, Pediatric Nephrology. The article will be published under a CC BY 4.0 license, http://creativecommons.org/licenses/by/4.0/.*

3.2.2.5 Computer phantom

The computer phantom method from Dorniak et al. (229), was used to calculate the required temporal resolution needed for accurate PWV measurements. Vessel lengths, set to approximate the minimal lengths of the aortic arch and the entire thoracic aorta for neonates and adolescents, respectively, were used as input in the phantom. Image data from neonates but not adolescents had sufficient timeframes per cardiac cycle for construction of a high-resolution computer phantom. One additional adolescent individual was included to provide this data to the computer phantom. Computer phantoms with PWV velocities between 2-10 m/s were created, to include the physiological ranges of velocities in both cohorts (230). The ascending and descending flow curves were calculated and the delay between them calculated as vessel length divided by the respective pulse wave velocity, PWV. The flow profile was down sampled to between 20-60 time frames per cardiac cycle, to mimic different temporal resolutions. The time to foot method was used to calculate PWV at different combinations of reference PWV and time frames per cardiac cycle. Differences between time to foot measurements and reference PWV were presented as percent error.

3.2.2.6 Aortic distensibility

Distensibility in the ascending aorta and descending aorta at diaphragm level was calculated as $\frac{A_{Max} - A_{Min}}{A_{Min} \times \Delta P}$. A_{max} denotes the maximum and A_{min} denotes the minimum cross- sectional areas during the cardiac cycle, and ΔP equals the brachial blood pressure difference between systole and diastole (231). Brachial blood pressure was acquired directly after the respective flow acquisition.

3.2.2.7 Cardiac volumes

Ventricular and atrial volumes were planimetrically derived from manually delineated short-axis images and trabeculations and papillary muscles were included in the cavity volumes according to guidelines (183) (Figure 3.6). Left ventricular mass (LVM) was calculated as the left ventricular wall volume multiplied with the ventricular myocardial density (1.05g/ml). End-diastole and end-systole were defined as the time frames with the maximum and minimum mid-ventricular area, respectively. Left atrial and right atrial volumes were delineated in ventricular end diastole and end systole for left and right atrial maximal and minimum volume. Total heart volume (THV) was measured by manual delineation of the epicardial contours at end-diastole in short-axis cine images covering the entire heart (Figure 3.6) (152). Cardiac volumes were indexed to BSA to enable group and sex comparisons. Ventricular and atrial volumes were also normalized to THV to assess the relation in size between atrial and ventricular volumes (232). Planimetrically derived stroke volume were calculated as EDV-ESV.

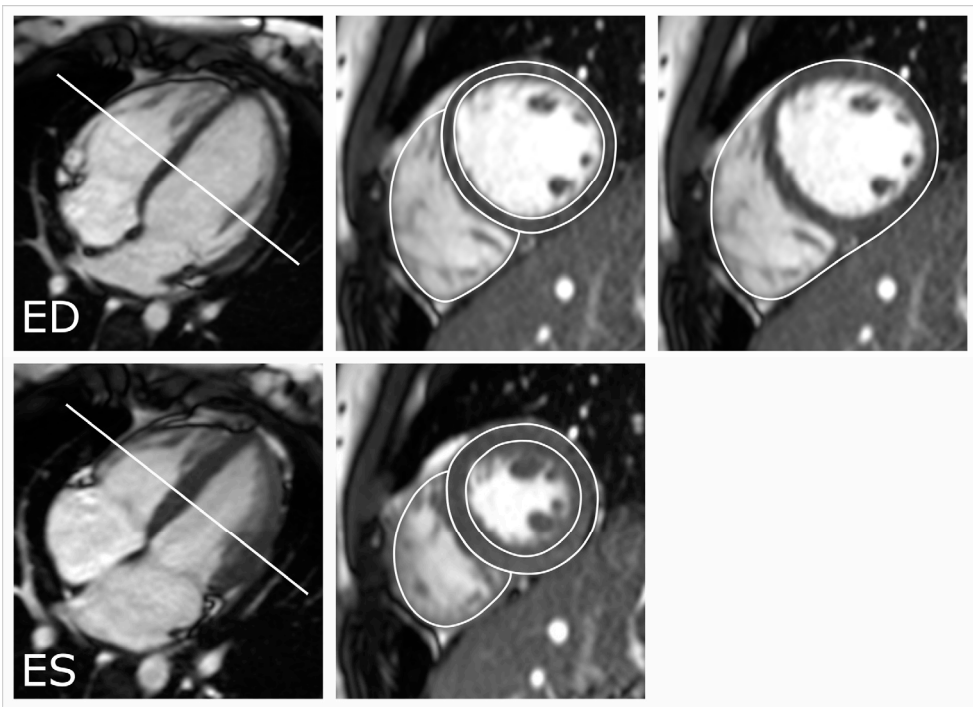

Figure 3.6. Delineations of cardiac volumes.
A 4-chamber view of the heart (**left column**) showing the corresponding imaging plane for the short-axis images in the other columns. Delineations for left and right ventricular volumes (**middle column**) and delineations for total heart volume (**right column**) are shown with white solid lines. Upper row shows end-diastole and lower row shows end-systole. For left and right ventricular volume assessment, short axis images for the entire myocardium were delineated and for total heart volume, short axis images fo the entire heart, including the greater vessels, were delineated.

3.2.2.8 Longitudinal contribution to stroke volume

Figure 3.7 show atrioventricular plane displacement (AVPD). Atrioventricular plane displacement was measured using a validated automated method for time-resolved AV-plane tracking, with manual correction as needed (184). In short, eight input points of the AV-plane position throughout the cardiac cycle were manually marked in 2-, 3-, and 4-chamber long axis views (Figure 3.7). Left ventricular AVPD was calculated using two input points from each of the long-axis views for the left ventricle whereas right ventricular AVPD was calculated using the mean of the two septal points together with the input points from the right lateral point of the 4-chamber and the input point by the right ventricular outflow tract in the 3-chamber view as previously described (150,151,184). To calculate AVPD relative to the length of the ventricle, AVPD ratio, an input point was also placed at the apex in long-axis images (Figure 3.7).

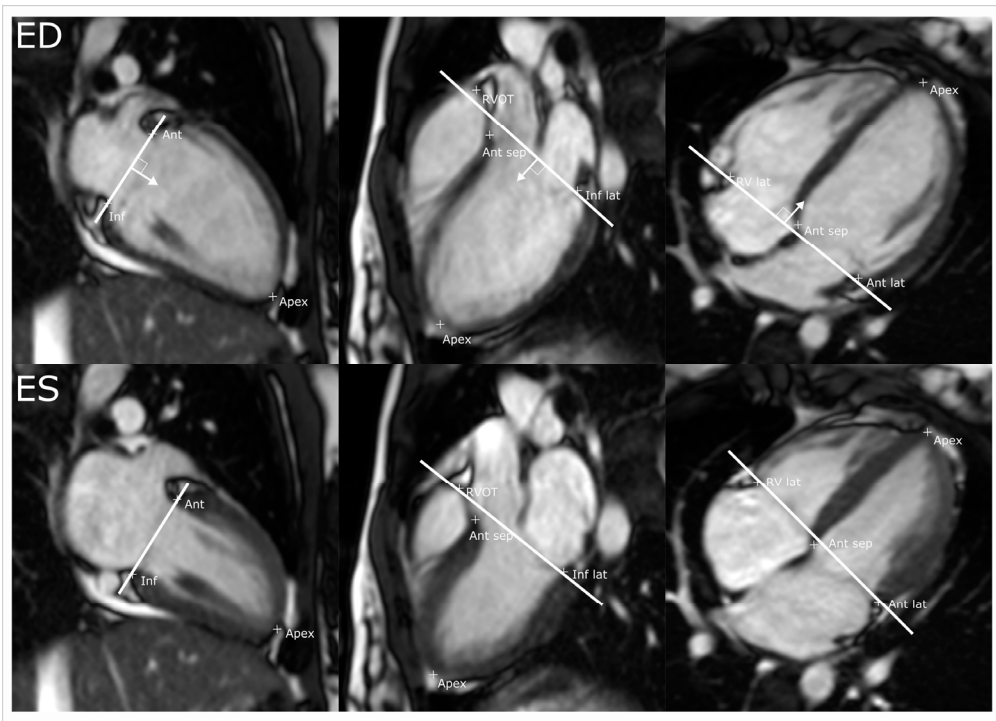

Figure 3.7 Measurement of atrioventricular plane displacement (AVPD).
Cardiac MR long axis images showing the input points for the AVPD algorithm and a vizualisation of the AV-plane movement from end-diastole (**upper row**) to end-systole (**lower row**) in a 2-chamber view (**left**) a 3-chamber view (**middle**) and a 4-chamber view (**right**). In addition to the eight standard points, depicted as crosses at their respective position, apex were marked in order to calculate the AVPD ratio (AVPD divided by the length of the ventricules). Ant=anterior, inf=inferior, lat=lateral, RVOT=right ventricular outflow tract.

Figure 3.8 show a visualization of longitudinal stroke volume. Stroke volume generated by the AVPD was calculated for the left and right ventricle as the AVPD in centimeters multiplied by the mean epicardial area (cm^2) of the short-axis slices (6 or 8mm depending on the scanner) within the AV-plane movement (184). Longitudinal contribution was calculated as stroke volume generated by the AVPD for the respective ventricle divided by the planimetrically derived stroke volume.

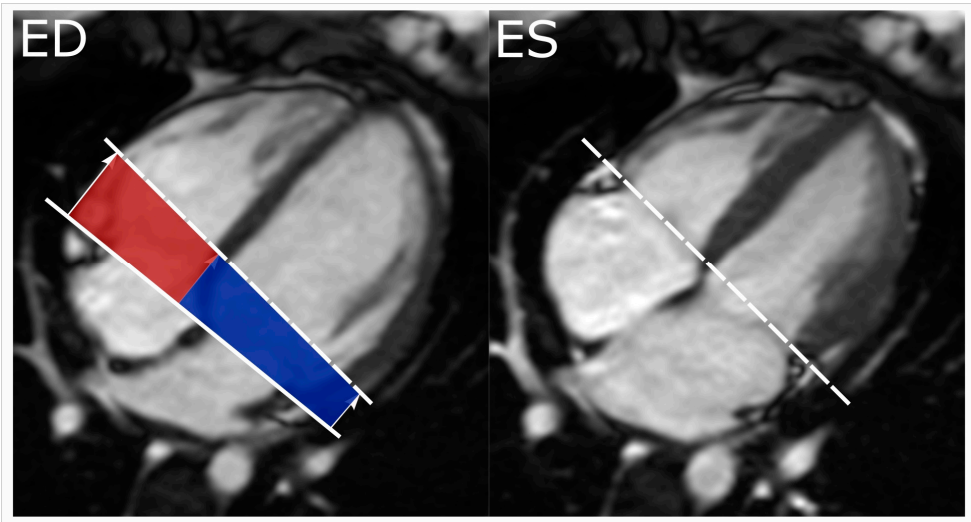

Figure 3.8 Longitudinal contribution to stroke volume.
Cardiac MR images showing a 4-chamber view of the heart in end-diastole (**left**) and in end-systole (**right**). The solid line represents the position of the AV-plane in end-diastole whereas the dashed line represents the AV-plane in end systole. The end-systolic AV-plane is transposed to the end-diastolic image. Longitudinal contributon to stroke volume for the respective ventricle is calculated as the blood volume transposed by the atrioventricular plane displacement. Longitudinal contribution to stroke volume is depicted in blue for the left ventricle and red for the right ventricle.

3.2.2.9 Radial contribution to stroke volume

Figure 3.9 show a visualization of radial contribution to stroke volume. Radial contribution to left and right ventricular stroke volume, respectively, was defined as the volume difference caused by the inward displacement of the epicardial border from end-diastole to end-systole divided by the planimetrically derived stroke volume. The right ventricular insertion points towards the left ventricle were manually marked and used to subdivide the radial contribution of the left ventricular stroke volume into septal and lateral contributions (233).

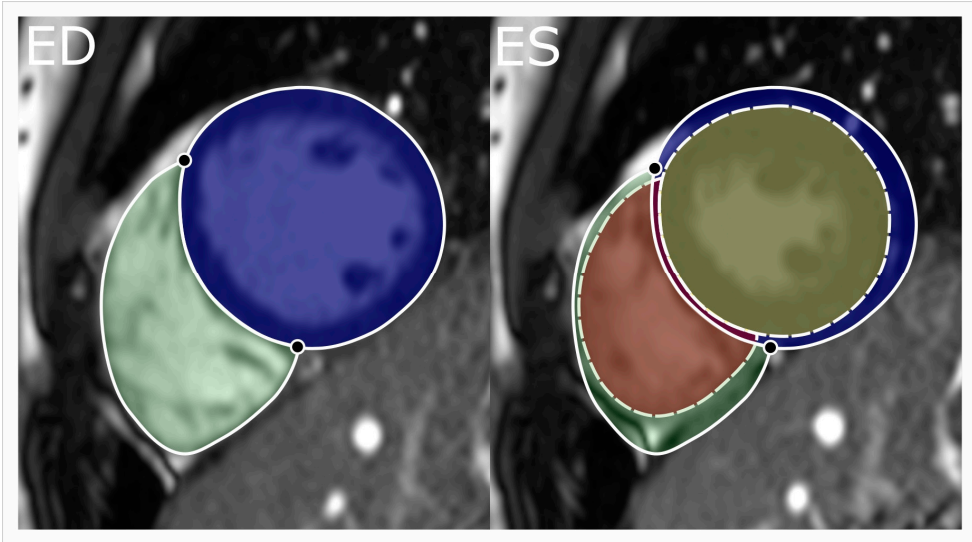

Figure 3.9. Radial contribution to stroke volume.
Cardiac MR images of the heart in a midventricular short axis view in end-diastole (**left**) and in end-systole (**right**). Solid lines indicate epicardial borders and dashed lines indicate endocardial borders.The black circles with white borders indicate RV insertion points. The end-diastolic volumes are marked with blue and green and the end-systolic volumes are marked in red and yellow to the right. The end-diastolic contours to the left are interpolated to the end-systolic image to the right. The green area in the image to the right represents the lateral contribution to stroke volume for the right ventricle, the darker red area between the solid and dashed lines between the RV insertion points represents septal contribution to stroke volume and the blue area between the solid and dashed lines around the left ventricle represents lateral contribution to left ventricular stroke volume. The respective areas were summed from all short-axis slices to calculate the respective volume.

3.3 24-hour ambulatory blood pressure measurements

Systolic, diastolic, and mean arterial blood pressure were measured every 20 minutes over 24 hours as per clinical routine (SpaceLabs Medical ABP-monitor model 90207 or Ultralite TM 90217A, Issaquah, USA). Activity and potential symptoms were reported. Generally, >80% of successful readings was deemed sufficient for inclusion.

Reference values for children and adolescents are based on sex, age, and height (234). Daytime and nighttime periods were reviewed both separately and in combination and related to the activity diary for evaluation, in line with ESC guidelines (175,234). Mean systolic and diastolic blood pressures were graded as normal (<90th percentile), prehypertension (≥90th to <95th percentile) or hypertension (≥95th percentile) for daytime and nighttime separately. A day-to-night ratio of mean arterial blood pressure <10% was graded as pathological. Normal values for adult blood pressure were defined for 24 hours as <130/80 mmHg, for daytime <135/85 mmHg, and for nighttime <120/70 mmHg (175).

Blood pressure above these values were, in addition to reference values for adolescents, graded as hypertension.

3.4 Biochemical markers in blood and urine

Sampling of blood and urine was performed in conjunction with MRI or with 24-hour ambulatory blood pressure measurements. Due to logistics, participants were not instructed to be in a fasted state and the sampling could have been performed any time during the day. Blood was collected in EDTA test tubes whereas urine was collected in sterile test tubes. Samples were directly centrifuged (Thermo Scientific Megafuge 8, Thermo Fisher Scientific, Waltham, USA) for ten minutes at 1,500 G, pipetted into cryotubes and stored at -80°C.

Plasma concentrations of cystatin C, N-terminal pro B-type natriuretic peptide (NT-proBNP), creatinine and renin as well as urine samples of creatinine, albumin, IgG, kappa, and lambda were quantified at the hospital laboratory. Cystatin C concentration was quantified using a Atellica Solution immunoassay Analyzer (Siemens Healthineers, Erlangen, Germany). Plasma renin concentration was quantified using an automated Chemiluminescence Immunoassay (CLIA) (WHO International Standard for Direct Renin, 68/356).

Urine was analyzed using standard protein electrophoresis, with quantification of creatinine, albumin, IgG, kappa, and lambda.

Urine angiotensinogen (u-AGT), a potential biochemical marker of intra-renal RAAS activation (235), was quantified using a solid-phase sandwich enzyme-linked immunosorbent assay (ELISA) (Human Total Angiotensinogen Assay Kit -IBL, Cat. no.- 27412, 1091-1 Naka Aza-Higashida, Fujioka-Shi, Gunma 375-0005, Japan) on an ELISA absorbance microplate reader (Infinite F50 with software Magellan 7.2, Tecan Trading AG, Switzerland). Four samples had been remeasured and thus thawed twice, and as angiotensinogen is sensitive to temperature changes these four samples were removed from further analysis.

The ratio of u-IgG, u-albumin, u-kappa, u-lambda and u-AGT to u-creatinine were calculated. Estimated glomerular filtration rate (eGFR) was calculated as per clinical routine for children and adolescents (<18 years of age), using the Caucasian, Asian, Pediatric and Adult (CAPA) equation based on Cystatin C ($eGFR_{Cystatin\ C}$) (159). For comparison, the updated Schwartz equation based on creatinine ($eGFR_{Creatinine}$) (160) and the average of $eGFR_{Cystatin\ C}$ and $eGFR_{Creatinine}$ ($eGFR_{Average}$) were assessed.

3.5 Statistical analyses

Statistical analyses were performed using SPSS versions 26 or 27 (IBM Corp, Armonk, NY) and/or GraphPad Prism 9 (GraphPad Software, La Jolla, California, USA). The open-source vector graphics editor Inkscape (https://inkscape.org/) were used for artwork.

Nonparametric tests were generally performed as normal distribution could not be assumed for the greater parts of the variables investigated. Normal distributions were visually assessed using histograms. Continuous variables were expressed median (range) or median [interquartile range] where appropriate. Categorical variables were expressed as absolute numbers or proportion. Kruskal-Wallis with post hoc Dunn's or Bonferroni's multiple comparison test and Mann-Whitney U-test assessed group differences. Pearson's or Spearman's correlation was used for correlation analyses as appropriate. Simple linear regression was used to calculate causation. Pearson's chi square test or Fisher's exact test was used for categorical variables as appropriate. The Jonckheere-Terpsta and Kendall's Tau-b tests were used for assessing trends between groups. The Bland-Altman method evaluated intra-and interobserver differences as well as agreement between methods as appropriate. All tests were two sided and p-values < 0.05 were considered to show statistically significant differences.

4 Results and comments

The major findings together with short comments of *studies I–V* are presented in this section. More detailed description of the study results for each paper are presented in part II at the end of the thesis summary.

4.1 Study I: Validation of renal cortical and medullary volume assessment with MRI

4.1.1 Agreement between MRI and ex vivo quantification

Figure 4.1 shows agreement between MRI and ex-vivo quantification. Agreement between MRI and ex-vivo quantification of renal parenchymal volumes is presented as median and 95% limits of agreement (LoA; 2.5th–97.5th percentile) and shown for one observer with intermediate MRI experience (~3 years) and for two experienced observers in consensus (~15–20 years of MRI experience). Agreement was for total parenchymal volume -7ml (-10 to 0) ml, for cortical volume -4ml (-9 to 3) ml and for medullary volume -2ml (-7 to 2) ml (Observer 1). The respective results for the consensus observers were for total parenchymal volume -3 (-9 to 4) ml, for cortical volume -2 (-9 to 4) ml and for medullary volume 0 (-4 to3) ml. The medullary fraction, i.e., medullary volume divided by total parenchymal volume was 15% (range 13–20%) in pigs 35% (range 27–38%) in human.

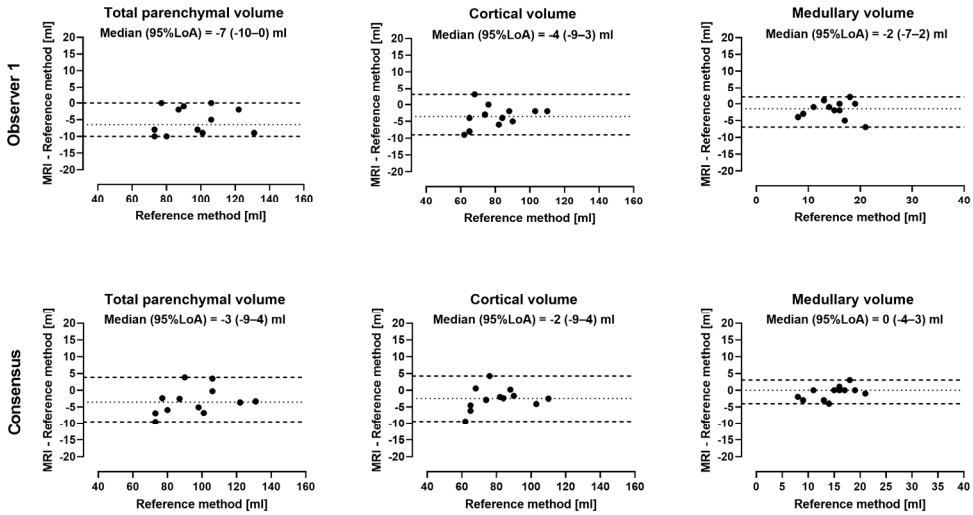

Figure 4.1. Agreement between MRI and ex-vivo reference standard for quantification of renal parenchymal volumes. Upper row shows observer I and lower row shows consensus observers. Dotted lines indicate median and dashed lines 95% Limits of agreement. *Liefke et al.* (221), *under a CC BY 4.0 License (https://creativecommons.org/licenses/by/4.0/)*

4.1.2 Intra-and interobserver variability

Figure 4.2 shows intra- and interobserver variability of renal parenchymal volume quantification by non-contrast enhanced MRI in pig and in human. Median interobserver variability for both pig and human were < 5% whereas median interobserver variability were between < 4% for total parenchymal volume and cortical volume and between 6–12% for medullary volume quantification.

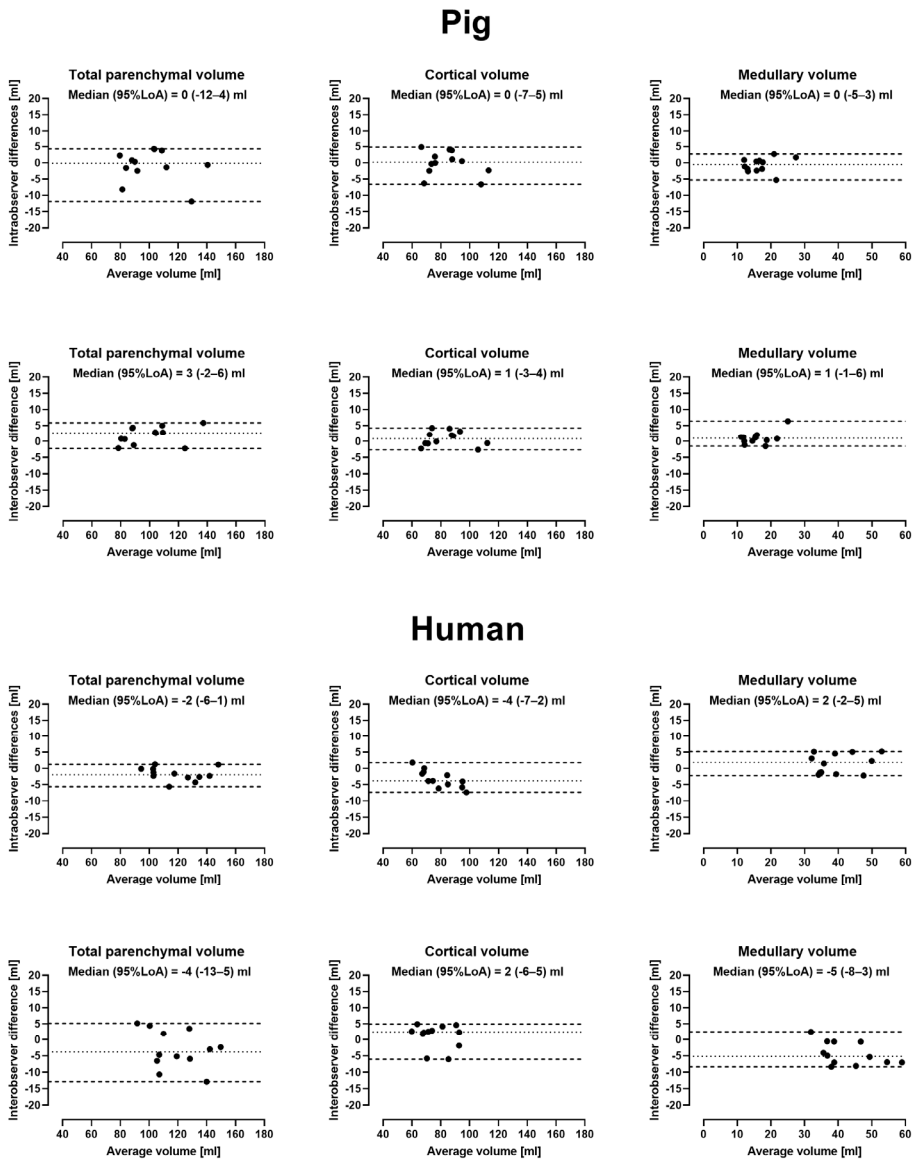

Figure 4.2. Intra- and interobserver variability of renal parenchymal volume quantification by non-contrast enhanced magnetic resonance imaging.

Bland-Altman plots showing intra- (**top row**) and interobserver (**bottom row**) in pig (**upper panels**) and in human (**lower panels**). Dotted lines indicate median and dashed lines 95% limits of agreement. *Adapted and reprinted from Liefke et al.* (221)*, under a CC BY 4.0 License (https://creativecommons.org/licenses/by/4.0/)*

4.2 Study II: Validation of pulse wave velocity acquisition using MRI in neonates and in adolescents

4.2.1 Computer phantom

Figure 4.3 shows the computer phantom results for neonates and adolescents. The phantom experiment shows the required time frames per cardiac cycle needed for accurate assessment of pulse wave velocities at different aortic lengths, derived from actual flow curves from neonates and adolescents respectively. A cut off value, suggestive of the minimum required timeframes per cardiac cycle for minimum PWV errors, dependent on vessel length and pulse wave velocity are depicted and were 42 for the aortic arch and 41 for the thoracic aorta in neonates and 39 and 32 for corresponding vessel segments in adolescents.

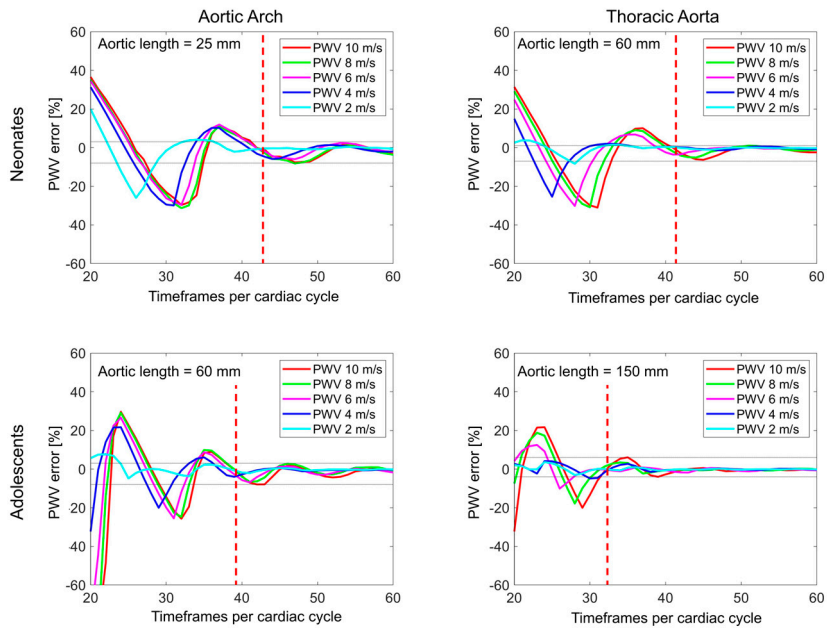

Figure 4.3. Pulse wave velocity errors at different pulse wave velocities dependent on the acquired timeframes per cardiac cycle. Computer phantom based on neonatal (**top row**) and adolescent (**bottom row**) flow data for the aortic arch (**left column)** and the thoracic aorta (**right column**). Vessel lengths approximates the minimal lengths in the respective cohorts. Vertical red dashed lines denote the cut-off for required timeframes per cardiac cycle for all pulse wave velocities. Horizontal gray dotted lines denote the mean error (min–max) after the cut-off line. Shorter aortic lengths and higher pulse wave velocities independently increased the number of time frames per cardiac cycle needed for accurate estimation of pulse wave velocitiy. X-axis offset between neonatal and adolescent curves is likely related to the shorter diastolic period in neonates due to their higher heartrate. *Reprinted with permission from Lundström et al.* (228), *under a CC BY 4.0 license, (http://creativecommons.org/licenses/by/4.0/).*

4.2.2 Aortic length measurements

Figure 4.4 shows aortic center-line measurements and agreement between coronal overview images and the reference standard 3D angiography. The current study investigated whether coronal overview images of the thoracic aorta, which is part of the standard clinical protocol for cardiac MRI, could be used interchangeably with the reference standard 3D angiography for calculations of vessel length. This would enable retrospective analysis of PWV in patients who has undergone cardiac MRI and would also lessen the need to add additional sequences, i.e., 3D angiography, to the clinical protocol. However, although showing a low median bias, the intra-individual variation was (95% LoA) -16 to 18 mm for the aortic arch and -25 to 30 mm for the thoracic aorta, indicating a low reliability. As non- contrast enhanced 3D angiography can be acquired in a few minutes, adding this sequence to the standard clinical protocol is preferred if accurate PWV measurements are to be assessed.

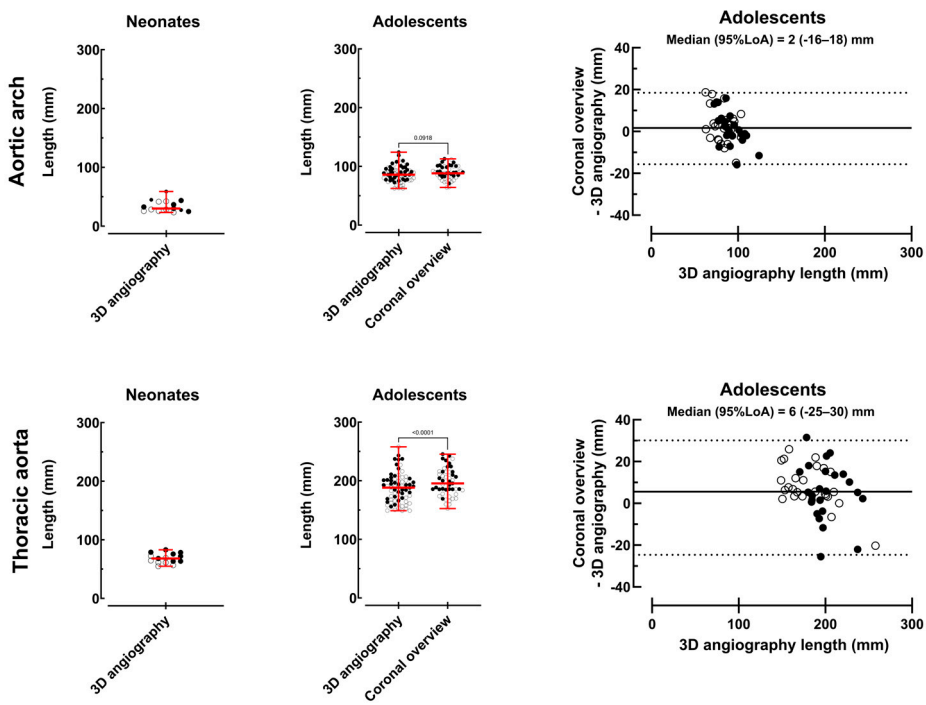

Figure 4.4. Aortic centerline measurements and agreement between coronal overview images and the reference standard 3D angiography. Aortic centerline measurements for the aortic arch (**upper row**) and the thoracic aorta (**lower row**) in neonates (**left column**) and in adolescents (**middle column**). Agreement between centerline measurements performed in the coronal overview images and the reference standard 3D angiography (n=49 adolescents) (**right column**). Solid circles represent males and open circles females. Red lines with error bars denote median (range). Solid black lines represent bias and dashed lines represent 95% limits of agreement. *Reprinted with permission from Lundström et al.* (228)*, under a CC BY 4.0 license, (http://creativecommons.org/licenses/by/4.0/).*

4.2.3 Pulse wave transit time

Figure 4.5 shows comparison of three methods for the assessment of pulse wave transit time: the time-to-foot method with automatic baseline correction (TTF), the maximum upslope method and the time-to -peak (TTP) method, based on flow and velocity curves, respectively. In neonates, there were no statistically significant difference between the thoracic aortic PWV based on flow curves for TTF (4.1 ± 0.9 m/s) vs maximum upslope (6.4 ± 3.5 m/s) or the TTP method (5.3 ± 5.6 m/s); $p \geq 0.43$. The corresponding PWV based on velocity curves were 4.2 ± 1.0 m/s for TTF, 6.1 ± 2.4 m/s for maximum upslope, and 1.8 ± 5.4 m/s for TTP ($p \geq 0.19$).

In adolescents, thoracic aortic PWV based on flow curves were higher for TTF (3.8 ± 0.5 m/s) as compared to TTP (2.7 ± 1.0 m/s); $p < 0.0001$ and for maximum upslope (3.7 ± 0.6 m/s) as compared to TTP (2.7 ± 1.0 m/s); $p < 0.0001$. There was no difference between the TTF and maximum upslope methods ($p = 0.8$). Pulse wave velocity measurements with the TTF and maximum upslope showed high agreement.

Although not statistically different, the wide range of pulse wave velocities in neonates, between all methods, but especially for velocity based PWV and the TTP method, shows that PWV is highly dependent on the method used. The TTP method, showing a wide range of velocities, a low agreement between flow and velocity-based flow curve derived values and showing negative values, cannot reliably be used for PWV assessment in neonates. For adolescents, the TTP method did not show negative values but was markedly lower as compared to the other method and showed higher variability between flow and velocity based PWV.

The TTF method showed the lowest ranges and the highest agreement between flow and velocity based PWV.

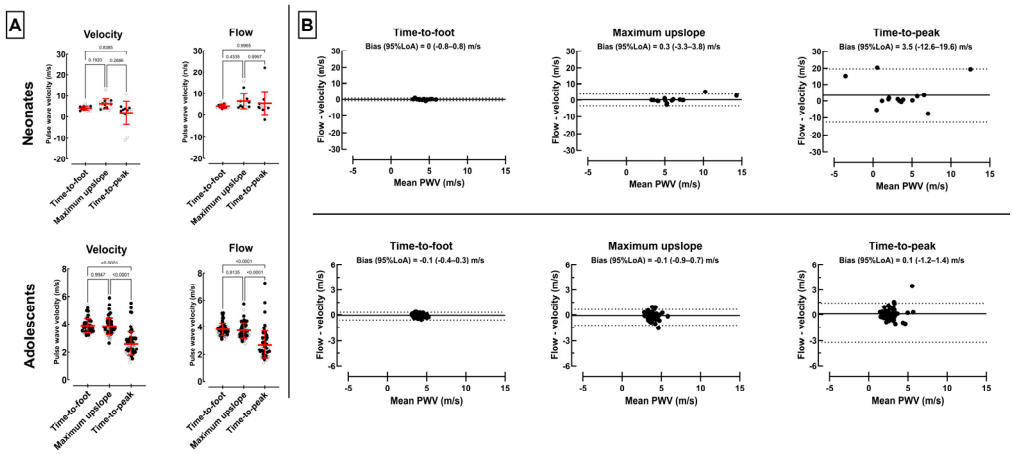

Figure 4.5. Transit time measurements and method agreement. Method comparisons (**panel A**) for neonates (**upper row**) and adolescents (**lower row**). Thoracic aortic PWV for velocity and flow are shown for time-to-foot with automatic baseline correction, maximum upslope, and time-to-peak algorithms. Time-to-peak was lower for both velocity and flow curves. Solid circles represent males and open circles females. Red line with error bars denotes mean ± SD. Bland–Altman plots (**panel B**) for neonates (**top row**) and adolescents (**bottom row**) with comparison of thoracic aorta velocity and flow-based maximum upslope (**left**), time-to-foot with automatic baseline correction (**middle**), and time-to-peak (**right**) algorithms. Note the difference in y-axis ranges for neonates and adolescents. Negative PWV values are due to curve shapes with no definitive peak, which worked poorly with the TTP algorithm. Solid black lines represent bias and dashed lines represent 95% limits of agreement. *Reprinted with permission from Lundström et al.* (228)*, under a CC BY 4.0 license, (http://creativecommons.org/licenses/by/4.0/).*

4.2.4 Baseline correction

Figure 4.6 shows agreement between baseline correction methods for neonates and adolescents. For both neonates and adolescents there was a high agreement between the manual and the proposed automatic baseline correction method, using the average from the 80th–95th % segment of the flow curve to approximate the ascending and descending curve.

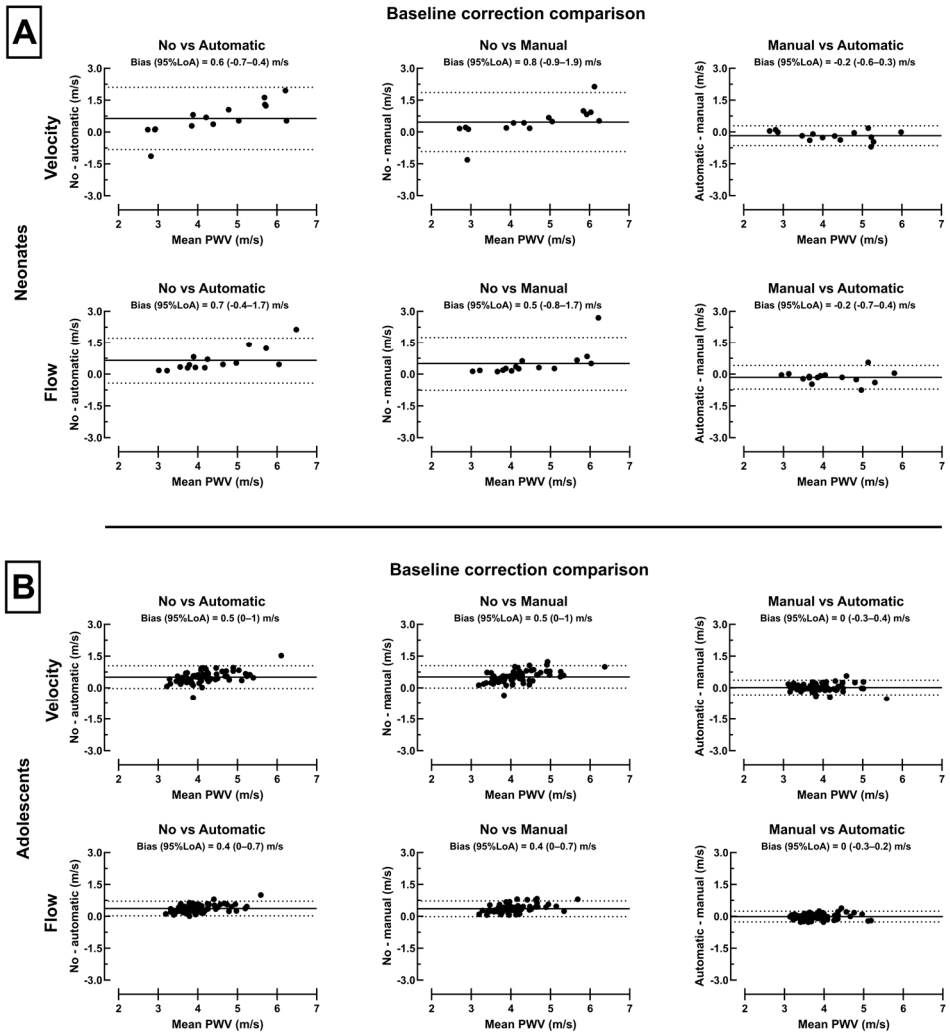

Figure 4.6 Baseline correction comparison. Bland Altman plots showing comparison of thoracic aortic pulse wave velocity based on velocity and flow curves for neonates (**panel A**) and adolescents (**panel B**). Agreement between no baseline correction and automatic baseline correction (**left**), no and manual baseline correction (**middle**), and manual and automatic baseline correction (**right**) is presented in both rows. Manual and automatic baseline correction agreed for both velocity and flow curves, which indicates that these baseline correction methods can be used interchangeably in neonates and adolescents. Solid black lines represent bias and dashed lines represent 95% limits of agreement. *Reprinted with permission from Lundström et al.* (228)*, under a CC BY 4.0 license, (http://creativecommons.org/licenses/by/4.0/).*

4.3 Study III: Blood pressure and arterial stiffness

In this study, measures of blood pressure and arterial stiffness were assessed in adolescents born very preterm due to early onset fetal growth restriction and compared with the two control groups born with appropriate birth weight, one in similar gestation and one born at term. This study included the entire cohort, prospectively included for follow up in adolescence who underwent either 24-hour ambulatory blood pressure measurements (24-hour ABPM) or MRI. In addition to 24-hour ABPM, the pulse wave velocity method proposed in *study II* were implemented.

4.3.1 Study population

A total of 79 adolescents (14 (13–17) years 52% girls were included. Table 4.1 shows subject characteristics and neonatal morbidity. Preeclampsia (33% vs 4%; p <0.01), Cesarean section (100% vs 56%; p<0.0001), bronchopulmonary dysplasia (75% vs 26%; p = 0.001) and septicemia (54 vs 22%; p =0.02) were more prevalent in the preterm FGR group as compared to the preterm AGA group. Although not statistically different, smoking was almost three times as common for mothers in the preterm AGA group to smoke as compared to the preterm FGR group (22 vs 8%; p = 0.3).

Table 4.2 shows comparisons of perinatal characteristics and neonatal morbidity between those who participated in the current study and those included in the original cohort who opted out from follow-up in the current study. For the preterm FGR group, maternal age was higher for those who participated in the study vs those who opted out (33 vs 28 years; p = 0.01). For preterm AGA, median birth weight was higher (1100 vs 875g; p = 0.04), the incidence of ablatio placentae lower (12 vs 57%; p = 0.03) and postnatal steroid treatment lower (15 vs 57%; p = 0.04) in the group who participated versus those who dropped out. There were no differences in the term AGA group.

Table 4.1 Subject characteristics and neonatal morbidity

				P values			
	Preterm FGR	**Preterm AGA**	**Term AGA**	**Between Groups**	**Preterm FGR vs Preterm AGA**	**Preterm FGR vs Term AGA**	**Preterm AGA vs Term AGA**
Peri-and neonatal characteristics	*n=24*	*n=27*	*n=28*				
Gestational age at birth (days)	188 (172 – 204)	193 (171 – 208)	280 (269 – 285)	**0.0001**	> 0.99	**0.0001**	**0.0001**
Gestational age at birth (weeks+days)	26+6 (24+4 – 29+1)	27 +4 (24+3 – 29+5)	40+0 (38+3 – 40+5)	**0.0001**	> 0.99	**0.0001**	**0.0001**
Birthweight (g)	643 (395 – 976)	1100 (660 – 1790)	3485 (2850 – 4390)	**0.0001**	**0.003**	**0.0001**	**0.0001**
Birthweight deviation (%)	-34.6 (-62.7 – -22.5)	-3.6 (-23.3 – 14.30)	-1.6 (-16.8 – 28.8)	**0.0001**	**0.0001**	**0.0001**	> 0.99
Maternal age (years)	33 (20 – 42)	31 (17 – 41)	31 (21 – 41)	0.2			
Preeclampsia (n (%))	8 (33%)	1 (4%) #	0	**<0.01***			
Antenatal steroid treatment (n (%))	23 (96%)	26 (100%) #	0	0.5*			
Multiple birth (n (%))	5 (21%)	6 (22%)	0	>0.99*			
Cesarean section (n (%))	24 (100%)	15 (56%)	0	**<0.0001***			
Smoking in pregnancy (n (%))	2 (8%)	6 (22%)	3 (11%)	0.3			
Ablatio placentae (n (%))	0	3 (11%) ##	0	0.2*			
Neonatal morbidity							
Severe IVH grade III-IV (n (%))	2 (8%)	3 (11%)	0	>0.99*			
Any grades of IVH (n (%))	3 (13%)	7 (26%)	0	0.3*			
Bronchopulmonary dysplasia (n (%))	18 (75%)	7 (26%)	0	**0.001***			
Severe retinopathy of prematurity (n (%))	2 (8%)	3 (11%)	0	>0.99*			
Necrotizing enterocolitis (n (%))	2 (8%)	0	0	0.2*			
Surgical treatment for PDA (n (%))	3 (13%)	3 (11%)	0	0.6*			
Pharmaceutical treatment for PDA (n (%))	10 (42%)	9 (33%)	0	0.5			
Septicemia (n (%))	13 (54%)	6 (22%)	0	**0.02***			

				P values			
	Preterm FGR	**Preterm AGA**	**Term AGA**	**Between Groups**	**Preterm FGR vs Preterm AGA**	**Preterm FGR vs Term AGA**	**Preterm AGA vs Term AGA**
Asphyxia; Apgar score <7 at 5 min (n (%))	1 (4%)	6 (22%)	0	0.1*			
Periventricular leukomalacia (n (%))	1 (4%)	1 (4%)	0	>0.99*			
Inotropic support (n (%))	10 (42%)	8 (30%)	0	0.4*			
Surfactant treatment (n (%))	13 (54%)	15 (56%)	0	>0.99*			
Postnatal steroid treatment (n (%))	9 (38%) [##]	4 (15%) [#]	0	0.06*			
Ventilatory support at 36 GW (n (%))	4 (17%)	2 (7%)	0	0.4*			
Characteristics in adolescence							
Age (years)	15 (13 – 17)	15 (13 – 16)	15 (13 – 16)	0.9			
Weight (kg)	51 (30 – 90)	56 (37 – 75)	58 (37 – 89)	0.1			
Weight deviation (SD)	-1(-4.6 – 2.9)	0.1 (-3 – 1.5)	0.4 (-2.3 – 2.6)	0.07			
Length (cm)	160 (150 – 180) [1]	167 (149 – 183)	167 (155 – 189)	**0.01**	**0.03**	**0.02**	> 0.99
BMI (kg/m²)	20 (13 –28)	21 (15 – 24)	21 (15 – 25)	0.9			
BSA (m²)	1.5 (1.1 – 2.1)	1.6 (1.2 – 2-0)	1.7 (1.3 – 2.2)	0.06			
Systolic blood pressure (mmHg)	105 (87 – 123)	107 (88 – 120)	102 (89 – 130)	0.37			
Diastolic blood pressure (mmHg)	53 (41 – 74)	54 (45 – 65)	50 (44 – 80)	0.08			

Data are presented as median (range). [1]Girls born preterm FGR were shorter than girls born term AGA ((157 (150 – 165cm) vs (164 (157 – 176cm); p = 0.003). *=comparison performed between preterm FGR and preterm AGA. Neonatal data missing in one (#) and two (##) individuals. FGR=fetal growth restriction, AGA=birth weight appropriate for gestational age, IVH=intraventricular hemorrhage, PDA=persistent ductus arteriosus, GW=gestational week, N/A=not applicable, SD=standard deviation, BMI=body mass index, BSA=body surface area.

Table 4.2 Comparison of perinatal characteristics and neonatal morbidity between study participants in the current cohort (opted in) and those who opted out from follow-up (opted out) from the original cohort.

	Preterm FGR			Preterm AGA			Term AGA		
	Opted in *n=24*	Opted out *n=10*	P	Opted in *n=27*	Opted out *n=7*	P	Opted in *n=28*	Opted out *n=6*	P
Perinatal characteristics									
Girls (%)	54	33	0.3	52	29	0.4	50	33	0.7
Gestational days (days)	188	191	0.6	193	180	0.1	280	279	0.7
Birth weight (g)	643	660	0.8	1100	875	**0.04**	3485	3580	0.3
Birth weight deviation (%)	-34.6	-43.4	0.3	-3.6	-11.4	0.1	-1.6	-1.2	0.7
Maternal age (years)	33	28	**0.01**	31	32	0.4	31	29	0.2
Preeclampsia (%)	33	0,3	1	4	0 #	1	0	0	N/A
Antenatal steroid treatment (%)	96	90	0.5	100	86 #	0.2	0	0	N/A
Multiple birth (%)	21	30	0.7	22	14 #	1	0	0	N/A
Cesarean section (%)	100	100	1	56	86 #	0.2	0	0	N/A
Primipara (%)	67	40	0.3	44	60 #	0.7	25	33	1
Smoking during pregnancy (%)	8	30	0.1	22	0 #	0.3	11	33	0.2
Ablatio placentae (%)	0	0	N/A	12	57 #	**0.03**	0	0	N/A
Neonatal morbidity									
Severe IVH grade III-IV (%)	8	10	1	11	29	0.6	0	0	N/A
Bronchopulmonary dysplasia (%)	75	60	0.4	26	43 #	0.6	0	0	N/A
Severe retinopathy of prematurity (%)	8	30	0.1	11	14 #	1	0	0	N/A
Necrotizing enterocolitis (%)	8	20	0.6	0	0	N/A	0	0	N/A
Treatment for PDA (%)	46	40	0.8	33	43 #	0.6	0	0	N/A
Septicemia (%)	54	50	1	22	14 #	0.4	0	0	N/A
Asphyxia; Apgar score <7 at 5 min (%)	4	20	0.2	22	14 #	1	0	0	N/A

	Preterm FGR			Preterm AGA			Term AGA		
	Opted in *n=24*	Opted out *n=10*	P	Opted in *n=27*	Opted out *n=7*	P	Opted in *n=28*	Opted out *n=6*	P
Periventricular leukomalacia (%)	4	0	1	4	14 #	0.4	0	0	N/A
Inotropic support (%)	42	1	0.1	30	57 #	0.2	0	0	N/A
Surfactant treatment (%)	54	60	1	56	86 #	0.2	0	0	N/A
Postnatal steroid treatment (%)	41	38	1	15	57 #	**0.04**	0	0	N/A
Ventilatory support at w36 (%)	17	40	0.2	7	0	1	0	0	N/A

FGR=fetal growth restriction, AGA=birth weight appropriate for gestational age, IVH=intraventricular hemorrhage, PDA=Persistent ductus arteriosus, N/A=not appropriate. Neonatal data missing in one (#) individual.

4.3.2 Blood pressure

Figure 4.7 and Tables 4.1 and 4.3 shows blood pressure data. There were no group differences in systolic ($p = 0.37$) or diastolic ($p = 0.08$) office blood pressure measurements (Table 4.1). The clinical evaluation of the 24-hour ambulatory blood pressure measurements revealed no group differences in the prevalence of pre-hypertension, hypertension or pathological day-to-night ratio (all $p \geq 0.1$) (Table 4.3).

For 24-hour ABPM, systolic blood pressure did not differ between groups for either sex (all $p > 0.21$). In boys, in addition to showing higher daytime mean arterial blood pressure (93 mmHg vs 86 mmHg; $p=0.03$) and 24-hour mean arterial blood pressure (88 vs 82 mmHg; $p=0.03$) in the preterm FGR group as compared to the term AGA group, trend analyses showed increasing diastolic and mean arterial blood pressures from term AGA to preterm AGA to preterm FGR for 24-hour and for daytime blood pressure (all $p \leq 0.03$) (Figure 4.7). In girls, no group differences or trends were observed in any blood pressure variables (all $p \geq 0.1$) (Figure 4.7).

4.3.3 Arterial stiffness

Figure 4.8 shows pulse wave velocity and distensibility in the ascending aorta and in the descending aorta at diaphragm level. There were no group differences in measures of arterial stiffness (all $p \geq 0.5$). When stratifying for sex, girls born preterm AGA showed higher median PWV (3.9 vs 3.5 m/s; $p = 0.04$) as compared to the term AGA group.

4.3.4 Renal function

Cystatin C based eGFR were for the preterm FGR group 94 [IQR 78–109] ml/min/1.73m^2, for the preterm AGA group 100 [IQR 85 – 118] ml/min/1.73m^2 and for the 243 term AGA group 100 [IQR 89 – 110] ml/min/1.73m^2 ($p = 0.35$).

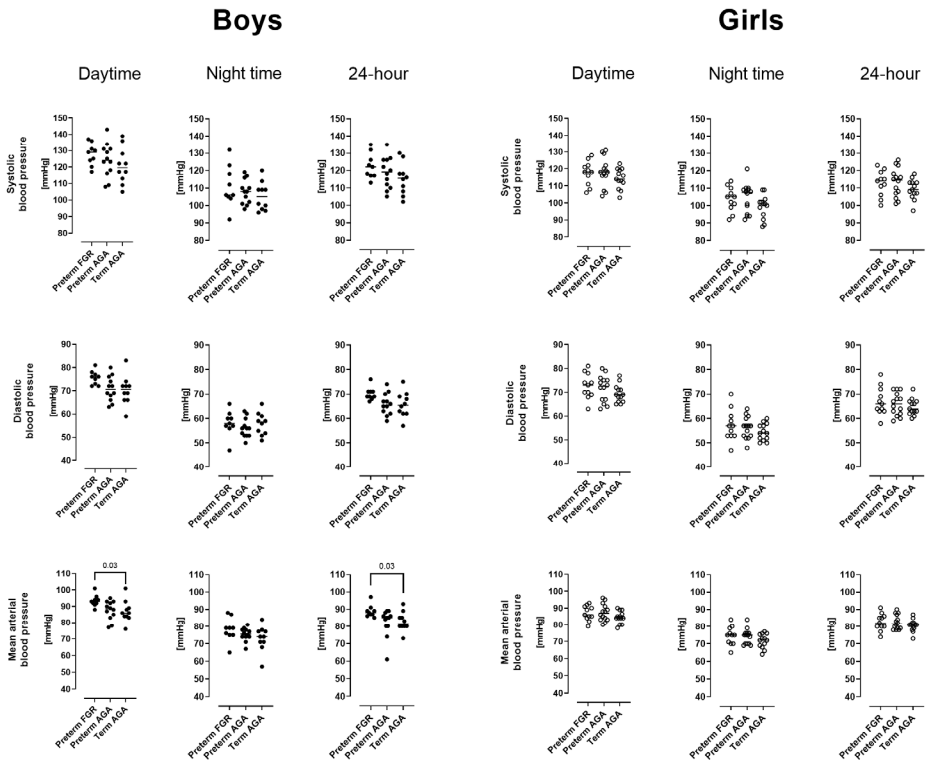

Figure 4.7 24-hour ambulatory blood pressure measurements. Systolic (**upper row**), diastolic (**middle row**) and mean arterial blood pressure (**lower row**) in boys (**left panel**) and girls (**right panel**) for daytime (**left column**), nighttime (**middle column**) and for 24-hour measurements (**right column**). For boys, median daytime and 24-hour mean arterial blood pressures were higher in the preterm FGR group as compared to the term AGA group ((93 (88-101 mmHg) vs 86 (76-101 mmHg); p = 0.03) and (88 (85-97 mmHg) vs 82 (73-93mmHg); p = 0.03, respectively)). FGR=fetal growth restriction, AGA=birth weight appropriate for gestational age. Lines indicate median. *To be published in Pediatric Research. Accepted manuscript. The article will be published open access under a CC BY 4.0 license (Creative Commons Attribution 4.0 International license).*

Table 4.3 24-hour ambulatory blood pressure measurements.

	Preterm FGR *n=20*	Preterm AGA *n=27*	Term AGA *n=23*	P values
Daytime				
Systolic blood pressure				
Prehypertensive (n (%))	1 (5%)	2 (7%)	0	0.63
Hypertensive (n (%))	2 (10%)	4 (15%)	1 (4%)	0.48
Diastolic blood pressure				
Prehypertensive (n (%))	2 (10%)	1 (4%)	1 (4%)	0.68
Hypertensive (n (%))	0	0	0	N/A
Night-time				
Systolic blood pressure				
Prehypertensive (n (%))	2 (10%)	0	0	0.08
Hypertensive (n (%))	3 (15%)	1 (4%)	0	0.1
Diastolic blood pressure				
Prehypertensive (n (%))	1 (5%)	0	0	0.29
Hypertensive (n (%))	1 (5%)	0	1 (4)	0.52
Nocturnal dip (<10%)	3 (15%)	3 (11%)	2 (9%)	0.9

Data are presented as number (%). FGR=fetal growth restriction, AGA=birth weight appropriate for gestational age, N/A=not applicable. *To be published in Pediatric Research. Accepted manuscript. The article will be published open access under a CC BY 4.0 license (Creative Commons Attribution 4.0 International license).*

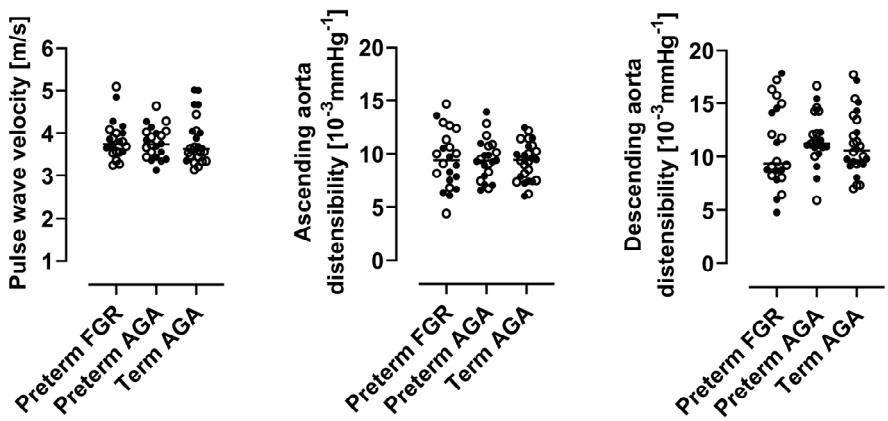

Figure 4.8 Thoracic aortic pulse wave velocity and aortic distensibility. Pulse wave velocity (**left graph**), distensibility in the ascending aorta (**middle graph)** and distensibility in the descending aorta at diaphram level (**right graph**). Closed circles indicate boys and open circles indicate girls. For girls, median pulse wave velocity was higher in preterm AGA group as compared to the term AGA group (3.9 m/s vs 3.5 m/s; p = 0.04). FGR=fetal growth restriction, AGA=birth weight appropriate for gestational age. Lines indicate median. *To be published in Pediatric Research. Accepted manuscript. The article will be published open access under a CC BY 4.0 license (Creative Commons Attribution 4.0 International license).*

4.4 Study IV: Cardiac morphology and function

In this paper measures of cardiac morphology and function were assessed in adolescents born very preterm due to early onset fetal growth restriction and compared with the two control groups born with appropriate birth weight, one in similar gestation and one born at term. Twenty-two participants in the preterm FGR group, 22 in the preterm AGA group and 26 in the term AGA group were included for analysis.

4.4.1 Cardiac volumes

Figure 4.9 and Table 4.4 shows cardiac volumes. Adolescents born very preterm AGA showed smaller left (80 vs 88 ml/m^2; p = 0.02) and right (85 vs 97 ml/m^2; p = 0.03) ventricles compared to term AGA. No differences were observed between preterm FGR and term AGA for the left or right ventricle, respectively (82 vs 88 ml/m^2; p = 0.39, and 94 vs 97 ml/m^2; p = 0.82). Left ventricular mass was not different between preterm FGR, preterm AGA, and term AGA (47 vs 43 vs 47 ml/m^2; p=0.22). The preterm FGR group showed smaller median right atrial end-diastolic volumes (46 vs 54 ml/m^2; p = 0.045) as compared to the term AGA group.

Total heart volume did not differ between groups (all $p \geq 0.2$) and simple linear regression showed that THV was dependent on BSA in the respective group; preterm FGR ($R^2 = 0.70$, $p < 0.0001$), preterm AGA ($R^2 = 0.74$, $p < 0.0001$), and term AGA ($R^2 = 0.71$, $p < 0.0001$).

Sex stratification indicated that differences in cardiac volumes as shown above for the whole group might be driven by differences in girls. Girls born preterm AGA had smaller left ventricular end-diastolic volumes (80 ml/m^2 (71 – 88 ml/m2) vs 88 ml/m^2 (73 – 101 ml/m^2); p = 0.04) and right ventricular end-diastolic volumes (84 ml/m2 (74 – 92 ml/m^2) vs 96 ml/m^2 (80 – 113 ml/m^2); p = 0.01) and end-systolic volumes (38 ml/m^2 (32 – 51 ml/m^2) vs 44 ml/m^2 (39 – 55 ml/m^2); p = 0.03) as compared to the term AGA group, and smaller right ventricular end-systolic volumes as compared to the preterm FGR group (38 ml/m^2 (32 – 51 ml/m^2) vs 45 ml/m^2 (30 – 62 ml/m^2);p = 0.04).

For boys, left ventricular mass normalized for THV were higher in the preterm FGR group (0.15 g (0.13 – 0.18g) as compared to the term AGA group (0.13 g (0.11 – 0.14g); p < 0.001). No other differences were observed for boys.

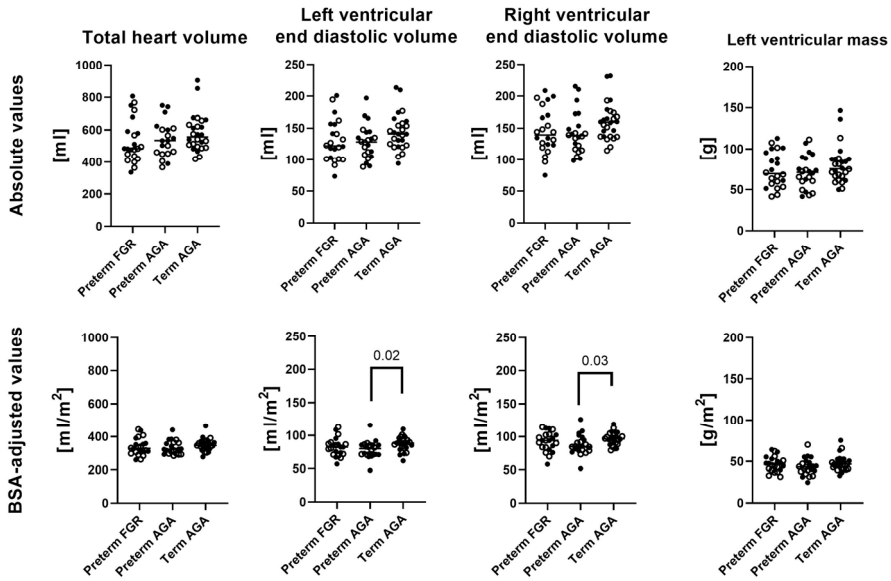

Figure 4.9 Cardiac volumes.
Absolute cardiac volumes (**upper row**) and BSA-adjusted values (**lower row**) for the three groups. Closed circles indicates boys and open circles indicates girls. Left and right end-diastolic BSA-adjusted volumes were lower in the preterm AGA group as compared to term AGA group (80 vs 88 ml/m^2;p=0.03, and 85 vs 97 ml/m^2;p = 0.03, respectively). FGR=fetal growth restriction, AGA=birth weight appropriate for gestational age. Lines indicate median.

4.4.2 Cardiac function

Table 4.4 shows planimetrically derived cardiac functional measures and Table 4.5 and Figure 4.10 shows measures of left and right cardiac function. Ejection fraction for the left and right ventricle was for preterm FGR (55% and 51%), for preterm AGA (56% and 52%) and for the term AGA group (54% and 52%), with no differences between groups for the left (p = 0.33) or right (p = 0.46) ventricle, respectively.

Atrioventricular plane displacement and longitudinal and radial contribution to stroke volume did not differ between groups for the left (all p ≥ 0.17) or right ventricle (all p ≥ 0.07) (Figure 4.10).

4.4.3 NT-proBNP

NT-proBNP was for preterm FGR 26 ng/l (5 – 80 ng/l), for preterm AGA 28 ng/l (14 – 87 ng/l) and for term AGA 18 ng/l (5 – 87 ng/l) with no difference between groups (p = 0.73).

Table 4.4 Cardiac volumes

	Preterm FGR n = 22	Preterm AGA n = 22	Term AGA n = 26	P values Between all groups	Preterm FGR vs Preterm AGA	Preterm FGR vs Term AGA	Preterm AGA vs Term AGA
Total heart volume	484 (336 – 807)	535 (368 – 751)#	557 (420 – 905)	0.2			
Total heart volume/BSA	329 (260 – 445)	324 (285 – 441)#	346 (278 – 465)	0.27			
Left ventricle							
LVM (g)	70 (42 – 113)	71 (42 – 112)	76 (50 – 147)	0.48			
LVM/BSA (g/m²)	47 (32 – 64)	43 (25 – 70)	47 (33 – 75)	0.22			
LVM/THV	0.14 (0.1 – 0.18)	0.13 (0.11 – 0.19)	0.14 (0.1 – 0.17)	0.07*			
LVEDV (ml)	122 (74 – 201)	128 (89 – 197)	141 (94 – 213)	0.11			
LVEDV/BSA (ml/m²)	82 (57 – 113)	80 (47 – 116)	88 (62 – 110)	0.02¤	1	0.26	0.02
LVEDV/THV	0.25 (0.21 – 0.27)	0.24 (0.21 – 0.28)	0.25 (0.2 – 0.27)	0.12			
LVESV (ml)	56 (33 – 101)	52 (37 – 92)	64 (37 – 97)	0.049	1	0.39	0.049
LVESV/BSA (ml/m^2)	36 (25 – 55)	34 (23 – 54)	41 (24 – 50)	0.03	0.37	0.88	0.02
LVESV/THV	0.11 (0.09 – 0.14)	0.1 (0.09 – 0.13)	0.11 (0.08 – 0.13)	0.06			
LVSV (ml)	68 (41 – 104)	70 (46 – 105)	78 (54 – 117)	0.12			
LVSV/BSA (ml/m^2)	44 (32 – 61)	42 (24 – 62)	47 (37 – 60)	0.24			
LVEF (%)	55 (46 – 62)	56 (51 – 69)	54 (46 – 62)	0.33			
CO (l/min)	4.9 (2.4 – 7.9)	5.1 (2.8 – 7.8)	5.4 (3.7 –9.2)	0.5			
CI (l//min/m^2)	3.3 (1.6 – 4.6)	3.1 (1.7 – 4.4)	3.2 (2.4 – 5.2)	0.85			
CO/THV	0.01 (0.005 –0.01)	0.009 (0.007 – 0.01)	0.01 (0.007 –0.01)	0.94			
Heart rate (bpm)	76 (44 – 93)	75 (48 – 128)	76 (57 – 99)	0.76			
Right ventricle							
RVEDV (ml)	140 (75 – 209)	138 (99 – 215)	159 (115 – 232)	0.09			
RVEDV/BSA (ml/m²)	94 (58 – 114)	85 (52 – 126)	97 (80 – 119)	0.03¤	0.45	0.82	0.03
RVEDV/THV	0.27 (0.22 – 0.32)	0.27 (0.23 – 0.3)	0.28 (0.24 – 0.31)	0.17			
RVESV (ml)	68 (41 – 122)	62 (42 – 110)	75 (55 – 128)	0.09			
RVESV/BSA (ml/m²)	46 (30 – 66)	40 (24 – 64)	44 (38 – 66)	0.06¤			
RVESV/THV	0.13 (0.1 – 0.17)	0.13 (0.09 – 0.15)	0.14 (0.11 – 0.15)	0.053¤			
RVSV (ml)	73 (31 – 107)	73 (49 – 112)	80 (58 – 112)	0.09			

				P values			
	Preterm FGR n = 22	**Preterm AGA n = 22**	**Term AGA n = 26**	**Between all groups**	**Preterm FGR vs Preterm AGA**	**Preterm FGR vs Term AGA**	**Preterm AGA vs Term AGA**
RVSV/BSA (ml/m2)	47 (24 – 61)	46 (28 –62)	51 (41 – 58)	0.13			
RVEF (%)	51 (41 – 63)	52 (42 – 62)	52 (43 – 59)	0.46			
Left atrium							
LAEDV (ml)	22 (13 – 39)	26 (12 – 36)	24 (13 – 37)	0.23			
LAEDV/BSA (ml/m²)	15 (10 – 23)	16 (8 – 21)	15 (9 – 19)	0.59			
LAEDV/THV	0.04 (0.03 – 0.05)	0.05 (0.03 – 0.06)	0.04 (0.03 – 0.05)	0.09¤			
LAESV (ml)	52 (23 – 82)	58 (34 – 87)	56 (35 – 92)	0.36			
LAESV/BSA (ml/m²)	33 (18 – 47)	38 (25 – 45)	35 (27 – 45)	0.6			
LAESV/THV	0.1 (0.07 – 0.14)	0.11 (0.08 – 0.14)	0.1 (0.08 – 0.12)	0.14			
Right atrium							
RAEDV (ml)	38 (17 – 77)	41 (24 – 61)	46 (31 – 69)	0.18			
RAEDV/BSA (ml/m²)	24 (13 – 42)	26 (17 – 36)	28 (19 – 39)	0.14			
RAEDV/THV	0.07 (0.05 – 0.12)	0.07 (0.06 – 0.1)	0.08 (0.06 – 0.1)	0.39			
RAESV (ml)	72 (28 –135)	75 (47 – 107)	81 (65 – 138)	0.04	0.8	0.03	0.51
RAESV/BSA (ml/m²)	46 (21 – 73)	47 (32 – 64)	54 (40 – 71)	0.02	1	0.045	0.06
RAESV/THV	0.14 (0.08 – 0.17)	0.14 (0.1 – 0.18)	0.15 (0.12 – 0.18)	0.04	1	0.03	0.31

n=20, for all of the measures in the preterm AGA group adjusted for THV, * and ¤ indicate differences for boys and girls, respectively (data presented in results). FGR = fetal growth restriction. AGA = birth weight appropriate for gestational age, BSA=body surface area, LV=Left ventricle, LVM=left ventricular mass, EDV=end diastolic volume, ESV=end systolic volume, THV=total heart volume, SV=stroke volume, CO=cardiac output, CI=cardiac index, EF=Ejection fraction, bpm=beats per minute, RV=right ventricle, LA=left atrium, RA=Right atrium.

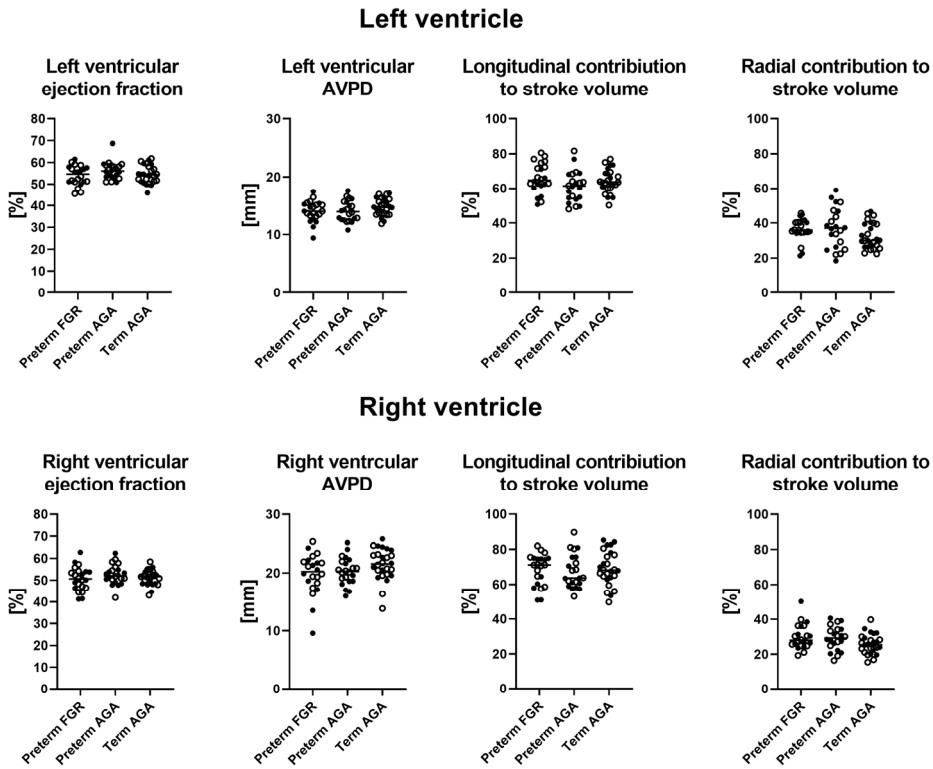

Figure 4.10 Measures of cardiac function.
Left ventricular function (**upper row**) and right ventricular function (**lower row**) in the three groups. Closed circles indicates boys and open circles indicates girls. There were no differences in any measure of cardiac function (all $p \geq 0.07$) FGR=fetal growth restriction, AGA=birth weight appropriate for gestational age. Lines indicate median.

Table 4.5 Longitudinal and radial contribution to stroke volume.

	Preterm FGR *n = 22*	**Preterm AGA** *n = 22*	**Term AGA** *n = 26*	**P between groups**
Left ventricle				
LV_{AVPD} (mm)	14 (9 – 17)	14 (11 – 18)	15 (12 – 17)	0.24
LV_{AVPD} (ratio)	0.15 (0.11 – 0.17)	0.15 (0.11 – 0.21)	0.16 (0.12 – 0.18)	0.77
SV_{Long} (ml)	44 (27 – 71)	42 (30 – 67)	48 (33 – 78)	0.08
SV_{Long} (%)	65 (51 – 81)	61 (48 – 82)	64 (50 – 77)	0.17
SV_{Sept} (ml)	5.2 (0.2 –15.9)	6 (0.2 – 9.6)	5.2 (0.43 – 13.8)	0.91
SV_{Sept} (%)	8 (0 – 18)	8 (0 – 14)	7 (1 – 14)	0.78
SV_{Lat} (ml)	21 (9 – 32)	22 (9 – 41)	19 (10 – 35)	0.84
SV_{Lat} (%)	32 (20 – 39)	31 (12 – 59)	24 (17 – 42)	0.14
Right Ventricle				
RV_{AVPD} (mm)	20 (10 – 25)	20 (16 –25)	22 (14 – 26)	0.13
RV_{AVPD} (ratio)	0.22 (0.13 – 0.29)	0.22 (0.17 – 0.3)	0.24 (0.16 – 0.27)	0.35
SV_{LONG} (ml)	54 (16–76)	50 (30 – 83)	56 (32 – 85)	0.22
SV_{Long} (%)	71 (51 –82)	64 (53 – 90)	68 (50 –85)	0.71
RV_{Lat} (ml)	21 (14 – 37)	22 (11 – 30)	29 (11 – 41)	0.81
RV_{Lat} (%)	28 (19 – 50)	29 (16 – 41)	25 (15 –40)	0.07

FGR=fetal growth restriction, AGA=birth weight appropriate for gestational age, LV=Left ventricle, AVPD=atrioventricular plane displacement, SV=stroke volume, long=longitudinal contribution to stroke volume, sept=septal contribution to stroke volume, lat=lateral contribution to stroke volume, RV=right ventricle.

4.5 Study V: Kidney volumes and function

In this study, measures of kidney volume and function were assessed in adolescents born very preterm due to early onset fetal growth restriction and compared with the two control groups born with appropriate birth weight, one in similar gestation and one born at term. In this study, the newly validated non-contrast-enhanced MRI method from study I was implemented and biochemical markers in blood and urine of kidney function and RAAS-activation were sampled.

4.5.1 Kidney volumes

Figure 4.11 and Table 4.6 shows total kidney-, cortical- and medullary volumes in absolute and BSA-adjusted values. Total kidney volume and medullary volume were smaller in the preterm FGR group as compared to the term AGA group, (66 vs 75 ml/m^2; p = 0.01) and (19 vs 24 ml/m^2; p < 0.0001), respectively. Further, medullary volume was smaller in the preterm FGR group as compared to the preterm AGA group (19 vs 23 ml/m^2; p = 0.02). Trend analyses showed a decrease in median total kidney volume (75 vs 73 vs 66 ml/m^2; p = 0.02) and medullary volume (24 vs 23 vs 19 ml/m^2; p = 0.001) from term AGA to preterm AGA to preterm FGR.

The preterm FGR group showed a higher corticomedullary volume ratio as compared to the term AGA group (2.4 vs 1.9; p = 0.01). The corticomedullary volume ratio decreased from preterm FGR (2.4) to preterm AGA (2.2) to term AGA (1.9; p=0.004) for both sexes combined and for boys (p = 0.02) and girls (p = 0.04), separately.

When stratifying for sex, no group differences in kidney volumes were observed after adjusting for BSA in boys (all p ≥ 0.08). Girls born preterm FGR had smaller median total kidney volume (65 vs 76 ml/m^2; p = 0.001), smaller cortical volume (44 vs 50 ml/m^2; p = 0.03), and smaller medullary volume (19 vs 26 ml/m^2; p < 0.0001) as compared to the term AGA group. Further, in girls, trend analyses showed smaller total (65 vs 72 vs 76 ml/m^2; p=0.004), cortical (44 vs 47 vs 50 ml/m^2; p=0.045) and medullary (19 vs 23 vs 26 ml/m^2; p=0.001) volumes for preterm FGR vs preterm AGA vs term AGA, respectively.

BSA adjusted kidney volumes were compared within the respective group and sex differences was only observed in the preterm FGR group, with girls showing smaller median total kidney volume (95 vs 116 ml; p = 0.049), cortical volume (66 vs 86 ml; p = 0.003) and BSA-adjusted cortical volume (44 vs 51 ml/m^2; p=0.02) compared to boys. No sex differences were observed in either absolute or BSA-adjusted kidney volumes in the other groups (all p ≥ 0.13).

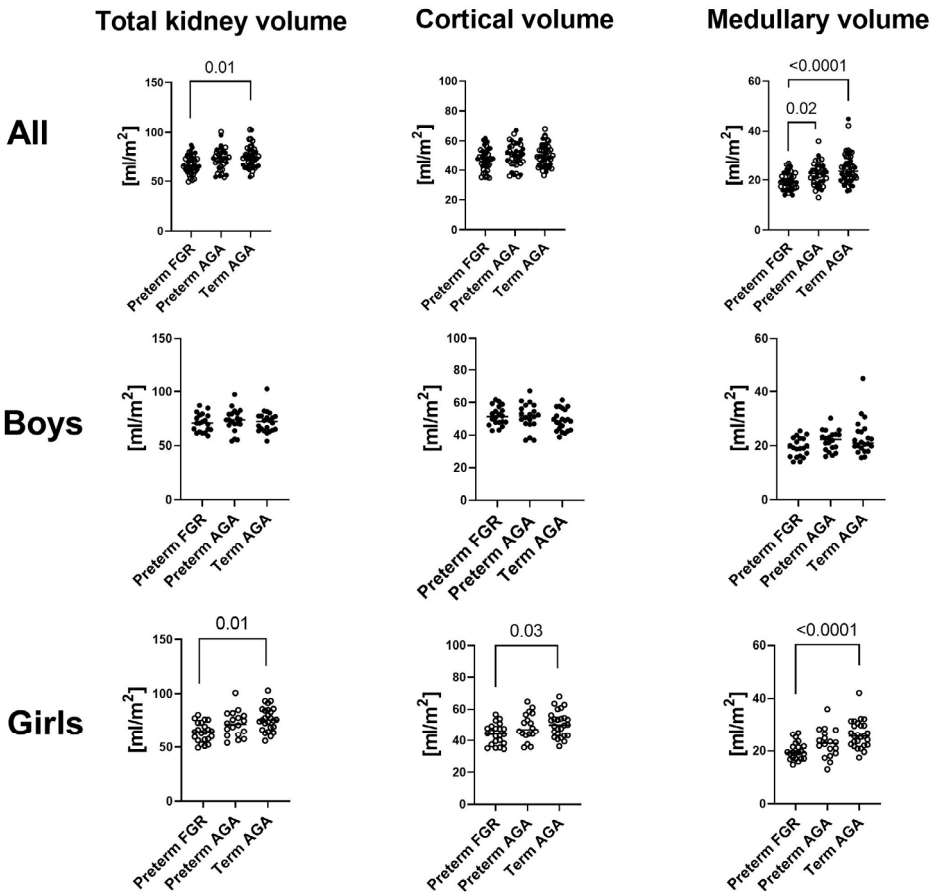

Figure 4.11 Kidney volumes adjusted for body surface area.
Total kidney volume (**left column**), cortical volume (**middle column**) and medullary volume (**right column**) for all individuals (**upper row**), and stratified for boys (**middle row**) and girls (**lower row**) in adolescents born very preterm due to fetal growth restriction (preterm FGR), very preterm with appropriate birth weight (preterm AGA) and at term after a healthy pregnancy (term AGA). Fetal growth restriction was assoiated with smaller total kidney volumes as compared to the term AGA group and smaller medullary volumes as compared to the preterm and term AGA groups, mostly driven by lower volumes in girls. FGR=fetal growth restriction, AGA=appropriate for gestational age.

Table 4.6 Kidney volumes and parenchymal T1 and T2* values.

	Preterm FGR	Preterm AGA	Term AGA	P Between groups	P Preterm FGR vs Preterm AGA	P Preterm FGR vs Term AGA	P Preterm AGA vs Term AGA	P Trend across groups
All	*n=21*	*n=19*	*n=24*					
Total parenchymal volume (ml)	105 (66 – 161)	121 (74 – 180)	122 (80 – 177)	**0.004**	0.06	**0.004**	>0.99	**0.02**
Total parenchymal volume (ml/m²)	66 (50 – 87)	73 (54 – 101)	75 (54 – 103)	**0.01**	0.12	**0.01**	>0.99	**0.02**
Cortical volume (ml)	77 (45 – 114)	84 (49 – 124)	82 (52 – 133)	0.1	N/A	N/A	N/A	0.24
Cortical volume (ml/m²)	48 (35 – 62)	51 (36 – 67)	50 (36 – 68)	0.34	N/A	N/A	N/A	0.41
Medullary volume (ml)	30 (20 – 48)	36 (20 – 57)	38 (27 – 71)	**<0.0001**	**0.01**	**<0.0001**	0.2	**0.0002**
Medullary volume (ml/m²)	19 (14 – 27)	23 (13 – 34)	24 (16 – 45)	**<0.0001**	**0.02**	**<0.0001**	0.33	**0.001**
Corticomedullary ratio	2.41 (1.97 – 3.51)	2.23 (1.62 – 3.14)	1.91 (1.47 – 2.95)	**0.018**	0.77	**0.014**	0.34	**0.004**
Boys	*n=10*	*n=10*	*n=11*					
Total parenchymal volume (ml)	116 (80 – 161)	125 (74 – 180)	124 (94 – 177)	0.31	N/A	N/A	N/A	0.45
Total parenchymal volume (ml/m²)	71 (59 – 87)	74 (54 – 97)	72 (54 – 103)	0.7	N/A	N/A	N/A	0.66
Cortical volume (ml)	86 (60 – 114)	87 (49 – 124)	85 (66 – 133)	0.54	N/A	N/A	N/A	0.91
Cortical volume (ml/m²)	51 (43 – 62)	52 (37 – 67)	49 (39 – 62)	0.34	N/A	N/A	N/A	0.33
Medullary volume (ml)	30 (20 – 47)	38 (25 – 56)	37 (27 – 71)	**0.02**	0.1	**0.03**	>0.99	0.0503
Medullary volume (ml/m²)	19 (14 – 25)	22 (16 – 30)	21 (16 – 45)	0.08	N/A	N/A	N/A	0.14
Corticomedullary ratio	2.79 (2.1 – 3.5)	2.28 (1.95 – 3.1)	2.2 (1.47 – 2.95)	0.07	N/A	N/A	N/A	**0.019**
Girls	*n=11*	*n=9*	*n=13*					
Total parenchymal volume (ml)	95 (66 – 140)	106 (82 – 160)	121 (80 – 154)	**0.002**	**0.021**	**0.001**	0.37	**0.008**
Total parenchymal volume (ml/m²)	65 (50 – 80)	72 (54 – 101)	76 (56 – 103)	**0.002**	0.15	**0.001**	0.53	**0.004**
Cortical volume (ml)	66 (45 – 92)	70 (51 – 103)	80 (52 – 104)	**0.02**	0.22	**0.02**	>0.99	**0.041**
Cortical volume (ml/m²)	44 (35 – 57)	47 (36 – 65)	50 (36 – 68)	**0.03**	0.18	**0.03**	>0.99	**0.045**
Medullary volume (ml)	29 (21 – 48)	33 (20 – 57)	39 (27 – 63)	**<0.0001**	0.23	**<0.0001**	0.054	**0.001**

	Preterm FGR	Preterm AGA	Term AGA	Between groups	P Preterm FGR vs Preterm AGA	P Preterm FGR vs Term AGA	P Preterm AGA vs Term AGA	P Trend across groups
Medullary volume (ml/m²)	19 (15 – 27)	23 (13 – 36)	26 (17 – 42)	**0.0001**	0.17	**<0.0001**	0.13	**0.001**
Corticomedullary ratio	2.09 (1.97 – 2.64)	2.07 (1.62 – 3.13)	1.81 (1.51 – 2.64)	0.1	N/A	N/A	N/A	**0.038**
T1 values	*n = 19*	*n = 19*	*n = 22*					
T1 cortex (ms)	1,032 (927 – 1,311)	1,056 (926 – 1,137)*	1,034 (970 – 1,165)	0.34	N/A	N/A	N/A	0.50
T1 medulla (ms)	1,574 (1,478 – 1,712)	1,568 (1,455 – 1,703)	1,600 (1,389 – 1,692)	0.39	N/A	N/A	N/A	0.56
Corticomedullary T1 differentiation (%)	64 (54 – 71)	67 (62 – 73)	65 (58 – 81)	0.08	N/A	N/A	N/A	0.62
T2* values	*n = 21*	*n = 19*	*n = 21*					
T2* Cortex (ms)	76 (70 – 90)	79 (64 – 83)	76 (63 – 84)	0.51	N/A	N/A	N/A	0.37
T2*parenchyma (ms)	76 (68 – 88)	77 (63 – 87)	77 (65 – 87)	0.99	N/A	N/A	N/A	0.89

Data presented as median (range). Renal parenchymal volumes are presented in absolute and BSA-adjusted values. * Indicates differences between groups for girls (data presented in Results). FGR = fetal growth restriction, AGA = appropriate for gestational age.

4.5.2 Renal T1 and T2* mapping

Table 4.6 shows renal T1 and T2* mapping values for the three groups. There were no differences in renal T1 or T2* mapping values between groups (all $p \geq 0.34$) or for corticomedullary T1 differentiation (all $p \geq 0.08$). When stratifying for sex, girls born preterm AGA showed higher cortical T1 values (1086 ms) as compared to the preterm FGR group (1037 ms; $p = 0.02$) and to the term AGA group (1027 ms; $p = 0.03$). Girls born preterm AGA also showed higher median corticomedullary T1 differentiation compared to the preterm FGR group (67 vs. 64%; $p = 0.005$). With no group differences observed for boys (all $p \geq 0.29$).

4.5.3 Biochemical markers

Table 4.7 shows biochemical markers of kidney function and RAAS activation. When stratifying for sex, boys in the preterm AGA group showed a lower median IgG/creatinine index compared to the term AGA group (0.35 vs 0.78 g/mol; $p = 0.04$).

Table 4.7 Biochemical markers

	Preterm FGR	Preterm AGA	Term AGA	P Between groups	Reference values
	n = 17	*n = 15*	*n = 23*		
eGFR (Cystatin C) ml/min/1.73m^2	91 (68 – 114)	102 (76 – 133)	100 (76 – 122)	0.2	86 – 134 ml/min/1.73m2
eGFR (Creatinine) ml/min/1.73m^2	97 (76 – 127)	89 (64 – 126)	99 (74 – 140)	0.31	86 – 134 ml/min/1.73m2
eGFR (Average) ml/min/1.73m^2	92 (81 – 119)	92 (75 – 127)	99 (85 – 125)	0.46	86 – 134 ml/min/1.73m2
P-Renin [mIE/L]	31 (10 – 74)	28 (6 – 68)	31 (8 – 72)	0.75	5 – 80 [mIE/L][1]
	n = 19	*n = 17*	*n = 23*		
U-Albumin/Creatinine [g/mol]	0.61 (0.13 – 7.35)	0.34 (0.08 – 7.53)	0.9 (0.05 – 14.54)	0.09	< 3.0 g/mol[1]
U-Albumin/Creatinine [mg/g]	54 (11 – 650)	30 (7 – 666)	79 (5 – 1285)	0.09	< 30 mg/g[1]
U-IgG/Creatinine [g/mol]	0.43 (0.16 – 2.11)	0.33 (0.18 – 0.76)*	0.57 (0.23 – 2.56)	0.051	< 0.8 g/mol
U-Kappa/Creatinine [g/mol]	0.09 (0.03 – 0.57)	0.12 (0.03 – 0.59)	0.14 (0.07 – 0.84)	0.14	< 0.6 g/mol
U-Lambda/Creatinine [g/mol]	0.01 (0 – 0.18)	0.02 (0 – 0.06)	0.02 (0 – 0.3)	0.64	< 0.6 g/mol
U-AGT/Creatinine ([ng/ml/ [µmol/L])	0.73 (0.24 – 2.29)	0.48 (0 – 1.6)	0.55 (0 – 7.5)	0.53	N/A

Data are presented as median (range).[1] Indicates reference values for morning samples. * Indicates lower values for boys born preterm AGA compared to term AGA (0.35 (0.23 – 0.74) vs 0.78 (0.23 – 1.74); p=0.04. GFR=glomerular filtration rate, IgG=Immunoglobulin gamma, AGT angiotensinogen, FGR=fetal growth restriction, AGA=appropriate for gestational age. *Manuscript accepted, Pediatric Nephrology. The article will be published under a CC BY 4.0 license, http://creativecommons.org/licenses/by/4.0/.*

Fetal growth restriction followed by very preterm birth is associated with smaller kidneys but preserved kidney function in adolescence

Graphical Abstract

HYPOTHESIS: Very preterm birth due to fetal growth restriction verified by abnormal fetal blood flow velocimetry is associated with structural and functional kidney changes in adolescence.

DESIGN & OUTCOMES:

A prospective cohort study in adolescence

- Term AGA (healthy controls) n = 24
- Very preterm AGA n = 19
- Very preterm FGR n = 21

Non-contrast enhanced MRI

Blood and urine

Normal kidney function
No RAAS activation

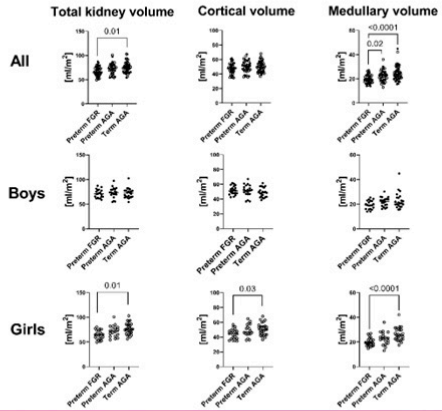

CONCLUSION: Fetal growth restriction is associated with reduced kidney volumes, but not with kidney dysfunction or markers of RAAS activation in adolescence.

Liefke et al. 2022

Pediatric Nephrology
Journal of the International Pediatric Nephrology Association
IPNA

5 Discussion

5.1 Study I

The current study validated the proposed non- contrast enhanced MRI method and showed that it is accurate and precise in quantifying cortical and medullary volumes in pigs and that intra- and interobserver variability is low in both pigs and in humans.

The method is widely available, and accuracy and precision were similar between observers with intermediate and high level of experience. The method could thus be implemented clinically and in research where ionizing radiation or contrast is preferred to be avoided. This might be especially important in pediatric populations or populations who either have renal failure or who will undergo serial assessment of kidney volumes.

This study enabled *Study V* in which the non-contrast enhanced MRI method was implemented to investigate whether very preterm birth due to fetal growth restriction (FGR) verified by abnormal fetal blood flow velocimetry is associated with alterations in kidney structure in adolescence.

5.1.1 Method comparison

This study is the first to validate quantification of medullary parenchymal volumes using non-contrast enhanced MRI. The current study shows similar or lower variability in quantification of total parenchymal and cortical volumes as compared to previous studies using contrast-enhanced MRI or advanced post-processing techniques (236,237). The current study thus adds to the previous studies in that MRI can be used for accurate volumetric quantification of kidney volumes, also when applying a widely available sequence without contrast administration.

For accurate and precise quantification of kidney volumes using MRI, the gold standard volumetric method should be used (206,236,238). The method is similar to cardiac volumetry, using planimetry for volume assessment (183) (*study IV)*. However, ultrasound is commonly used for the assessment of kidney volumes in both in the clinical setting and in research. The acoustic window of ultrasound does not enable visualization and quantification of the entire kidney parenchyma. Instead, kidney length and width are used to estimate kidney volume using the ellipsoid shape as reference. Although group comparisons might be made with this method, the accuracy and precision is limited and repeatability is substantially lower as

compared to the gold standard MRI method, also when input variables are measured with MRI (204,206).

Intra and interobserver variability were in the current study low for both pig and human kidney volume assessment. Previous studies, also using non-contrast enhanced MRI, show similar observer variability for total kidney volume and cortical volume assessment, while medullary measurements showed slightly higher variability using an automated algorithm (204,208,239). The study strengthens the findings of these previous studies and further enables the use of MRI for both cortical and medullary volume quantification in the clinical setting.

Manual delineations of cortical and medullary boundaries for the assessment of volumes are used in the current study. The use of semi- or fully automated methods for parenchymal volume assessment show higher variability but may, if widely available, increase the applicability of kidney volume quantification using non-contrast enhanced MRI clinically, mainly by lessening time for analysis (239,240). New methods for automatic analysis are being developed and a study, using a fully automated method, based on a convolutional neural network for total kidney volume quantification in CKD patients, showed high agreement with manual assessment and higher repeatability as compared to manual assessment, although assessing images <10s (241). However, for accurate and precise quantification of cortical and medullary volumes, manual delineation is at present time the only available option.

5.1.2 Clinical aspects

The worldwide prevalence of CKD is 11-13%, with diabetes and hypertension being the main contributors (164). Both of these diseases impact kidney volumes as well as function, and the prevalence is rising steadily (165,166). Kidney volume change has been observed in several diseases and often shows prognostic value, also in the absence of kidney dysfunction. Diabetic nephropathy induces initial renal hypertrophy and large diabetic kidneys have indeed been shown to be prognostic of future renal functional decline (242,243). Total kidney volume is suggested to be a valuable biomarker in measuring CKD progression, often showing smaller kidneys with declining function, and in renal transplant sequele where hypertrophy of the renal parenchyma is associated with increased renal function of the remaining kidney (238,244). In addition, studies also show that prematurity with or without birth weight deviation, associate with smaller kidney volumes from infancy (201,245) throughout life (108,109,113,114,246). A major limitation is the use of ultrasound for volume assessment, showing low accuracy and repeatability (204,206) and lacking the ability to quantify cortical and medullary volumes.

In summary, the current study shows that cortical and medullary volumes can be quantified using a widely available non-contrast enhanced MRI method with high accuracy and precision. As cortical and medullary volumes associate differently with age, kidney function and common risk markers of chronic kidney disease (CKD) (198), separate quantification of cortical and medullary volumes might well

be warranted. This validation work thus increases availability of separate cortical and medullary quantification and can be directly implemented both clinically and in research.

5.2 Study II

This study showed the required temporal resolution needed for accurate measurements of pulse wave velocity (PWV) in neonates and adolescents, respectively. The study further showed that a dedicated 3D angiography of the aorta should be used for vessel length measurements and that the time-to-foot method should be used to calculate the transit time for accurate and reliable measurements of PWV.

This study enabled *Study III* in which the method was implemented to investigate whether very preterm birth due to FGR verified by abnormal fetal blood flow velocimetry is associated with alterations arterial stiffness in adolescence.

5.2.1 Method comparison

Although PWV measurement's using MRI agrees with invasive measurements (186), lack of standardization hinders widespread clinical implementation (229,247). And further, for comparison with reference values, several potential differences in methodology need to be considered. In the validation study by Grotenhuis et al. (186), flow measurements were acquired with a temporal resolution of 6-10ms, and PWV was calculated using the time to foot method without baseline correction based on oblique sagittal images covering the entire aorta (186).

The current study showed that 3D angiography, similar to the images used in the validation paper by Grotenhuis et al. (186), should be used to calculate pulse wave travelling distance. The time to foot method, also used in the validation paper, showed the lowest limits of agreement of the compared and commonly used methods. The study further showed the temporal resolution needed for accurate PWV assessment, depending on vessel length and the pulse wave velocity. Pulse wave velocity varies depending on both age and thus biometry of the patient and also depending on which segment of the aorta that is being measured, e.g., the aortic arch or the entire thoracic aorta. Flow measurements should be acquired with at least 42 and 41 timeframes per cardiac cycle in the neonatal aortic arch and thoracic aorta, respectively, and 39 and 32 timeframes per cardiac cycle for corresponding vessel segments in adolescents. This corresponds to typical temporal resolutions of 10 ms, 11 ms, 21 ms, and 26 ms, respectively.

For clinical implementation, normal values for PWV are needed, and have been published for both children and young adults (247,248). Both studies used one

imaging plane for acquisition of blood flow in the ascending and descending aorta, respectively, but used different transit time methods for PWV measurements. Voges et al. publishing reference values throughout childhood to young adulthood (247), used the maximum upslope method while Caterini et al. assessing PWV in adolescents (248), used the time to half peak method. In the current study, although showing wider limits of agreement, the maximum upslope method showed similar pulse wave velocities compared to the time to foot method indicating that these measures can be used interchangeably. The PWV values acquired with the time to peak method was similar to the values presented for the time to half peak by Caterini et al. (248). As this method showed unphysiological values for the neonate population and significantly different PWV values as compared to the other methods, this method might not be reliable for all age ranges and is not interchangeable with the other two tested methods.

Data not published for the current study suggest that PWV is higher in the segment between the ascending and descending aorta as compared to measurements in the ascending to abdominal aorta. As the current study and the other two studies uses different segments of the aorta, the actual pulse wave velocities are likely not completely interchangeable. Further, applying a dedicated flow acquisition for the respective vessel is preferable as flow quantification is most accurate when the imaging plane is perpendicular to the flow (249,250).

5.2.2 Clinical aspects

Pulse wave velocity is a surrogate marker of arterial stiffness and is an independent predictor of cardiovascular morbidity and mortality (103,251,252). Arterial stiffness is in turn dependent on the atherosclerotic process in the vessel walls, gradually developing with increasing age. The atherosclerotic process begins in childhood and adolescence but the prevalence and extent increases with age and in the presence of well-known risk factors of increased arterial stiffness, such as smoking and diabetes (153–155). In addition, preterm birth and low birth weight are associated with increased arterial stiffness and increases can be observed already in childhood and adolescence (91,253–255). Applanation tonometry can be used to assess PWV (256) but lacks the ability to accurately measure vessel length resulting in non-interchangeable values as compared to MRI (248,257–259).

In summary, this study shows how commonly used methods influence PWV values by MRI in neonates and adolescents. The study proposes that 3D angiography and the time to foot method should be used for accurate PWV measurements and show the required temporal resolution needed for reliable assessment of pulse wave velocity in the respective group. The study thereby enables implementation of PWV assessment in the clinical setting.

5.3 Study III

The current study implemented the newly validated pulse wave velocity method from *Study II* to investigate whether very preterm birth due to fetal growth restriction (FGR) verified by abnormal fetal blood flow velocimetry is associated with alterations in arterial stiffness in adolescence. Adolescents also underwent 24-hour ambulatory blood pressure measurements (24-hour ABPM) and assessment of renal function.

The current study shows that very preterm birth due to early onset FGR is associated with higher blood pressure in adolescent boys and that a similar trend was observed in boys born very preterm with appropriate birth weight. The increase in blood pressure was not associated with increases in arterial stiffness. Although not showing increases in arterial stiffness on a group level, girls born preterm AGA showed increased PWV as compared to the term AGA group. These changes were not associated with differences in renal function, which was within normal levels in all groups.

5.3.1 Blood pressure

The clinical evaluation of the 24-hour ABPM showed no differences in either prehypertension or hypertension between groups. This is similar to the recent study by Rakow et al. (113), showing normal 24-hour ambulatory blood pressures in young children born extremely preterm. However, in the study by Rakow et al. (113), the prevalence of non-dippers in mean arterial blood pressure were higher than in the current study. Differences between the studies might be explained by a lower day-to-night ratio in mean arterial blood pressures in infants and young children as compared to older subjects (260). As the clinical evaluation of the 24-hour ABPM is based on age, sex, and height it can be seen as an adjusted comparison of blood pressures across groups.

In boys, a stepwise increase in diastolic and mean arterial blood pressures was observed from term AGA to preterm AGA to preterm FGR. No such trend statistically or visually was observed in girls. This sex-specificity, showing higher blood pressures for boys born preterm was also recently observed in the 'Extremely Preterm Infants in Sweden Study' (EXPRESS) cohort' although using office blood pressure (261). The prevalence of FGR was however not known.

The current and these two recent studies indicate that preterm birth and fetal growth restriction are associated with higher but still normal blood pressure in childhood and adolescence (113,261). It is however important to note that both preterm birth (5,81) and low birth weight (262,263) independently are associated with an increased long term risk for hypertension, although a possible lessened effect of preterm birth on blood pressure has been observed in individuals born after the 1990's (81). Even a small increase or decrease in blood pressures might have a

substantial impact on long term cardiovascular morbidity (264,265). The association between increased blood pressure and preterm birth and low birth weight likely also contribute to the increased prevalence of CKD and cardiovascular disease in those born preterm (4,82,85). This association was however not observed for the current study population in adolescence, showing normal cardiac function (*Study IV*) and normal kidney function (*Study V*).

Both standard office blood pressures and 24-hour ABPM are presented in this paper but only the 24-hour ABPM were sensitive enough to detect differences between groups. Ambulatory measurements have been shown to be more sensitive for detecting changes and also show higher predicative value as compared to office blood pressure (175–177). If the findings of the current and other recent studies, showing only subtle blood pressure increases in those born preterm with and without FGR, are generalizable and persistent throughout ages, assessment of future cardiovascular risk in these cohorts should be performed using 24-hour ABPM.

5.3.2 Arterial stiffness

Pulse wave velocity and aortic distensibility were similar between groups in the current study. The results are thus only partly in line with the hypothesis that FGR would exacerbate the effects of preterm birth on blood pressure and arterial stiffness, as previously observed by Cheung et al. (91). Preterm birth and low birth weight have been shown to be associated with increased arterial stiffness in childhood and adolescence (87,91,101,255). Increases in arterial stiffness are often accompanied with increases also in blood pressure (101,254,266). The current and other recent studies indicate a lessened effect on both arterial stiffness (267,268) and blood pressure in these recent cohorts, especially for girls (113,261,267).

Arterial intima media thickness, pulse wave velocity, distensibility of the aortic wall and augmentation index are all proxies for arterial stiffness and are predictive of future cardiovascular disease (103,252,269–271). The association between these measures of arterial stiffness and preterm birth or low birth weight are well described (87,255,266,272). Anatomical differences in vessel size and the composition of the arterial walls have been suggested to contribute to these changes (144,145), where smaller vessels and increased intima media thickness would indicate increased afterload and arterial stiffness, respectively. Studies on intima media thickness, after preterm birth are incongruent but seem to indicate that preterm birth alone show increased intima media thickness (255,272) while FGR show a decreased thickness (216,273).

A recent study by Mohlkert et al. (268), showed no differences in intima media thickness or vessel size after normalizing for BSA in children born extremely preterm. Similarly, in childhood, the preterm AGA group in the current study showed higher aortic stiffness as compared to the preterm FGR group while the preterm FGR group showed lower intima media thickness as compared to the term AGA group (216). When stratifying for sex in the current study, girls born term

AGA in the current study showed higher PWV as compared to term AGA. Similarly, Bonamy et al. (255), showed increased arterial stiffness in adolescent girls, with no additive effect of low birth weight to that of preterm birth. These studies thus suggest differences in vascular development and response to extrauterine life after very preterm birth and FGR, respectively. This effect might be influenced by sex.

In summary, this study shows that very preterm birth due to early onset FGR is associated with higher, yet normal blood pressure in adolescent boys and also suggests alterations in arterial stiffness after very preterm birth in girls. These differences suggest an existing but limited impact of very preterm birth on cardiovascular risk in adolescence, possibly enhanced by male sex and FGR.

5.4 Study IV

The current study applied magnetic resonance imaging to investigate the effects of very preterm birth due to fetal growth restriction on cardiac morphology and function in adolescence.

Left and right ventricular volumes but not total heart volume were smaller in the preterm AGA group as compared to the term AGA group. A visual trend in smaller volumes was observed also for the preterm FGR group, who showed smaller right atrial volumes as compared to the term AGA group. Left ventricular mass (LVM) and measures of left and right cardiac function including longitudinal and radial pumping, as well as plasma concentration of NT-proBNP, did not differ between groups.

5.4.1 Cardiac volumes

This study investigated the effects of very preterm birth and FGR on left and right ventricular and atrial volumes as well as total heart volume (THV). This comprehensive approach is usually not undertaken and studies investigating the long term effects of preterm birth and FGR have focused solely on the left or right side of the heart (83, 262–264).

In line with previous studies, the preterm FGR group in the current study was shorter as compared to the term AGA group, indicating differing growth patterns with possible differences also in final height (202,265). Although a difference in height was observed, the preterm FGR group has gone through a partial catch up in both height and weight, as was observed already in childhood (214). Relating the different cardiac volumes to BSA might thus be important for comparison and also indicates whether the heart is proportional to the body. Relating cardiac volumes to THV indicates whether the respective volume is proportional in respect to the entire heart, which might indicate whether the ratios are physiological or pathophysiological (232,278).

The current study showed smaller left and right ventricular volumes, in absolute and BSA- but not THV adjusted volumes, in the preterm AGA group as compared to the term AGA group. A similar non-significant trend was also observed for the preterm FGR group. These findings are in line with previous studies showing smaller left ventricular volumes relative to BSA after preterm birth and after being born SGA (93,274). As ventricular volumes were smaller in the preterm groups, THV could be hypothesized to also be smaller, but no statistically significant differences in THV were observed, and BSA was a strong predictor of THV in all groups. The preterm FGR group showed smaller right atrial volumes as compared to the term AGA group, both in absolute values and when adjusted for BSA and THV. In a recent study of adolescents born very preterm during the same time period as the current population, Harris et al. (279), showed smaller cardiac volumes, including ventricular and atrial volumes, lower LVM normalized for BSA and preserved cardiac function using echocardiography. In addition, no differences in systolic or diastolic blood pressure were observed. Being born with modern neonatal intensive care was suggested as a contributing factor to these findings.

The current study showed no group differences in LVM, either in absolute or in BSA adjusted values. Increases in LVM is a common finding after preterm birth and low birth weight (92,93,274), showing an inverse relationship with gestational age. Increased LVM in earlier studies may have been a result of increased blood pressure and arterial stiffness, which is commonly observed in these populations (5,7,266). These findings could also be an effect of an intrinsic alteration in cardiac structure after preterm birth and FGR as shown in both animal (139) and human (99,141) studies. Conversely, recent studies indicates a lessened effect on LVM, even showing smaller volumes in those born very- and extremely preterm (275,279).

However, when stratifying for sex in the current study, boys in the preterm FGR group, who also showed higher blood pressures as compared to the other groups (*Study III*), showed increased LVM normalized to THV as compared to the term AGA group. This finding might be thus be indicative of increased blood pressure and afterload, as previously observed when comparing men and women, with men showing higher LVM/THV as compared to women (232). Left ventricular mass normalized to BSA were however within normal ranges (280). This finding might indicate that normalizing for total heart volume increases sensitivity for cardiac alterations as compared to normalizing for BSA.

Differences observed for left and right ventricular volumes between preterm AGA and term AGA group in the current study seems to be driven mostly by girls, who generally showed comparatively smaller cardiac volumes. A similar finding was observed in *Study V* where preterm birth, and especially very preterm birth due to FGR, were associated with smaller kidney volumes (both absolute and BSA adjusted), a difference that was driven by smaller volumes in girls.

5.4.2 Cardiac function

Although showing smaller cardiac volumes, neither very preterm birth nor FGR were associated with alterations in cardiac function in the current study. Both planimetrically derived functional measures such as stroke volume, cardiac index and ejection fraction as well as flow measurements were similar between groups. This is contrary to earlier studies of young adults born preterm showing smaller ventricles and lower ejection fraction for both left and right ventricles (274,281). However, as in the current study, Harris et al (279), showed smaller cardiac volumes without alterations in cardiac function in adolescents born very preterm during the same period as the current study population (279). Ejection fraction, measures of late- and early filling and measures of cardiac longitudinal pumping such tricuspid annular plane of systolic excursion (TAPSE) and left and right ventricular global longitudinal strain (GLS) were similar as compared to healthy controls (279).

The effect of very preterm birth and FGR on atrioventricular plane displacement and longitudinal and radial contribution to stroke volume have not previously been investigated using MRI. However, none of these measures differed between groups in the current study. MRI derived AVPD has been shown to be similar in assessing longitudinal function to that of TAPSE and mitral annular late diastolic velocity (MAPSE) (185). Measures of longitudinal shortening, such as TAPSE, MAPSE and GLS, are predictive for future CVD in apparently healthy, albeit older populations (282–284).

The AVPD ratio, the relative longitudinal shortening along the left and right ventricular length axis, respectively, showed no difference between groups in the current study. This measure is one way to study the relative longitudinal shortening of the ventricles and show some resemblance to GLS, measured as the longitudinal shortening of the myocardium as a percentage of the total length of the ventricle using echocardiography. Longitudinal strain has previously been shown to be affected after preterm birth and low birth weight (98,274). I line with the current study and the study by Harris et al. (279), Mohlkert et al., (275) also studying the EXPRESS (Extremely Preterm Infants in Sweden Study) cohort previously described, showed no differences GLS in children born extremely preterm. Mohlkert et al. did however show alterations in MAPSE and other makers of systolic and diastolic function for the left ventricle in those born extremely preterm.

Cardiac MRI is sensitive to detect also small differences in cardiac structure and function (179,187,188). Although not including all of the potential individuals from the original cohort, resulting in a limited number of participants in each group, especially when stratifying for sex, the use of cardiac MRI decreases sample size compared to 2D echo between 55-95% in left and right ventricular variables (187–189). It might thus be that the current study population, with only subtle and sex-dependent differences in blood pressure and arterial stiffness (*Study III*) and normal renal function without signs of RAAS activation (*Study V*) are healthier than

previous cohorts investigated, as was indicated in the study by Harris et al. (279) and partly by the recent EXPRESS studies (261,268,275).

In summary, this study shows that very preterm birth is associated with smaller ventricular volumes without alterations in longitudinal or radial pumping in adolescence. Sex-specific results suggested that changes in cardiac volumes were driven by girls born very preterm. Early onset FGR did not exacerbate the effects of very preterm birth suggesting that preterm birth rather than FGR is associated with smaller cardiac volumes.

5.5 Study V

This study implemented the newly validated MRI method from *Study I* to investigate the effects of very preterm birth due to FGR on kidney structure in adolescence. Renal parenchymal T1 and T2* values as well as biochemical markers of kidney function were also assessed.

This study showed that FGR followed by very preterm birth is associated with smaller total kidney volumes and medullary volumes in adolescence. T1 and T2* did not differ between group and biochemical markers of kidney function and RAAS activation were within normal levels.

5.5.1 Kidney volume

As the method used for renal parenchymal quantification was just recently validated (*Study I*), this is the first study to quantify the effects of very preterm birth and early onset FGR on medullary and cortical volumes using non-contrast enhanced MRI. The current study confirms the previous ultrasound studies in that very preterm birth, especially when due to early onset fetal growth restriction, is associated with smaller kidney volumes in adolescence. Both cortical and medullary volumes were smaller in the preterm FGR group as compared to the term AGA group, but only medullar were significantly smaller. Differences were more pronounced in girls, showing smaller absolute and BSA adjusted cortical and medullary volumes as compared to the term AGA group. A similar finding was observed in *study IV* where group differences in left, and right ventricular size was driven by smaller volumes in girls born very preterm AGA. Studies have previously indicated smaller kidney volumes in females born preterm (113,246). Lillås et al. (246) showed that middle age women with smaller kidneys also showed lower kidney function (285). Whether smaller kidney volumes per se is a direct sign of pathology and thus a risk factor for future kidney disease is however not known and renal function was within normal levels in the current study.

Several pathologies impact kidney volume (198,242,286) and although preterm birth and FGR are associated with a low nephron count at birth (108,109) and

smaller kidney volumes throughout life (113,117,246,287,288), the relationship between total kidney volume and nephron count can´t be inferred with certainty. The gold standard for quantification of the number of nephrons is however invasive (289), and is thus not widely used or applicable.

5.5.2 Biomarkers of kidney structure and function

The current study further investigated the effects of preterm birth and FGR on kidney structure and function using T1 and T2* mapping and biochemical markers of kidney function and RAAS activation. As in *study III* and *study IV* the current study indicates subtle and sex-specific differences between groups, with increased cortical T1 in the preterm AGA group as compared to the term AGA group for girls. No other group differences were observed.

Congenital oligonephropathy, as observed in the preterm infant, has been proposed as a pathway towards adult hypertension through a process of increased glomerular pressure and subsequent glomerular hyperfiltration, hypertrophy and glomerulosclerosis (107,290,291). Cortical hypertrophy has indeed been suggested after preterm birth using ultrasound (115) and was indicated by the current study, where the ratio between cortical and medullary volumes increased from term AGA to preterm AGA to preterm FGR. Glomerulosclerosis, or renal fibrosis, could potentially be quantified using T1 mapping (211,292) and as increases in cortical T1 and loss of corticomedullary differentiation has been observed in patients with CKD and hypertension (210,223), T1 mapping could potentially also be used also for risk assessment in cohorts born preterm or with low birth weight (4,5). As the current study showed no differences in renal function or RAAS activation and the previous studies in adolescence showed normal cardiac function (*study IV*) and only subtle sex-specific changes in blood pressure (boys) and arterial stiffness (girls) (*Study III*) the subtle differences in renal T1 or T2* might be expected.

In summary, this study shows that FGR with abnormal fetal blood flow followed by very preterm birth is associated with smaller total kidney and medullary kidney volumes, but not with markers of kidney dysfunction or RAAS activation in adolescence. The study further indicates that these changes are more pronounced in girls.

6 Conclusions

This thesis is one of the first presenting cardiovascular and renal outcomes in a population of adolescents who were actively delivered very preterm due to early onset fetal growth restriction into a modern neonatal intensive care. This thesis concludes that adolescents born very preterm with and without preceding fetal growth restriction show alterations in cardiovascular and renal morphology. Changes were more pronounced in girls. Cardiovascular and kidney function were however normal, possibly indicating a lessened long-term effect of very preterm birth and fetal growth restriction on these organ systems compared to earlier studies, where clear signs of increased risk were observed already in childhood and adolescence. As indicated by increases in blood pressure, male sex and fetal growth restriction might increase cardiovascular risk in those born preterm. Morphological changes in both the heart and in the kidneys may still precede functional decline in this population, and the alterations observed could potentially be used as prognostic markers in the future.

This thesis concludes that:

I. The proposed non-contrast enhanced MRI method can be used for accurate and precise measures of cortical and medullary volumes.

II. The validity of pulse wave velocity measurements is significantly influenced by the acquired temporal resolution, the image used for measurements and the method used for calculating the transit time.

III. Very preterm birth due to early onset FGR is associated with higher, yet normal blood pressure in adolescent boys and increased arterial stiffness after very preterm birth in girls is suggested.

IV. Very preterm birth is associated with smaller ventricular volumes without alterations in longitudinal or radial pumping in adolescence. Early onset FGR did not exacerbate the effects of very preterm birth, suggesting that preterm birth rather than FGR is associated with smaller cardiac volumes.

V. Very preterm birth due to early onset FGR is associated with smaller total kidney and medullary kidney volumes, but not with markers of kidney dysfunction or RAAS activation in adolescence.

7 Future aspects

At the time of publication of this thesis, individuals with early onset fetal growth restriction born into an era of modern obstetric and neonatal care, have reached young adulthood. Follow-up studies on these cohorts to support or contrast the findings are needed. Whether these more recent cohorts are at a lower risk for future cardiovascular and kidney disease, as suggested in the current thesis remains to be confirmed.

Several landmark improvements in both obstetric and neonatal management have been implemented during the last decades and have in concert drastically reduced morbidity and mortality in high-risk pregnancies (13,14,76). Early improvements include introduction of maternal and fetal surveillance programs and the wide use of ultrasound for fetal biometry and the use of Doppler velocimetry and CTG for identification and prediction of fetal demise (12). The criteria for both diagnosis and management of fetal growth restriction are however still up for debate and differ depending on site and country. However, with active management, perinatal morbidity and mortality is similar in infants born very preterm due to early onset FGR as compared to being born very preterm due to other causes (76,293).

Antenatal corticosteroid administration and post-natal surfactant administration became widely available during the mid-1990s and has markedly lessened perinatal mortality and morbidity (9,10). Delayed umbilical cord clamping, better and age-adjusted nutrition, development of ventilators to better suit the very preterm infant and implementation of kangaroo care are other factors that impact at least short-term morbidity and mortality (32,294–296).

The long-term effects and cardiovascular and renal outcomes following these improvements are yet to be fully elucidated, especially as several improvements have been implemented quite recently. It may however be hypothesized that long term outcomes in cohorts born during in the era of modern medicine will differ in many aspects as compared to earlier cohorts.

As in all research, more and larger studies are needed but it is also important to use sound and robust methods and methodologies. To increase transparency and to enable comparison between studies, future work should include more detailed perinatal characteristics, including the obstetric and neonatal management, and whether guidelines for the definition of fetal growth restriction or SGA are being followed.

This thesis validated and implemented assessment of renal cortical and medullary volumes using non-contrast enhanced MRI. Future studies should implement this

technique to increase the understanding of the separate processes in the renal cortex and medulla in various diseases. Not only for the long-term outcomes after preterm birth and FGR but also for other pathologies with known kidney changes, such as diabetic nephropathy and the sequele of nephrectomy. In the current study, apparently healthy adolescents with normal kidney function were imaged, and therefore the reliability in patients with manifest renal pathologies need further investigation.

Preterm birth and early onset fetal growth restriction increase the risk of neurodevelopmental disorders and cognitive delay (45,214,293), but this was not within the scope of this thesis. Neurodevelopmental disorders (297,298) as well as preterm birth and low birth weight (28,299) are in turn associated with an increased risk for obesity and the metabolic syndrome. The association between cognitive function and future cardiovascular and renal disease burden in these cohorts remains to be studied.

References

1. Chawanpaiboon S, Vogel JP, Moller AB, Lumbiganon P, Petzold M, Hogan D, et al. Global, regional, and national estimates of levels of preterm birth in 2014: a systematic review and modelling analysis. Lancet Glob Health. 2019 Jan;7(1):e37–46.
2. Liu L, Oza S, Hogan D, Chu Y, Perin J, Zhu J, et al. Global, regional, and national causes of under-5 mortality in 2000–15: an updated systematic analysis with implications for the Sustainable Development Goals. The Lancet. 2016 Dec;388(10063):3027–35.
3. Lees CC, Stampalija T, Baschat AA, Silva Costa F, Ferrazzi E, Figueras F, et al. ISUOG Practice Guidelines: diagnosis and management of small-for-gestational-age fetus and fetal growth restriction. Ultrasound Obstet Gynecol. 2020 Aug;56(2):298–312.
4. Crump C, Sundquist J, Winkleby MA, Sundquist K. Preterm birth and risk of chronic kidney disease from childhood into mid-adulthood: national cohort study. BMJ. 2019 May 1;l1346.
5. Crump C, Winkleby MA, Sundquist K, Sundquist J. Risk of hypertension among young adults who were born preterm: a Swedish national study of 636,000 births. Am J Epidemiol. 2011 Apr 1;173(7):797–803.
6. Barker DJP, Osmond C, Winter PD, Margetts B, Simmonds SJ. WEIGHT IN INFANCY AND DEATH FROM ISCHAEMIC HEART DISEASE. The Lancet. 1989 Sep;334(8663):577–80.
7. Sipola-Leppänen M, Karvonen R, Tikanmäki M, Matinolli HM, Martikainen S, Pesonen AK, et al. Ambulatory Blood Pressure and Its Variability in Adults Born Preterm. Hypertension. 2015 Mar;65(3):615–21.
8. Effect of corticosteroids for fetal maturation on perinatal outcomes. NIH Consens Statement. 1994 Mar 28;12(2):1–24.
9. Antenatal corticosteroid therapy: A meta-analysis of the randomized trials, 1972 to 1994. Am J Obstet Gynecol. 1995 Jul 1;173(1):322–35.
10. Polin RA, Carlo WA, COMMITTEE ON FETUS AND NEWBORN, Papile LA, Polin RA, Carlo W, et al. Surfactant Replacement Therapy for Preterm and Term Neonates With Respiratory Distress. Pediatrics. 2014 Jan 1;133(1):156–63.
11. Philip AGS. The Evolution of Neonatology. Pediatr Res. 2005 Oct;58(4):799–815.
12. Campbell S. A short history of sonography in obstetrics and gynaecology. Facts Views Vis ObGyn. 2013;5(3):213–29.

13. Norman M, Hallberg B, Abrahamsson T, Björklund LJ, Domellöf M, Farooqi A, et al. Association Between Year of Birth and 1-Year Survival Among Extremely Preterm Infants in Sweden During 2004-2007 and 2014-2016. JAMA. 2019 Mar 26;321(12):1188.
14. Ancel PY, Goffinet F, Kuhn P, Langer B, Matis J, Hernandorena X, et al. Survival and Morbidity of Preterm Children Born at 22 Through 34 Weeks' Gestation in France in 2011: Results of the EPIPAGE-2 Cohort Study. JAMA Pediatr. 2015 Mar 1;169(3):230.
15. Use of Antenatal Corticosteroids at 22 Weeks of Gestation [Internet]. [cited 2022 Sep 17]. Available from: https://www.acog.org/en/clinical/clinical-guidance/practice-advisory/articles/2021/09/use-of-antenatal-corticosteroids-at-22-weeks-of-gestation
16. Brodszki J, Morsing E, Malcus P, Thuring A, Ley D, Maršál K. Early intervention in management of very preterm growth-restricted fetuses: 2-year outcome of infants delivered on fetal indication before 30 gestational weeks. Ultrasound Obstet Gynecol. 2009 Sep;34(3):288–96.
17. Barker DJ. The fetal and infant origins of adult disease. BMJ. 1990 Nov 17;301(6761):1111.
18. Notkola V, Punsar S, Karvonen MJ, Haapakoski J. Socio-economic conditions in childhood and mortality and morbidity caused by coronary heart disease in adulthood in rural Finland. Soc Sci Med 1982. 1985;21(5):517–23.
19. Barker D. INFANT MORTALITY, CHILDHOOD NUTRITION, AND ISCHAEMIC HEART DISEASE IN ENGLAND AND WALES. The Lancet. 1986 May;327(8489):1077–81.
20. Barker DJP, Gelow J, Thornburg K, Osmond C, Kajantie E, Eriksson JG. The early origins of chronic heart failure: impaired placental growth and initiation of insulin resistance in childhood. Eur J Heart Fail. 2010 Aug;12(8):819–25.
21. Barker DJ, Bull AR, Osmond C, Simmonds SJ. Fetal and placental size and risk of hypertension in adult life. BMJ. 1990 Aug 4;301(6746):259–62.
22. Forsdahl A. Are poor living conditions in childhood and adolescence an important risk factor for arteriosclerotic heart disease? Br J Prev Soc Med. 1977 Jun;31(2):91–5.
23. Barker DJ, Osmond C. Death rates from stroke in England and Wales predicted from past maternal mortality. Br Med J Clin Res Ed. 1987 Jul 11;295(6590):83–6.
24. Waaler HT. Height, weight and mortality. The Norwegian experience. Acta Med Scand Suppl. 1984;679:1–56.
25. Leon DA, Koupilova I, Lithell HO, Berglund L, Mohsen R, Vagero D, et al. Failure to realise growth potential in utero and adult obesity in relation to blood pressure in 50 year old Swedish men. BMJ. 1996 Feb 17;312(7028):401–6.
26. Hult M, Tornhammar P, Ueda P, Chima C, Edstedt Bonamy AK, Ozumba B, et al. Hypertension, Diabetes and Overweight: Looming Legacies of the Biafran Famine. Miranda JJ, editor. PLoS ONE. 2010 Oct 22;5(10):e13582.
27. Leunissen RWJ. Timing and Tempo of First-Year Rapid Growth in Relation to Cardiovascular and Metabolic Risk Profile in Early Adulthood. JAMA. 2009 Jun 3;301(21):2234.

28. Lapillonne A, Griffin IJ. Feeding Preterm Infants Today for Later Metabolic and Cardiovascular Outcomes. J Pediatr. 2013 Mar;162(3):S7–16.
29. Lumey LH, Van Poppel FWA. The Dutch Famine of 1944-45: Mortality and Morbidity in Past and Present Generations. Soc Hist Med. 1994;7(2):229–46.
30. Lumey L, Stein AD, Kahn HS, van der Pal-de Bruin KM, Blauw G, Zybert PA, et al. Cohort Profile: The Dutch Hunger Winter Families Study. Int J Epidemiol. 2007 Dec 1;36(6):1196–204.
31. Roseboom T, de Rooij S, Painter R. The Dutch famine and its long-term consequences for adult health. Early Hum Dev. 2006 Aug;82(8):485–91.
32. Lagercrantz H, Hellstr??m-Westas L, Norman M. Neonatologi. Lund: Studentlitteratur; 2015.
33. Nägele F Carl. Erfahrungen und Abhandlungen aus dem Gebiethe der Krankheiten des weiblichen Geschlechtes: nebst Grundzügen einer Methodenlehre der Geburtshülfe. Vol. 1812. Löffler;
34. Pay ASD, Wiik J, Backe B, Jacobsson B, Strandell A, Klovning A. Symphysis-fundus height measurement to predict small-for-gestational-age status at birth: a systematic review. BMC Pregnancy Childbirth. 2015 Dec;15(1):22.
35. Pay ASD, Frøen JF, Staff AC, Jacobsson B, Gjessing HK. Symphysis-fundus measurement - the predictive value of a new reference curve. Tidsskr Den Nor Laegeforening Tidsskr Prakt Med Ny Raekke. 2017 May;137(10):717–20.
36. Stirnemann J, Villar J, Salomon LJ, Ohuma E, Ruyan P, Altman DG, et al. International estimated fetal weight standards of the INTERGROWTH-21 st Project: International estimated fetal weight standards. Ultrasound Obstet Gynecol. 2017 Apr;49(4):478–86.
37. Hadlock FP, Harrist RB, Martinez-Poyer J. In utero analysis of fetal growth: a sonographic weight standard. Radiology. 1991 Oct;181(1):129–33.
38. Monier I, Ego A, Benachi A, Ancel PY, Goffinet F, Zeitlin J. Comparison of the Hadlock and INTERGROWTH formulas for calculating estimated fetal weight in a preterm population in France. Am J Obstet Gynecol. 2018 Nov;219(5):476.e1-476.e12.
39. Persson PH, Weldner BM. Intra-uterine weight curves obtained by ultrasound. Acta Obstet Gynecol Scand. 1986;65(2):169–73.
40. Maršál K, Persson PH, Larsen T, Lilja H, Selbing A, Sultan B. Intrauterine growth curves based on ultrasonically estimated foetal weights. Acta Paediatr. 1996 Jul;85(7):843–8.
41. Gordijn SJ, Beune IM, Thilaganathan B, Papageorghiou A, Baschat AA, Baker PN, et al. Consensus definition of fetal growth restriction: a Delphi procedure. Ultrasound Obstet Gynecol Off J Int Soc Ultrasound Obstet Gynecol. 2016 Sep;48(3):333–9.
42. Buonocore G, Bracci R, Weindling M, editors. Neonatology: A Practical Approach to Neonatal Management. New York: Springer; 2011.
43. Salomon LJ, Alfirevic Z, Da Silva Costa F, Deter RL, Figueras F, Ghi T, et al. ISUOG Practice Guidelines: ultrasound assessment of fetal biometry and growth. Ultrasound Obstet Gynecol. 2019 Jun;53(6):715–23.

44. Unterscheider J, Daly S, Geary MP, Kennelly MM, McAuliffe FM, O'Donoghue K, et al. Optimizing the definition of intrauterine growth restriction: the multicenter prospective PORTO Study. Am J Obstet Gynecol. 2013 Apr;208(4):290.e1-290.e6.
45. Shand AW, Hornbuckle J, Nathan E, Dickinson JE, French NP. Small for gestational age preterm infants and relationship of abnormal umbilical artery Doppler blood flow to perinatal mortality and neurodevelopmental outcomes. Aust N Z J Obstet Gynaecol. 2009 Feb;49(1):52–8.
46. Statistikdatabaser - Förlossningsstatistik - Resultat [Internet]. Socialstyrelsen. [cited 2022 Sep 8]. Available from: https://sdb.socialstyrelsen.se/if_mfr_004/resultat.aspx
47. Lee AC, Kozuki N, Cousens S, Stevens GA, Blencowe H, Silveira MF, et al. Estimates of burden and consequences of infants born small for gestational age in low and middle income countries with INTERGROWTH-21st standard: analysis of CHERG datasets. BMJ. 2017 Aug 17;358:j3677.
48. Sankaran S, Kyle PM. Aetiology and Pathogenesis of IUGR. Best Pract Res Clin Obstet Gynaecol. 2009 Dec;23(6):765–77.
49. Suhag A, Berghella V. Intrauterine Growth Restriction (IUGR): Etiology and Diagnosis. Curr Obstet Gynecol Rep. 2013 Jun;2(2):102–11.
50. Kingdom J, Huppertz B, Seaward G, Kaufmann P. Development of the placental villous tree and its consequences for fetal growth. Eur J Obstet Gynecol Reprod Biol. 2000 Sep;92(1):35–43.
51. Meekins JW, Pijnenborg R, Hanssens M, McFadyen IR, van Asshe A. A study of placental bed spiral arteries and trophoblast invasion in normal and severe pre-eclamptic pregnancies. Br J Obstet Gynaecol. 1994 Aug;101(8):669–74.
52. Mitra SC, Seshan SV, Riachi LE. Placental vessel morphometry in growth retardation and increased resistance of the umbilical artery Doppler flow. J Matern Fetal Med. 2000 Oct;9(5):282–6.
53. Guzin K, Tomruk S, Tuncay YA, Naki M, Sezginsoy S, Zemheri E, et al. The relation of increased uterine artery blood flow resistance and impaired trophoblast invasion in pre-eclamptic pregnancies. Arch Gynecol Obstet. 2005 Dec;272(4):283–8.
54. Kim YM, Chaemsaithong P, Romero R, Shaman M, Kim CJ, Kim JS, et al. Placental lesions associated with acute atherosis. J Matern-Fetal Neonatal Med Off J Eur Assoc Perinat Med Fed Asia Ocean Perinat Soc Int Soc Perinat Obstet. 2015 Sep;28(13):1554–62.
55. Zimmermann P, Eiriö V, Koskinen J, Kujansuu E, Ranta T. Doppler assessment of the uterine and uteroplacental circulation in the second trimester in pregnancies at high risk for pre-eclampsia and/or intrauterine growth retardation: comparison and correlation between different Doppler parameters. Ultrasound Obstet Gynecol Off J Int Soc Ultrasound Obstet Gynecol. 1997 May;9(5):330–8.
56. Su EJ. Role of the fetoplacental endothelium in fetal growth restriction with abnormal umbilical artery Doppler velocimetry. Am J Obstet Gynecol. 2015 Oct;213(4):S123–30.

57. Bilardo CM, Hecher K, Visser GHA, Papageorghiou AT, Marlow N, Thilaganathan B, et al. Severe fetal growth restriction at 26-32 weeks: key messages from the TRUFFLE study: Editorial. Ultrasound Obstet Gynecol. 2017 Sep;50(3):285–90.
58. Khong TY, Wolf F, Robertson WB, Brosens I. Inadequate maternal vascular response to placentation in pregnancies complicated by pre-eclampsia and by small-for-gestational age infants. BJOG Int J Obstet Gynaecol. 1986 Oct;93(10):1049–59.
59. Bower S, Bewley S, Campbell S. Improved prediction of preeclampsia by two-stage screening of uterine arteries using the early diastolic notch and color Doppler imaging. Obstet Gynecol. 1993 Jul;82(1):78–83.
60. North RA, Ferrier C, Long D, Townend K, Kincaid-Smith P. Uterine artery Doppler flow velocity waveforms in the second trimester for the prediction of preeclampsia and fetal growth retardation. Obstet Gynecol. 1994 Mar;83(3):378–86.
61. Chappell L, Bewley S. Pre-eclamptic toxaemia: the role of uterine artery Doppler. BJOG Int J Obstet Gynaecol. 1998 Apr;105(4):379–82.
62. Ochi H, Matsubara K, Kusanagi Y, Taniguchi H, Ito M. Significance of a diastolic notch in the uterine artery flow velocity waveform induced by uterine embolisation in the pregnant ewe. BJOG Int J Obstet Gynaecol. 1998 Oct;105(10):1118–21.
63. Hernandez-Andrade E, Brodszki J, Lingman G, Gudmundsson S, Molin J, Maršál K. Uterine artery score and perinatal outcome: Uterine artery score and perinatal outcome. Ultrasound Obstet Gynecol. 2002 May 1;19(5):438–42.
64. FitzGerald DE, Drumm JE. Non-invasive measurement of human fetal circulation using ultrasound: a new method. BMJ. 1977 Dec 3;2(6100):1450–1.
65. Giles WB, Trudinger BJ, Baird PJ. Fetal umbilical artery flow velocity waveforms and placental resistance: pathological correlation. Br J Obstet Gynaecol. 1985 Jan;92(1):31–8.
66. Trudinger BJ, Giles WB, Cook CM, Bombardieri J, Collins L. Fetal umbilical artery flow velocity waveforms and placental resistance: clinical significance. Br J Obstet Gynaecol. 1985 Jan;92(1):23–30.
67. Trudinger BrianJ, Giles WarwickB, Cook ColleenM, Connelly A, Thompson RosemaryS. UMBILICAL ARTERY FLOW VELOCITY WAVEFORMS IN HIGH-RISK PREGNANCY. The Lancet. 1987 Jan;329(8526):188–90.
68. Laurin J, Marsal K, Persson PH, Lingman G. Ultrasound measurement of fetal blood flow in predicting fetal outcome. BJOG Int J Obstet Gynaecol. 1987 Oct;94(10):940–8.
69. Giles WB, Trudinger BJ, Baird PJ. Fetal umbilical artery flow velocity waveforms and placental resistance: pathological correlation. Br J Obstet Gynaecol. 1985 Jan;92(1):31–8.
70. Morrow RJ, Adamson SL, Bull SB, Knox Ritchie JW. Effect of placental embolization on the umbilical arterial velocity waveform in fetal sheep. Am J Obstet Gynecol. 1989 Oct;161(4):1055–60.
71. Johnson P, Stojilkovic T, Sarkar P. Middle cerebral artery Doppler in severe intrauterine growth restriction: MCA Doppler in IUGR. Ultrasound Obstet Gynecol. 2001 May;17(5):416–20.

72. Gramellini D, Folli MC, Raboni S, Vadora E, Merialdi A. Cerebral-umbilical Doppler ratio as a predictor of adverse perinatal outcome. Obstet Gynecol. 1992 Mar;79(3):416–20.
73. Bahado-Singh RO, Kovanci E, Jeffres A, Oz U, Deren O, Copel J, et al. The Doppler cerebroplacental ratio and perinatal outcome in intrauterine growth restriction. Am J Obstet Gynecol. 1999 Mar;180(3 Pt 1):750–6.
74. Baschat AA, Cosmi E, Bilardo CM, Wolf H, Berg C, Rigano S, et al. Predictors of Neonatal Outcome in Early- Onset Placental Dysfunction: Obstet Gynecol. 2007 Feb;109(2, Part 1):253–61.
75. Fratelli N, Amighetti S, Bhide A, Fichera A, Khalil A, Papageorghiou AT, et al. Ductus venosus Doppler waveform pattern in fetuses with early growth restriction. Acta Obstet Gynecol Scand. 2020 May;99(5):608–14.
76. Morsing E, Brodszki J, Thuring A, Maršál K. Infant outcome after active management of early-onset fetal growth restriction with absent or reversed umbilical artery blood flow. Ultrasound Obstet Gynecol Off J Int Soc Ultrasound Obstet Gynecol. 2021 Jun;57(6):931–41.
77. Lees C, Marlow N, Arabin B, Bilardo CM, Brezinka C, Derks JB, et al. Perinatal morbidity and mortality in early-onset fetal growth restriction: cohort outcomes of the trial of randomized umbilical and fetal flow in Europe (TRUFFLE). Ultrasound Obstet Gynecol Off J Int Soc Ultrasound Obstet Gynecol. 2013 Oct;42(4):400–8.
78. Gardosi J, Madurasinghe V, Williams M, Malik A, Francis A. Maternal and fetal risk factors for stillbirth: population based study. BMJ. 2013 Jan 24;346:f108.
79. Nkadi PO, Merritt TA, Pillers DAM. An overview of pulmonary surfactant in the neonate: Genetics, metabolism, and the role of surfactant in health and disease. Mol Genet Metab. 2009 Jun;97(2):95–101.
80. Htun ZT, Schulz EV, Desai RK, Marasch JL, McPherson CC, Mastrandrea LD, et al. Postnatal steroid management in preterm infants with evolving bronchopulmonary dysplasia. J Perinatol. 2021 Aug;41(8):1783–96.
81. de Jong F, Monuteaux MC, van Elburg RM, Gillman MW, Belfort MB. Systematic Review and Meta-Analysis of Preterm Birth and Later Systolic Blood Pressure. Hypertension. 2012 Feb;59(2):226–34.
82. Crump C, Howell EA, Stroustrup A, McLaughlin MA, Sundquist J, Sundquist K. Association of Preterm Birth With Risk of Ischemic Heart Disease in Adulthood. JAMA Pediatr. 2019 Aug 1;173(8):736.
83. Carr H, Cnattingius S, Granath F, Ludvigsson JF, Edstedt Bonamy AK. Preterm Birth and Risk of Heart Failure Up to Early Adulthood. J Am Coll Cardiol. 2017 May;69(21):2634–42.
84. Abitbol CL, DeFreitas MJ, Strauss J. Assessment of kidney function in preterm infants: lifelong implications. Pediatr Nephrol. 2016 Dec;31(12):2213–22.
85. Chehade H, Simeoni U, Guignard JP, Boubred F. Preterm Birth: Long Term Cardiovascular and Renal Consequences. Curr Pediatr Rev. 2018 Dec 21;14(4):219–26.

86. Evensen KAI, Steinshamn S, Tjønna AE, Stølen T, Høydal MA, Wisløff U, et al. Effects of preterm birth and fetal growth retardation on cardiovascular risk factors in young adulthood. Early Hum Dev. 2009 Apr;85(4):239–45.
87. Levent E, Atik T, Darcan Ş, Ülger Z, Gökşen D, Özyürek AR. The relation of arterial stiffness with intrauterine growth retardation: Arterial stiffness and intrauterine growth. Pediatr Int. 2009 Dec;51(6):807–11.
88. Burchert H, Lewandowski AJ. Preterm Birth Is a Novel, Independent Risk Factor for Altered Cardiac Remodeling and Early Heart Failure: Is it Time for a New Cardiomyopathy? Curr Treat Options Cardiovasc Med. 2019 Feb 14;21(2):8.
89. Washburn LK, Brosnihan KB, Chappell MC, Diz DI, Gwathmey TM, Nixon PA, et al. The renin-angiotensin-aldosterone system in adolescent offspring born prematurely to mothers with preeclampsia. J Renin-Angiotensin-Aldosterone Syst JRAAS. 2015 Sep;16(3):529–38.
90. Paquette K, Fernandes RO, Xie LF, Cloutier A, Fallaha C, Girard-Bock C, et al. Kidney Size, Renal Function, Ang (Angiotensin) Peptides, and Blood Pressure in Young Adults Born Preterm: The HAPI Study. Hypertension. 2018 Oct;72(4):918–28.
91. Cheung YF. Relation of arterial stiffness with gestational age and birth weight. Arch Dis Child. 2004 Mar 1;89(3):217–21.
92. Lewandowski AJ, Augustine D, Lamata P, Davis EF, Lazdam M, Francis J, et al. Preterm Heart in Adult LifeClinical Perspective: Cardiovascular Magnetic Resonance Reveals Distinct Differences in Left Ventricular Mass, Geometry, and Function. Circulation. 2013 Jan 15;127(2):197–206.
93. Toemen L, Gaillard R, Roest AA, van der Geest RJ, Steegers EA, van der Lugt A, et al. Fetal and infant growth patterns and left and right ventricular measures in childhood assessed by cardiac MRI. Eur J Prev Cardiol. 2020 Jan;27(1):63–74.
94. Crispi F, Hernandez-Andrade E, Pelsers MMAL, Plasencia W, Benavides-Serralde JA, Eixarch E, et al. Cardiac dysfunction and cell damage across clinical stages of severity in growth-restricted fetuses. Am J Obstet Gynecol. 2008 Sep;199(3):254.e1-254.e8.
95. Crispi F, Bijnens B, Sepulveda-Swatson E, Cruz-Lemini M, Rojas-Benavente J, Gonzalez-Tendero A, et al. Postsystolic shortening by myocardial deformation imaging as a sign of cardiac adaptation to pressure overload in fetal growth restriction. Circ Cardiovasc Imaging. 2014 Sep;7(5):781–7.
96. Cohen E, Whatley C, Wong FY, Wallace EM, Mockler JC, Odoi A, et al. Effects of foetal growth restriction and preterm birth on cardiac morphology and function during infancy. Acta Paediatr Oslo Nor 1992. 2018 Mar;107(3):450–5.
97. Sehgal A, Allison BJ, Gwini SM, Miller SL, Polglase GR. Cardiac Morphology and Function in Preterm Growth Restricted Infants: Relevance for Clinical Sequelae. J Pediatr. 2017 Sep;188:128-134.e2.
98. Änghagen O, Engvall J, Gottvall T, Nelson N, Nylander E, Bang P. Developmental Differences in Left Ventricular Strain in IUGR vs. Control Children the First Three Months of Life. Pediatr Cardiol. 2022 Aug;43(6):1286–97.

99. Sarvari SI, Rodriguez-Lopez M, Nuñez-Garcia M, Sitges M, Sepulveda-Martinez A, Camara O, et al. Persistence of Cardiac Remodeling in Preadolescents With Fetal Growth Restriction. Circ Cardiovasc Imaging. 2017 Jan;10(1):e005270.
100. Brodszki J, Länne T, Maršál K, Ley D. Impaired Vascular Growth in Late Adolescence After Intrauterine Growth Restriction. Circulation. 2005 May 24;111(20):2623–8.
101. Rossi P, Tauzin L, Marchand E, Boussuges A, Gaudart J, Frances Y. Respective Roles of Preterm Birth and Fetal Growth Restriction in Blood Pressure and Arterial Stiffness in Adolescence. J Adolesc Health. 2011 May;48(5):520–2.
102. Wentland AL, Grist TM, Wieben O. Review of MRI-based measurements of pulse wave velocity: a biomarker of arterial stiffness. Cardiovasc Diagn Ther. 2014 Apr;4(2):193–206.
103. Vlachopoulos C, Aznaouridis K, Stefanadis C. Prediction of cardiovascular events and all-cause mortality with arterial stiffness: a systematic review and meta-analysis. J Am Coll Cardiol. 2010 Mar 30;55(13):1318–27.
104. Laurent S, Boutouyrie P, Asmar R, Gautier I, Laloux B, Guize L, et al. Aortic stiffness is an independent predictor of all-cause and cardiovascular mortality in hypertensive patients. Hypertens Dallas Tex 1979. 2001 May;37(5):1236–41.
105. Kouis P, Kousios A, Kanari A, Kleopa D, Papatheodorou SI, Panayiotou AG. Association of non-invasive measures of subclinical atherosclerosis and arterial stiffness with mortality and major cardiovascular events in chronic kidney disease: systematic review and meta-analysis of cohort studies. Clin Kidney J. 2020 Oct;13(5):842–54.
106. Brenner BM, Garcia DL, Anderson S. Glomeruli and blood pressure. Less of one, more the other? Am J Hypertens. 1988 Oct;1(4 Pt 1):335–47.
107. Brenner BM, Chertow GM. Congenital oligonephropathy and the etiology of adult hypertension and progressive renal injury. Am J Kidney Dis Off J Natl Kidney Found. 1994 Feb;23(2):171–5.
108. Hinchliffe SA, Sargent PH, Howard CV, Chan YF, van Velzen D. Human intrauterine renal growth expressed in absolute number of glomeruli assessed by the disector method and Cavalieri principle. Lab Investig J Tech Methods Pathol. 1991 Jun;64(6):777–84.
109. Hinchliffe SA, Lynch MR, Sargent PH, Howard CV, Van Velzen D. The effect of intrauterine growth retardation on the development of renal nephrons. Br J Obstet Gynaecol. 1992 Apr;99(4):296–301.
110. Hughson M, Farris AB, Douglas-Denton R, Hoy WE, Bertram JF. Glomerular number and size in autopsy kidneys: The relationship to birth weight. Kidney Int. 2003 Jun;63(6):2113–22.
111. Rodríguez MM, Gómez AH, Abitbol CL, Chandar JJ, Duara S, Zilleruelo GE. Histomorphometric Analysis of Postnatal Glomerulogenesis in Extremely Preterm Infants. Pediatr Dev Pathol. 2004 Jan;7(1):17–25.
112. Mañalich R, Reyes L, Herrera M, Melendi C, Fundora I. Relationship between weight at birth and the number and size of renal glomeruli in humans: A histomorphometric study. Kidney Int. 2000 Aug;58(2):770–3.

113. Rakow A, Laestadius Å, Liliemark U, Backheden M, Legnevall L, Kaiser S, et al. Kidney volume, kidney function, and ambulatory blood pressure in children born extremely preterm with and without nephrocalcinosis. Pediatr Nephrol. 2019 Oct;34(10):1765–76.
114. Silver LE, Decamps PJ, Korst LM, Platt LD, Castro LC. Intrauterine growth restriction is accompanied by decreased renal volume in the human fetus. Am J Obstet Gynecol. 2003 May;188(5):1320–5.
115. Li J, Guandalini M, Mcinnes H, Kandasamy Y, Trnka P, Moritz K. The impact of prematurity on postnatal growth of different renal compartments. Nephrology. 2020 Feb;25(2):116–24.
116. Starzec K, Klimek M, Grudzień A, Jagła M, Kwinta P. Longitudinal assessment of renal size and function in extremely low birth weight children at 7 and 11 years of age. Pediatr Nephrol. 2016 Nov;31(11):2119–26.
117. Kwinta P, Klimek M, Drozdz D, Grudzień A, Jagła M, Zasada M, et al. Assessment of long-term renal complications in extremely low birth weight children. Pediatr Nephrol Berl Ger. 2011 Jul;26(7):1095–103.
118. Gilarska M, Raaijmakers A, Zhang ZY, Staessen JA, Levtchenko E, Klimek M, et al. Extremely Low Birth Weight Predisposes to Impaired Renal Health: A Pooled Analysis. Kidney Blood Press Res. 2019;44(5):897–906.
119. Bertram JF, Douglas-Denton RN, Diouf B, Hughson MD, Hoy WE. Human nephron number: implications for health and disease. Pediatr Nephrol Berl Ger. 2011 Sep;26(9):1529–33.
120. Keller G, Zimmer G, Mall G, Ritz E, Amann K. Nephron number in patients with primary hypertension. N Engl J Med. 2003 Jan 9;348(2):101–8.
121. White SL, Perkovic V, Cass A, Chang CL, Poulter NR, Spector T, et al. Is Low Birth Weight an Antecedent of CKD in Later Life? A Systematic Review of Observational Studies. Am J Kidney Dis. 2009 Aug;54(2):248–61.
122. South AM, Nixon PA, Chappell MC, Diz DI, Russell GB, Snively BM, et al. Antenatal corticosteroids and the renin-angiotensin-aldosterone system in adolescents born preterm. Pediatr Res. 2017 Jan;81(1):88–93.
123. Garovic VD, White WM, Vaughan L, Saiki M, Parashuram S, Garcia-Valencia O, et al. Incidence and Long-Term Outcomes of Hypertensive Disorders of Pregnancy. J Am Coll Cardiol. 2020 May 12;75(18):2323–34.
124. Wang W, Xie X, Yuan T, Wang Y, Zhao F, Zhou Z, et al. Epidemiological trends of maternal hypertensive disorders of pregnancy at the global, regional, and national levels: a population-based study. BMC Pregnancy Childbirth. 2021 May 8;21(1):364.
125. Roberts CL, Algert CS, Morris JM, Ford JB, Henderson-Smart DJ. Hypertensive disorders in pregnancy: a population-based study. Med J Aust. 2005 Apr 4;182(7):332–5.
126. Duley L. The Global Impact of Pre-eclampsia and Eclampsia. Semin Perinatol. 2009 Jun;33(3):130–7.

127. Alsnes IV, Vatten LJ, Fraser A, Bjørngaard JH, Rich-Edwards J, Romundstad PR, et al. Hypertension in Pregnancy and Offspring Cardiovascular Risk in Young Adulthood: Prospective and Sibling Studies in the HUNT Study (Nord-Trøndelag Health Study) in Norway. Hypertension. 2017 Apr;69(4):591–8.
128. McDonald SD, Malinowski A, Zhou Q, Yusuf S, Devereaux PJ. Cardiovascular sequelae of preeclampsia/eclampsia: a systematic review and meta-analyses. Am Heart J. 2008 Nov;156(5):918–30.
129. Davis EF, Lazdam M, Lewandowski AJ, Worton SA, Kelly B, Kenworthy Y, et al. Cardiovascular risk factors in children and young adults born to preeclamptic pregnancies: a systematic review. Pediatrics. 2012 Jun;129(6):e1552-1561.
130. Tranquilli AL, Dekker G, Magee L, Roberts J, Sibai BM, Steyn W, et al. The classification, diagnosis and management of the hypertensive disorders of pregnancy: A revised statement from the ISSHP. Pregnancy Hypertens Int J Womens Cardiovasc Health. 2014 Apr;4(2):97–104.
131. Sotiriadis A, Hernandez-Andrade E, da Silva Costa F, Ghi T, Glanc P, Khalil A, et al. ISUOG Practice Guidelines: role of ultrasound in screening for and follow-up of pre-eclampsia. Ultrasound Obstet Gynecol. 2019 Jan;53(1):7–22.
132. Melchiorre K, Sharma R, Thilaganathan B. Cardiovascular Implications in Preeclampsia: An Overview. Circulation. 2014 Aug 19;130(8):703–14.
133. Adorno M, Maher-Griffiths C, Grush Abadie HR. HELLP Syndrome. Crit Care Nurs Clin North Am. 2022 Sep;34(3):277–88.
134. Sibai BM. Diagnosis, prevention, and management of eclampsia. Obstet Gynecol. 2005 Feb;105(2):402–10.
135. Sadler TW. Langman's medical embryology. Fourteenth edition. Philadelphia: Wolters Kluwer; 2019. 432 p.
136. Symonds IM, Arulkumaran S, editors. Essential obstetrics and gynaecology. Sixth edition. Edinburgh: Elsevier; 2020.
137. Tan CMJ, Lewandowski AJ. The Transitional Heart: From Early Embryonic and Fetal Development to Neonatal Life. Fetal Diagn Ther. 2020;47(5):373–86.
138. Huttenbach Y, Ostrowski ML, Thaller D, Kim HS. Cell proliferation in the growing human heart: MIB-1 immunostaining in preterm and term infants at autopsy. Cardiovasc Pathol. 2001 May;10(3):119–23.
139. Bensley JG, Stacy VK, De Matteo R, Harding R, Black MJ. Cardiac remodelling as a result of pre-term birth: implications for future cardiovascular disease. Eur Heart J. 2010 Aug;31(16):2058–66.
140. Puente BN, Kimura W, Muralidhar SA, Moon J, Amatruda JF, Phelps KL, et al. The Oxygen-Rich Postnatal Environment Induces Cardiomyocyte Cell-Cycle Arrest through DNA Damage Response. Cell. 2014 Apr;157(3):565–79.
141. Bensley JG, Moore L, De Matteo R, Harding R, Black MJ. Impact of preterm birth on the developing myocardium of the neonate. Pediatr Res. 2018 Apr;83(4):880–8.
142. Creager MA, Beckman JA, Loscalzo J, editors. Vascular medicine: a companion to Braunwald's heart disease. Third edition. Philadelphia, PA: Elsevier/Saunders; 2020. 940 p.

143. Berry CL, Looker T, Germain J. Nucleic acid and scleroprotein content of the developing human aorta. J Pathol. 1972 Dec;108(4):265–74.
144. Tauzin L. Alterations in viscoelastic properties following premature birth may lead to hypertension and cardiovascular disease development in later life. Acta Paediatr. 2015;104(1):19–26.
145. Martyn CN, Greenwald SE. Impaired synthesis of elastin in walls of aorta and large conduit arteries during early development as an initiating event in pathogenesis of systemic hypertension. Lancet Lond Engl. 1997 Sep 27;350(9082):953–5.
146. Coleman C, Tambay Perez A, Selewski DT, Steflik HJ. Neonatal Acute Kidney Injury. Front Pediatr. 2022 Apr 7;10:842544.
147. Mohamed TH, Abdi HH, Magers J, Prusakov P, Slaughter JL. Nephrotoxic medications and associated acute kidney injury in hospitalized neonates. J Nephrol [Internet]. 2022 Feb 15 [cited 2022 Jul 15]; Available from: https://link.springer.com/10.1007/s40620-022-01264-6
148. Boubred F, Vendemmia M, Garcia-Meric P, Buffat C, Millet V, Simeoni U. Effects Of Maternally Administered Drugs On The Fetal And Neonatal Kidney: Drug Saf. 2006;29(5):397–419.
149. al-Dahan J, Stimmler L, Chantler C, Haycock GB. The effect of antenatal dexamethasone administration on glomerular filtration rate and renal sodium excretion in premature infants. Pediatr Nephrol Berl Ger. 1987 Apr;1(2):131–5.
150. Carlsson M, Ugander M, Heiberg E, Arheden H. The quantitative relationship between longitudinal and radial function in left, right, and total heart pumping in humans. Am J Physiol-Heart Circ Physiol. 2007 Jul;293(1):H636–44.
151. Carlsson M, Ugander M, Mosen H, Buhre T, Arheden H. Atrioventricular plane displacement is the major contributor to left ventricular pumping in healthy adults, athletes, and patients with dilated cardiomyopathy. AJP Heart Circ Physiol. 2006 Oct 20;292(3):H1452–9.
152. Carlsson M. Total heart volume variation throughout the cardiac cycle in humans. AJP Heart Circ Physiol. 2004 Apr 1;287(1):H243–50.
153. Kumar V, Abbas AK, Aster JC, Turner JR, Perkins JA, Robbins SL, et al., editors. Robbins & Cotran pathologic basis of disease. Tenth edition. Philadelphia, PA: Elsevier; 2021. 1379 p.
154. Pathobiological Determinants of Atherosclerosis in Youth (PDAY) Research Group, McGill HC, McMahan CA, Herderick EE, Malcom GT, Tracy RE, et al. Origin of atherosclerosis in childhood and adolescence. Am J Clin Nutr. 2000 Nov 1;72(5):1307s–15s.
155. Strong JP, Malcom GT, McMahan CA, Tracy RE, Newman WP, Herderick EE, et al. Prevalence and extent of atherosclerosis in adolescents and young adults: implications for prevention from the Pathobiological Determinants of Atherosclerosis in Youth Study. JAMA. 1999 Feb 24;281(8):727–35.
156. Visseren FLJ, Mach F, Smulders YM, Carballo D, Koskinas KC, Bäck M, et al. 2021 ESC Guidelines on cardiovascular disease prevention in clinical practice. Eur Heart J. 2021 Sep 7;42(34):3227–337.

157. Tsamis A, Krawiec JT, Vorp DA. Elastin and collagen fibre microstructure of the human aorta in ageing and disease: a review. J R Soc Interface. 2013 Jun 6;10(83):20121004.
158. Faber M, Møller-Hou G. THE HUMAN AORTA. Acta Pathol Microbiol Scand. 2009 Aug 18;31(3):377–82.
159. Grubb A, Horio M, Hansson LO, Björk J, Nyman U, Flodin M, et al. Generation of a new cystatin C-based estimating equation for glomerular filtration rate by use of 7 assays standardized to the international calibrator. Clin Chem. 2014 Jul;60(7):974–86.
160. Schwartz GJ, Muñoz A, Schneider MF, Mak RH, Kaskel F, Warady BA, et al. New equations to estimate GFR in children with CKD. J Am Soc Nephrol JASN. 2009 Mar;20(3):629–37.
161. Björk J, Nyman U, Berg U, Delanaye P, Dubourg L, Goffin K, et al. Validation of standardized creatinine and cystatin C GFR estimating equations in a large multicentre European cohort of children. Pediatr Nephrol. 2019 Jun;34(6):1087–98.
162. Chapter 1: Definition and classification of CKD. Kidney Int Suppl. 2013 Jan;3(1):19–62.
163. Chapter 2: Definition, identification, and prediction of CKD progression. Kidney Int Suppl. 2013 Jan;3(1):63–72.
164. Hill NR, Fatoba ST, Oke JL, Hirst JA, O'Callaghan CA, Lasserson DS, et al. Global Prevalence of Chronic Kidney Disease – A Systematic Review and Meta-Analysis. Remuzzi G, editor. PLOS ONE. 2016 Jul 6;11(7):e0158765.
165. NCD Risk Factor Collaboration (NCD-RisC). Worldwide trends in hypertension prevalence and progress in treatment and control from 1990 to 2019: a pooled analysis of 1201 population-representative studies with 104 million participants. Lancet Lond Engl. 2021 Sep 11;398(10304):957–80.
166. Ogurtsova K, da Rocha Fernandes JD, Huang Y, Linnenkamp U, Guariguata L, Cho NH, et al. IDF Diabetes Atlas: Global estimates for the prevalence of diabetes for 2015 and 2040. Diabetes Res Clin Pract. 2017 Jun;128:40–50.
167. Bock JS, Gottlieb SS. Cardiorenal Syndrome: New Perspectives. Circulation. 2010 Jun 15;121(23):2592–600.
168. Shchekochikhin D, Schrier RW, Lindenfeld J. Cardiorenal Syndrome: Pathophysiology and Treatment. Curr Cardiol Rep [Internet]. 2013 Jul [cited 2017 Feb 21];15(7). Available from: http://link.springer.com/10.1007/s11886-013-0380-4
169. Blecker S, Matsushita K, Köttgen A, Loehr LR, Bertoni AG, Boulware LE, et al. High-Normal Albuminuria and Risk of Heart Failure in the Community. Am J Kidney Dis. 2011 Jul;58(1):47–55.
170. Chronic Kidney Disease Prognosis Consortium. Association of estimated glomerular filtration rate and albuminuria with all-cause and cardiovascular mortality in general population cohorts: a collaborative meta-analysis. The Lancet. 2010 Jun;375(9731):2073–81.

171. Waheed S, Matsushita K, Sang Y, Hoogeveen R, Ballantyne C, Coresh J, et al. Combined Association of Albuminuria and Cystatin C–Based Estimated GFR With Mortality, Coronary Heart Disease, and Heart Failure Outcomes: The Atherosclerosis Risk in Communities (ARIC) Study. Am J Kidney Dis. 2012 Aug;60(2):207–16.
172. He J, Shlipak M, Anderson A, Roy JA, Feldman HI, Kallem RR, et al. Risk Factors for Heart Failure in Patients With Chronic Kidney Disease: The CRIC (Chronic Renal Insufficiency Cohort) Study. J Am Heart Assoc. 2017 May;6(5):e005336.
173. Moore RA. The total number of glomeruli in the normal human kidney. Anat Rec. 1931 Jan;48(1):153–68.
174. Denic A, Lieske JC, Chakkera HA, Poggio ED, Alexander MP, Singh P, et al. The Substantial Loss of Nephrons in Healthy Human Kidneys with Aging. J Am Soc Nephrol. 2017 Jan;28(1):313–20.
175. Williams B, Mancia G, Spiering W, Agabiti Rosei E, Azizi M, Burnier M, et al. 2018 ESC/ESH Guidelines for the management of arterial hypertension. Eur Heart J. 2018 Sep 1;39(33):3021–104.
176. Hermida RC, Smolensky MH, Ayala DE, Portaluppi F. Ambulatory Blood Pressure Monitoring (ABPM) as the reference standard for diagnosis of hypertension and assessment of vascular risk in adults. Chronobiol Int. 2015 Nov 26;32(10):1329–42.
177. Piper MA, Evans CV, Burda BU, Margolis KL, O'Connor E, Whitlock EP. Diagnostic and predictive accuracy of blood pressure screening methods with consideration of rescreening intervals: a systematic review for the U.S. Preventive Services Task Force. Ann Intern Med. 2015 Feb 3;162(3):192–204.
178. Lurbe E, Agabiti-Rosei E, Cruickshank JK, Dominiczak A, Erdine S, Hirth A, et al. 2016 European Society of Hypertension guidelines for the management of high blood pressure in children and adolescents. J Hypertens. 2016 Oct;34(10):1887–920.
179. Leiner T, Bogaert J, Friedrich MG, Mohiaddin R, Muthurangu V, Myerson S, et al. SCMR Position Paper (2020) on clinical indications for cardiovascular magnetic resonance. J Cardiovasc Magn Reson Off J Soc Cardiovasc Magn Reson. 2020 Nov 9;22(1):76.
180. MRI Questions & Answers; MR imaging physics & technology [Internet]. Questions and Answers in MRI. [cited 2022 Oct 30]. Available from: http://mriquestions.com/
181. Pahlm O, Wagner GS. Multimodal cardiovascular image principles and clinical applications. New York: McGraw-Hill Medical;
182. Olsson A. Ekokardiografi. Upplaga 5. Stockholm: Ultraview; 2022.
183. Schulz-Menger J, Bluemke DA, Bremerich J, Flamm SD, Fogel MA, Friedrich MG, et al. Standardized image interpretation and post-processing in cardiovascular magnetic resonance - 2020 update: Society for Cardiovascular Magnetic Resonance (SCMR): Board of Trustees Task Force on Standardized Post-Processing. J Cardiovasc Magn Reson. 2020 Dec;22(1):19.
184. Seemann F, Pahlm U, Steding-Ehrenborg K, Ostenfeld E, Erlinge D, Dubois-Rande JL, et al. Time-resolved tracking of the atrioventricular plane displacement in Cardiovascular Magnetic Resonance (CMR) images. BMC Med Imaging. 2017 Feb 28;17(1):19.

185. Sepúlveda-Martínez A, Steding-Ehrenborg K, Rodríguez-López M, Ostenfeld E, Valenzuela-Alcaráz B, Heiberg E, et al. Atrioventricular plane displacement versus mitral and tricuspid annular plane systolic excursion: A comparison between cardiac magnetic resonance and M-mode echocardiography. Clin Physiol Funct Imaging. 2021 May;41(3):262–70.
186. Grotenhuis HB, Westenberg JJM, Steendijk P, van der Geest RJ, Ottenkamp J, Bax JJ, et al. Validation and reproducibility of aortic pulse wave velocity as assessed with velocity-encoded MRI. J Magn Reson Imaging JMRI. 2009 Sep;30(3):521–6.
187. Bellenger N, Davies LC, Francis J, Coats A, Pennell D. Reduction in Sample Size for Studies of Remodeling in Heart Failure by the Use of Cardiovascular Magnetic Resonance. J Cardiovasc Magn Reson. 2000 Nov 1;2(4):271–8.
188. Grothues F, Smith GC, Moon JCC, Bellenger NG, Collins P, Klein HU, et al. Comparison of interstudy reproducibility of cardiovascular magnetic resonance with two-dimensional echocardiography in normal subjects and in patients with heart failure or left ventricular hypertrophy. Am J Cardiol. 2002 Jul;90(1):29–34.
189. Mooij CF, de Wit CJ, Graham DA, Powell AJ, Geva T. Reproducibility of MRI measurements of right ventricular size and function in patients with normal and dilated ventricles. J Magn Reson Imaging. 2008 Jul;28(1):67–73.
190. Al'Aref SJ, Min JK. Cardiac CT: current practice and emerging applications. Heart. 2019 Oct;105(20):1597–605.
191. Schroeder S, Achenbach S, Bengel F, Burgstahler C, Cademartiri F, de Feyter P, et al. Cardiac computed tomography: indications, applications, limitations, and training requirements: Report of a Writing Group deployed by the Working Group Nuclear Cardiology and Cardiac CT of the European Society of Cardiology and the European Council of Nuclear Cardiology. Eur Heart J. 2008 Jan 3;29(4):531–56.
192. Taylor AJ, Cerqueira M, Hodgson JMcB, Mark D, Min J, O'Gara P, et al. ACCF/SCCT/ACR/AHA/ASE/ASNC/NASCI/SCAI/SCMR 2010 Appropriate Use Criteria for Cardiac Computed Tomography. J Am Coll Cardiol. 2010 Nov;56(22):1864–94.
193. Greenland P, Blaha MJ, Budoff MJ, Erbel R, Watson KE. Coronary Calcium Score and Cardiovascular Risk. J Am Coll Cardiol. 2018 Jul;72(4):434–47.
194. Nakahara T, Dweck MR, Narula N, Pisapia D, Narula J, Strauss HW. Coronary Artery Calcification. JACC Cardiovasc Imaging. 2017 May;10(5):582–93.
195. Curie J, Curie P. Sur l'électricité polaire dans les cristaux hémièdres à faces inclinées. 91383-6. 1880.
196. Edler I, Hertz CH. The Use of Ultrasonic Reflectoscope for the Continuous Recording of the Movements of Heart Walls. Clin Physiol Funct Imaging. 2004 May;24(3):118–36.
197. Lin E, Alessio A. What are the basic concepts of temporal, contrast, and spatial resolution in cardiac CT? J Cardiovasc Comput Tomogr. 2009 Nov;3(6):403–8.
198. Wang X, Vrtiska TJ, Avula RT, Walters LR, Chakkera HA, Kremers WK, et al. Age, kidney function, and risk factors associate differently with cortical and medullary volumes of the kidney. Kidney Int. 2014 Mar;85(3):677–85.

199. Breau RH, Clark E, Bruner B, Cervini P, Atwell T, Knoll G, et al. A simple method to estimate renal volume from computed tomography. Can Urol Assoc J J Assoc Urol Can. 2013 Jun;7(5–6):189–92.
200. Sharma K, Caroli A, Quach LV, Petzold K, Bozzetto M, Serra AL, et al. Kidney volume measurement methods for clinical studies on autosomal dominant polycystic kidney disease. Long D, editor. PLOS ONE. 2017 May 30;12(5):e0178488.
201. Li J, Guandalini M, Mcinnes H, Kandasamy Y, Trnka P, Moritz K. The impact of prematurity on postnatal growth of different renal compartments. Nephrol Carlton Vic. 2020 Feb;25(2):116–24.
202. Schlesinger AE, Hernandez RJ, Zerin JM, Marks TI, Kelsch RC. Interobserver and intraobserver variations in sonographic renal length measurements in children. AJR Am J Roentgenol. 1991 May;156(5):1029–32.
203. Beland MD, Walle NL, Machan JT, Cronan JJ. Renal Cortical Thickness Measured at Ultrasound: Is It Better Than Renal Length as an Indicator of Renal Function in Chronic Kidney Disease? Am J Roentgenol. 2010 Aug;195(2):W146–9.
204. Bakker J, Olree M, Kaatee R, de Lange EE, Moons KGM, Beutler JJ, et al. Renal Volume Measurements: Accuracy and Repeatability of US Compared with That of MR Imaging. Radiology. 1999 Jun;211(3):623–8.
205. Emamian SA, Nielsen MB, Pedersen JF. Intraobserver and interobserver variations in sonographic measurements of kidney size in adult volunteers. A comparison of linear measurements and volumetric estimates. Acta Radiol Stockh Swed 1987. 1995 Jul;36(4):399–401.
206. Bakker J, Olree M, Kaatee R, de Lange EE, Beek FJ. In vitro measurement of kidney size: comparison of ultrasonography and MRI. Ultrasound Med Biol. 1998 Jun;24(5):683–8.
207. Karstoft K, Lødrup AB, Dissing TH, Sørensen TS, Nyengaard JR, Pedersen M. Different strategies for MRI measurements of renal cortical volume. J Magn Reson Imaging. 2007 Dec;26(6):1564–71.
208. Di Leo G, Di Terlizzi F, Flor N, Morganti A, Sardanelli F. Measurement of renal volume using respiratory-gated MRI in subjects without known kidney disease: Intraobserver, interobserver, and interstudy reproducibility. Eur J Radiol. 2011 Dec;80(3):e212–6.
209. Zöllner FG, Svarstad E, Munthe-Kaas AZ, Schad LR, Lundervold A, Rørvik J. Assessment of Kidney Volumes From MRI: Acquisition and Segmentation Techniques. Am J Roentgenol. 2012 Nov;199(5):1060–9.
210. Gillis KA, McComb C, Patel RK, Stevens KK, Schneider MP, Radjenovic A, et al. Non-Contrast Renal Magnetic Resonance Imaging to Assess Perfusion and Corticomedullary Differentiation in Health and Chronic Kidney Disease. Nephron. 2016;133(3):183–92.
211. Wolf M, de Boer A, Sharma K, Boor P, Leiner T, Sunder-Plassmann G, et al. Magnetic resonance imaging T1- and T2-mapping to assess renal structure and function: a systematic review and statement paper. Nephrol Dial Transplant. 2018 Sep 1;33(suppl_2):ii41–50.

212. World Medical Association Declaration of Helsinki: Ethical Principles for Medical Research Involving Human Subjects. JAMA. 2013 Nov 27;310(20):2191.
213. National Research Council (US) Committee for the Update of the Guide for the Care and Use of Laboratory Animals. Guide for the Care and Use of Laboratory Animals [Internet]. 8th ed. Washington (DC): National Academies Press (US); 2011 [cited 2022 Sep 9]. (The National Academies Collection: Reports funded by National Institutes of Health). Available from: http://www.ncbi.nlm.nih.gov/books/NBK54050/
214. Morsing E, Asard M, Ley D, Stjernqvist K, Marsal K. Cognitive Function After Intrauterine Growth Restriction and Very Preterm Birth. PEDIATRICS. 2011 Apr 1;127(4):e874–82.
215. Morsing E, Gustafsson P, Brodszki J. Lung function in children born after foetal growth restriction and very preterm birth: Lung function after very preterm IUGR. Acta Paediatr. 2012 Jan;101(1):48–54.
216. Morsing E, Liuba P, Fellman V, Maršál K, Brodszki J. Cardiovascular function in children born very preterm after intrauterine growth restriction with severely abnormal umbilical artery blood flow. Eur J Prev Cardiol. 2014 Oct;21(10):1257–66.
217. Shariat M, Mertens L, Seed M, Grosse-Wortmann L, Golding F, Mercer-Rosa L, et al. Utility of Feed-and-Sleep Cardiovascular Magnetic Resonance in Young Infants with Complex Cardiovascular Disease. Pediatr Cardiol. 2015 Apr;36(4):809–12.
218. Sjöberg P, Hedström E, Fricke K, Frieberg P, Weismann CG, Liuba P, et al. Comparison of 2D and 4D Flow MRI in Neonates Without General Anesthesia. J Magn Reson Imaging. 2022 Jun 21;jmri.28303.
219. Heiberg E, Sjögren J, Ugander M, Carlsson M, Engblom H, Arheden H akan. Design and validation of Segment-freely available software for cardiovascular image analysis. BMC Med Imaging. 2010;10(1):1.
220. Hollanders JJ, van der Pal SM, van Dommelen P, Rotteveel J, Finken MJJ. Growth pattern and final height of very preterm vs. very low birth weight infants. Pediatr Res. 2017 Aug;82(2):317–23.
221. Liefke J, Steding-Ehrenborg K, Asgeirsson D, Nordlund D, Kopic S, Morsing E, et al. Non-contrast-enhanced magnetic resonance imaging can be used to assess renal cortical and medullary volumes—A validation study. Acta Radiol Open. 2022 Jan;11(1):205846012110722.
222. Bidhult S, Kantasis G, Aletras AH, Arheden H, Heiberg E, Hedström E. Validation of T1 and T2 algorithms for quantitative MRI: performance by a vendor-independent software. BMC Med Imaging. 2016 Aug 8;16(1):46.
223. Lee VS, Kaur M, Bokacheva L, Chen Q, Rusinek H, Thakur R, et al. What causes diminished corticomedullary differentiation in renal insufficiency? J Magn Reson Imaging. 2007 Apr;25(4):790–5.
224. Bidhult S, Hedström E, Carlsson M, Töger J, Steding-Ehrenborg K, Arheden H, et al. A new vessel segmentation algorithm for robust blood flow quantification from two-dimensional phase-contrast magnetic resonance images. Clin Physiol Funct Imaging. 2019 Sep;39(5):327–38.

225. Nickander J, Lundin M, Abdula G, Jenner J, Maret E, Sörensson P, et al. Stationary tissue background correction increases the precision of clinical evaluation of intra-cardiac shunts by cardiovascular magnetic resonance. Sci Rep. 2020 Mar 19;10(1):5053.
226. Ljungman S, Laragh JH, Cody RJ. Role of the kidney in congestive heart failure. Relationship of cardiac index to kidney function. Drugs. 1990;39 Suppl 4:10–21; discussion 22-24.
227. Taylor MRH, Holland CV, Spencer R, Jackson JF, O'Connor GI, O'Donnell JR. Haematological reference ranges for schoolchildren. Clin Lab Haematol. 1997 Apr;19(1):1–15.
228. Lundström S, Liefke J, Heiberg E, Hedström E. Pulse Wave Velocity Measurements by Magnetic Resonance Imaging in Neonates and Adolescents: Methodological Aspects and Their Clinical Implications. Pediatr Cardiol. 2022 Apr 9;
229. Dorniak K, Heiberg E, Hellmann M, Rawicz-Zegrzda D, Wesierska M, Galaska R, et al. Required temporal resolution for accurate thoracic aortic pulse wave velocity measurements by phase-contrast magnetic resonance imaging and comparison with clinical standard applanation tonometry. BMC Cardiovasc Disord. 2016 Dec;16(1):110.
230. Thurn D, Doyon A, Sözeri B, Bayazit AK, Canpolat N, Duzova A, et al. Aortic Pulse Wave Velocity in Healthy Children and Adolescents: Reference Values for the Vicorder Device and Modifying Factors. Am J Hypertens. 2015 Dec;28(12):1480–8.
231. Hoeks APG. Non-invasive study of the local mechanical arterial characteristics in humans. In: Safar ME, O'Rourke MF, editors. The Arterial System in Hypertension [Internet]. Dordrecht: Springer Netherlands; 1993 [cited 2022 Feb 21]. p. 119–34. (Developments in Cardiovascular Medicine; vol. 144). Available from: http://link.springer.com/10.1007/978-94-011-0900-0_9
232. Steding K, Engblom H, Buhre T, Carlsson M, Mosén H, Wohlfart B, et al. Relation between cardiac dimensions and peak oxygen uptake. J Cardiovasc Magn Reson. 2010;12(1):8.
233. Asgeirsson D, Hedström E, Jögi J, Pahlm U, Steding-Ehrenborg K, Engblom H, et al. Longitudinal shortening remains the principal component of left ventricular pumping in patients with chronic myocardial infarction even when the absolute atrioventricular plane displacement is decreased. BMC Cardiovasc Disord. 2017 Dec;17(1):208.
234. Lurbe E, Cifkova R, Cruickshank JK, Dillon MJ, Ferreira I, Invitti C, et al. Management of high blood pressure in children and adolescents: recommendations of the European Society of Hypertension: J Hypertens. 2009 Sep;27(9):1719–42.
235. Kobori H, Alper AB, Shenava R, Katsurada A, Saito T, Ohashi N, et al. Urinary angiotensinogen as a novel biomarker of the intrarenal renin-angiotensin system status in hypertensive patients. Hypertens Dallas Tex 1979. 2009 Feb;53(2):344–50.
236. Coulam CH, Bouley DM, Sommer FG. Measurement of renal volumes with contrast-enhanced MRI. J Magn Reson Imaging. 2002 Feb;15:174–9.

237. Cheong B, Muthupillai R, Rubin MF, Flamm SD. Normal Values for Renal Length and Volume as Measured by Magnetic Resonance Imaging. Clin J Am Soc Nephrol. 2006 Nov 2;2(1):38–45.
238. Selby NM, Blankestijn PJ, Boor P, Combe C, Eckardt KU, Eikefjord E, et al. Magnetic resonance imaging biomarkers for chronic kidney disease: a position paper from the European Cooperation in Science and Technology Action PARENCHIMA. Nephrol Dial Transplant. 2018 Sep 1;33(suppl_2):ii4–14.
239. Will S, Martirosian P, Würslin C, Schick F. Automated segmentation and volumetric analysis of renal cortex, medulla, and pelvis based on non-contrast-enhanced T1- and T2-weighted MR images. Magn Reson Mater Phys Biol Med. 2014 Oct;27(5):445–54.
240. Kline TL, Edwards ME, Korfiatis P, Akkus Z, Torres VE, Erickson BJ. Semiautomated Segmentation of Polycystic Kidneys in T2-Weighted MR Images. Am J Roentgenol. 2016 Sep;207(3):605–13.
241. Daniel AJ, Buchanan CE, Allcock T, Scerri D, Cox EF, Prestwich BL, et al. Automated renal segmentation in healthy and chronic kidney disease subjects using a convolutional neural network. Magn Reson Med. 2021 Aug;86(2):1125–36.
242. Rigalleau V, Garcia M, Lasseur C, Laurent F, Montaudon M, Raffaitin C, et al. Large kidneys predict poor renal outcome in subjects with diabetes and chronic kidney disease. BMC Nephrol [Internet]. 2010 Dec [cited 2017 Nov 5];11(1). Available from: http://bmcnephrol.biomedcentral.com/articles/10.1186/1471-2369-11-3
243. Baumgartl HJ, Sigl G, Banholzer P, Haslbeck M, Standl E. On the prognosis of IDDM patients with large kidneys. Nephrol Dial Transplant Off Publ Eur Dial Transpl Assoc - Eur Ren Assoc. 1998 Mar;13(3):630–4.
244. Song T, Fu L, Huang Z, He S, Zhao R, Lin T, et al. Change in renal parenchymal volume in living kidney transplant donors. Int Urol Nephrol. 2014 Apr;46(4):743–7.
245. Brennan S, Watson DL, Rudd DM, Kandasamy Y. Kidney growth following preterm birth: evaluation with renal parenchyma ultrasonography. Pediatr Res [Internet]. 2022 Feb 4 [cited 2022 Apr 6]; Available from: https://www.nature.com/articles/s41390-022-01970-8
246. Lillås BS, Qvale TH, Richter BK, Vikse BE. Birth Weight Is Associated With Kidney Size in Middle-Aged Women. Kidney Int Rep. 2021 Nov;6(11):2794–802.
247. Voges I, Jerosch-Herold M, Hedderich J, Pardun E, Hart C, Gabbert D, et al. Normal values of aortic dimensions, distensibility, and pulse wave velocity in children and young adults: a cross-sectional study. J Cardiovasc Magn Reson. 2012;14(1):77.
248. Caterini JE, Banks L, Wells GD, Cifra B, Slorach C, McCrindle BW, et al. Magnetic resonance imaging reveals elevated aortic pulse wave velocity in obese and overweight adolescents. Clin Obes. 2017 Dec;7(6):360–7.
249. Wolf RL, Ehman RL, Riederer SJ, Rossman PJ. Analysis of systematic and random error in MR volumetric flow measurements. Magn Reson Med. 1993 Jul;30(1):82–91.

250. Arheden H, Saeed M, Törnqvist E, Lund G, Wendland MF, Higgins CB, et al. Accuracy of segmented MR velocity mapping to measure small vessel pulsatile flow in a phantom simulating cardiac motion. J Magn Reson Imaging. 2001 May;13(5):722–8.
251. Wentland AL, Grist TM, Wieben O. Review of MRI-based measurements of pulse wave velocity: a biomarker of arterial stiffness. Cardiovasc Diagn Ther. 2014 Apr;4(2):193–206.
252. Willum Hansen T, Staessen JA, Torp-Pedersen C, Rasmussen S, Thijs L, Ibsen H, et al. Prognostic Value of Aortic Pulse Wave Velocity as Index of Arterial Stiffness in the General Population. Circulation. 2006 Feb 7;113(5):664–70.
253. Flahault A, Oliveira Fernandes R, De Meulemeester J, Ravizzoni Dartora D, Cloutier A, Gyger G, et al. Arterial Structure and Stiffness Are Altered in Young Adults Born Preterm. Arterioscler Thromb Vasc Biol. 2020 Oct;40(10):2548–56.
254. te Velde SJ, Ferreira I, Twisk JWR, Stehouwer CDA, van Mechelen W, Kemper HCG, et al. Birthweight and arterial stiffness and blood pressure in adulthood--results from the Amsterdam Growth and Health Longitudinal Study. Int J Epidemiol. 2004 Feb;33(1):154–61.
255. Bonamy AKE, Bendito A, Martin H, Andolf E, Sedin G, Norman M. Preterm Birth Contributes to Increased Vascular Resistance and Higher Blood Pressure in Adolescent Girls. Pediatr Res. 2005 Nov;58(5):845–9.
256. Reference Values for Arterial Stiffness' Collaboration. Determinants of pulse wave velocity in healthy people and in the presence of cardiovascular risk factors: "establishing normal and reference values." Eur Heart J. 2010 Oct;31(19):2338–50.
257. Huybrechts SAM, Devos DG, Vermeersch SJ, Mahieu D, Achten E, de Backer TLM, et al. Carotid to femoral pulse wave velocity: a comparison of real travelled aortic path lengths determined by MRI and superficial measurements. J Hypertens. 2011 Aug;29(8):1577–82.
258. Weber T, Ammer M, Rammer M, Adji A, O'Rourke MF, Wassertheurer S, et al. Noninvasive determination of carotid-femoral pulse wave velocity depends critically on assessment of travel distance: a comparison with invasive measurement. J Hypertens. 2009 Aug;27(8):1624–30.
259. van Hout MJ, Dekkers IA, Westenberg JJ, Schalij MJ, Widya RL, de Mutsert R, et al. Normal and reference values for cardiovascular magnetic resonance-based pulse wave velocity in the middle-aged general population. J Cardiovasc Magn Reson Off J Soc Cardiovasc Magn Reson. 2021 Apr 19;23(1):46.
260. Varda NM, Gregorič A. Twenty-four-hour ambulatory blood pressure monitoring in infants and toddlers. Pediatr Nephrol. 2005 Jun;20(6):798–802.
261. Edstedt Bonamy AK, Mohlkert LA, Hallberg J, Liuba P, Fellman V, Domellöf M, et al. Blood Pressure in 6-Year-Old Children Born Extremely Preterm. J Am Heart Assoc. 2017 Aug 1;6(8).
262. Chen W, Srinivasan SR, Berenson GS. Amplification of the association between birthweight and blood pressure with age: the Bogalusa Heart Study. J Hypertens. 2010 Oct;28(10):2046–52.

263. Huxley RR, Shiell AW, Law CM. The role of size at birth and postnatal catch-up growth in determining systolic blood pressure: a systematic review of the literature. J Hypertens. 2000 Jul;18(7):815–31.
264. Cook NR, Cohen J, Hebert PR, Taylor JO, Hennekens CH. Implications of small reductions in diastolic blood pressure for primary prevention. Arch Intern Med. 1995 Apr 10;155(7):701–9.
265. Whelton SP, McEvoy JW, Shaw L, Psaty BM, Lima JAC, Budoff M, et al. Association of Normal Systolic Blood Pressure Level With Cardiovascular Disease in the Absence of Risk Factors. JAMA Cardiol. 2020 Sep 1;5(9):1011.
266. Tauzin L, Rossi P, Grosse C, Boussuges A, Frances Y, Tsimaratos M, et al. Increased systemic blood pressure and arterial stiffness in young adults born prematurely. J Dev Orig Health Dis. 2014 Dec;5(6):448–52.
267. Olander RFW, Sundholm JKM, Suonsyrjä S, Sarkola T. Arterial health during early childhood following abnormal fetal growth. BMC Pediatr. 2022 Dec;22(1):40.
268. Mohlkert LA, Hallberg J, Broberg O, Hellström M, Pegelow Halvorsen C, Sjöberg G, et al. Preterm arteries in childhood: dimensions, intima-media thickness, and elasticity of the aorta, coronaries, and carotids in 6-y-old children born extremely preterm. Pediatr Res. 2017 Feb;81(2):299–306.
269. Bots ML, Hoes AW, Hofman A, Witteman JCM, Grobbee DE. Cross-sectionally assessed carotid intima–media thickness relates to long-term risk of stroke, coronary heart disease and death as estimated by available risk functions. J Intern Med. 1999 Mar;245(3):269–76.
270. Santos LM dos, Gomes IC, Pinho JF, Neves-Alves CM, Magalhães GS, Campagnole-Santos MJ, et al. Predictors and reference equations for augmentation index, an arterial stiffness marker, in healthy children and adolescents. Clinics. 2021;76:e2350.
271. Redheuil A, Wu CO, Kachenoura N, Ohyama Y, Yan RT, Bertoni AG, et al. Proximal Aortic Distensibility Is an Independent Predictor of All-Cause Mortality and Incident CV Events. J Am Coll Cardiol. 2014 Dec;64(24):2619–29.
272. Hovi P, Turanlahti M, Strang-Karlsson S, Wehkalampi K, Järvenpää AL, Eriksson JG, et al. Intima-Media Thickness and Flow-Mediated Dilatation in the Helsinki Study of Very Low Birth Weight Adults. Pediatrics. 2011 Feb 1;127(2):e304–11.
273. Painter RC, de Rooij SR, Hutten BA, Bossuyt PMM, de Groot E, Osmond C, et al. Reduced intima media thickness in adults after prenatal exposure to the Dutch famine. Atherosclerosis. 2007 Aug;193(2):421–7.
274. Telles F, McNamara N, Nanayakkara S, Doyle MP, Williams M, Yaeger L, et al. Changes in the Preterm Heart From Birth to Young Adulthood: A Meta-analysis. Pediatrics. 2020 Aug;146(2).
275. Mohlkert L, Hallberg J, Broberg O, Rydberg A, Halvorsen CP, Liuba P, et al. The Preterm Heart in Childhood: Left Ventricular Structure, Geometry, and Function Assessed by Echocardiography in 6-Year-Old Survivors of Periviable Births. J Am Heart Assoc. 2018 Jan 23;7(2):e007742.

276. Kozák-Bárány A, Jokinen E, Saraste M, Tuominen J, Välimäki I. Development of left ventricular systolic and diastolic function in preterm infants during the first month of life: A prospective follow-up study. J Pediatr. 2001 Oct;139(4):539–45.
277. Derraik JGB, Lundgren M, Cutfield WS, Ahlsson F. Association Between Preterm Birth and Lower Adult Height in Women. Am J Epidemiol. 2017 Jan 1;185(1):48–53.
278. Engblom H, Steding K, Carlsson M, Mosén H, Hedén B, Buhre T, et al. Peak oxygen uptake in relation to total heart volume discriminates heart failure patients from healthy volunteers and athletes. J Cardiovasc Magn Reson. 2010;12(1):74.
279. Harris S, Perston L, More K, Graham P, Ellis N, Frampton C, et al. Cardiac structure and function in very preterm-born adolescents compared to term-born controls: A longitudinal cohort study. Early Hum Dev. 2021 Dec;163:105505.
280. Buechel EV, Kaiser T, Jackson C, Schmitz A, Kellenberger CJ. Normal right- and left ventricular volumes and myocardial mass in children measured by steady state free precession cardiovascular magnetic resonance. J Cardiovasc Magn Reson Off J Soc Cardiovasc Magn Reson. 2009 Jun 21;11:19.
281. Lewandowski AJ, Bradlow WM, Augustine D, Davis EF, Francis J, Singhal A, et al. Right Ventricular Systolic Dysfunction in Young Adults Born Preterm. Circulation. 2013 Aug 13;128(7):713–20.
282. Biering-Sørensen T, Biering-Sørensen SR, Olsen FJ, Sengeløv M, Jørgensen PG, Mogelvang R, et al. Global Longitudinal Strain by Echocardiography Predicts Long-Term Risk of Cardiovascular Morbidity and Mortality in a Low-Risk General Population: The Copenhagen City Heart Study. Circ Cardiovasc Imaging. 2017 Mar;10(3):e005521.
283. Modin D, Møgelvang R, Andersen DM, Biering-Sørensen T. Right Ventricular Function Evaluated by Tricuspid Annular Plane Systolic Excursion Predicts Cardiovascular Death in the General Population. J Am Heart Assoc. 2019 May 21;8(10):e012197.
284. Rangarajan V, Chacko SJ, Romano S, Jue J, Jariwala N, Chung J, et al. Left ventricular long axis function assessed during cine-cardiovascular magnetic resonance is an independent predictor of adverse cardiac events. J Cardiovasc Magn Reson. 2016 Dec;18(1):35.
285. Lillås BS, Tøndel C, Aßmus J, Vikse BE. Low birthweight is associated with lower glomerular filtration rate in middle-aged mainly healthy women. Nephrol Dial Transplant. 2021 Dec 31;37(1):92–9.
286. Gandy SJ, Armoogum K, Nicholas RS, McLeay TB, Houston JG. A clinical MRI investigation of the relationship between kidney volume measurements and renal function in patients with renovascular disease. Br J Radiol. 2007 Jan;80(949):12–20.
287. Restrepo JM, Torres-Canchala L, Cadavid JCA, Ferguson M, Villegas A, Ramirez O, et al. Renal volume of five-year-old preterm children are not different than full-term controls. J Pediatr (Rio J). 2021 Sep;S0021755721001182.
288. Keijzer-Veen MG, Devos AS, Meradji M, Dekker FW, Nauta J, van der Heijden BJ. Reduced renal length and volume 20 years after very preterm birth. Pediatr Nephrol. 2010 Mar;25(3):499–507.

289. Bertram JF, Cullen-McEwen LA, Egan GF, Gretz N, Baldelomar E, Beeman SC, et al. Why and how we determine nephron number. Pediatr Nephrol Berl Ger. 2014 Apr;29(4):575–80.
290. Hoogenboom LA, Wolfs TGAM, Hütten MC, Peutz-Kootstra CJ, Schreuder MF. Prematurity, perinatal inflammatory stress, and the predisposition to develop chronic kidney disease beyond oligonephropathy. Pediatr Nephrol. 2021 Jul;36(7):1673–81.
291. Brenner BM, Lawler EV, Mackenzie HS. The hyperfiltration theory: a paradigm shift in nephrology. Kidney Int. 1996 Jun;49(6):1774–7.
292. Friedli I, Crowe LA, Berchtold L, Moll S, Hadaya K, de Perrot T, et al. New Magnetic Resonance Imaging Index for Renal Fibrosis Assessment: A Comparison between Diffusion-Weighted Imaging and T1 Mapping with Histological Validation. Sci Rep. 2016 Jul;6(1):30088.
293. Lees CC, Marlow N, van Wassenaer-Leemhuis A, Arabin B, Bilardo CM, Brezinka C, et al. 2 year neurodevelopmental and intermediate perinatal outcomes in infants with very preterm fetal growth restriction (TRUFFLE): a randomised trial. Lancet Lond Engl. 2015 May 30;385(9983):2162–72.
294. Kc A, Rana N, Målqvist M, Jarawka Ranneberg L, Subedi K, Andersson O. Effects of Delayed Umbilical Cord Clamping vs Early Clamping on Anemia in Infants at 8 and 12 Months: A Randomized Clinical Trial. JAMA Pediatr. 2017 Mar 1;171(3):264.
295. Conde-Agudelo A, Díaz-Rossello JL. Kangaroo mother care to reduce morbidity and mortality in low birthweight infants. Cochrane Neonatal Group, editor. Cochrane Database Syst Rev [Internet]. 2016 Aug 23 [cited 2021 Aug 26];2017(2). Available from: http://doi.wiley.com/10.1002/14651858.CD002771.pub4
296. Hsiao CC, Tsai ML, Chen CC, Lin HC. Early optimal nutrition improves neurodevelopmental outcomes for very preterm infants. Nutr Rev. 2014 Aug;72(8):532–40.
297. Cortese S, Angriman M, Maffeis C, Isnard P, Konofal E, Lecendreux M, et al. Attention-deficit/hyperactivity disorder (ADHD) and obesity: a systematic review of the literature. Crit Rev Food Sci Nutr. 2008 Jun;48(6):524–37.
298. Wentz E, Björk A, Dahlgren J. Neurodevelopmental disorders are highly over-represented in children with obesity: A cross-sectional study: Neurodevelopmental Disorders in Children with Obesity. Obesity. 2017 Jan;25(1):178–84.
299. Markopoulou P, Papanikolaou E, Analytis A, Zoumakis E, Siahanidou T. Preterm Birth as a Risk Factor for Metabolic Syndrome and Cardiovascular Disease in Adult Life: A Systematic Review and Meta-Analysis. J Pediatr. 2019 Jul;210:69-80.e5.

Part II Research papers

Papers I-V

Author Contributions

	Study design	Ethical application	Data collection	Data analysis	Statistical analysis	Figures and tables	Interpretation of results	Preparation of manuscript	Revision of manuscript	Reply to reviewers
Study I	2	0	3	3	3	3	3	3	3	3
Study II	3	0	3	2	2	2	3	2	2	1
Study III	2	0	3	3	3	3	3	3	3	3
Study IV	2	0	3	3	3	3	3	3	-	-
Study V	2	0	3	3	3	3	3	3	3	3

Not applicable	-
No contribution	0
Limited contribution	1
Moderate contribution	2
Significant contribution	3

About the author

With a deep interest in human performance and physiology, Jonas Liefke begun his academic career by getting a BSc in Physiotherapy at Lund University. Six months later, after working as a licensed physiotherapist, Jonas enrolled in medical school. In 2018, still in medical school, he got a position as a PhD student in the Cardiac MR group at the department of Clinical Physiology and Nuclear Medicine, Lund, Sweden. Jonas earned his MD from Lund university in January 2021 and will be doing his internship at Skåne University Hospital, Lund, Sweden, which starts in the beginning of 2022.

Printed by Media-Tryck, Lund 2022 NORDIC SWAN ECOLABEL 3041 0903

LUND UNIVERSITY

FACULTY OF MEDICINE

Department of Clinical Physiology

Lund University, Faculty of Medicine
Doctoral Dissertation Series 2022:159
ISBN 978-91-8021-321-9
ISSN 1652-8220